7
CHAPTER 7
UPDATED EPRI (2004, 2006) GMM

7.1 General Methodology for Updating EPRI (2004, 2006) GMM

This chapter documents the development of the Updated EPRI (2004, 2006) Ground-Motion Model (GMM). The Updated GMM is intended for use in estimating ground motions for hard rock sites in the Central and Eastern United States (CEUS). The development of the Updated GMM draws on data and models that are applicable to the somewhat broader region of Central and Eastern North America (CENA). Therefore, both CEUS and CENA terms are used throughout this chapter interchangeably.

7.1.1 Overview and Road Map

This chapter documents the development of the Updated EPRI (2004, 2006) Ground-Motion Model (GMM). The material in this chapter is presented in the following sequence:

- The remainder of Section 7.1 provides a summary of the data and methodology used to develop the update.
- Sections 7.2 and 7.3 document the development of the ground-motion database and the adjustment of ground-motion amplitudes to reference rock site conditions (shear-wave velocity $\geq$ 2,800 m/s).
- Section 7.4 presents the technical basis for the approach used to develop an updated model for the median ground-motion amplitude for the Midcontinent and its epistemic uncertainty.
- Sections 7.5 through 7.9 documents the steps used to develop the updated model for the median (log mean) ground motion and its epistemic uncertainty.
- Section 7.10 documents the development of the updated model for aleatory variability.
- Section 7.11 presents an updated designation of the Gulf Coast region, quantifies anelastic attenuation in the Gulf Coast crustal region, and develops the Updated GMM for the Gulf Coast region.
- Sections 7.12 and 7.13 compare the Updated GMM to the EPRI (2004) GMM and summarize the results from a number of sensitivity analyses.
- Section 7.14 discusses the Updated GMM and the process used in its development.
- Section 7.15 summarizes the objectives and contents of the Hazard Input Document (Appendix G), which provides all the information required for implementing and using the Updated GMM.

7.1.2 Data and Data-Selection Criteria

This project took advantage of two significant data collection efforts: (1) the PEER NGA-East collection and uniform processing of strong-motion and seismograph data, and (2) the EPRI-sponsored effort to characterize site conditions at a number of recording stations (the latter supplemented by a parallel USGS effort that provided data for additional stations and by profile data from the literature compiled by PEER NGA-East). The station data were used to adjust the recorded ground-motion data to reference site conditions using two alternative approaches. In addition, this project used a small number of ground-motion data that were used in the EPRI (2004) study but were not included in the NGA-East database.

The selection criteria applied to the ground-motion data are discussed throughout Section 7.2 and are summarized below.

- Moment Magnitude (**M**). This project used only data from earthquakes with **M** 3.75 and greater. Although earthquakes in the **M** 3.75–4.75 range may differ in magnitude scaling from larger earthquakes, they provide useful information regarding geometric spreading and were retained by the TI team (albeit with a lower weight than larger earthquakes). The data from earthquakes with magnitudes less than **M** 3.75 were not used because these magnitudes are well below the magnitude range for which the candidate GMPEs were developed.
- Distance. This project used only data obtained at distances up to 500 km to develop the Updated GMM, because this is the distance range of primary engineering interest for the 0.1–100 Hz frequency range. Data from distances between 500 and 1,000 km are displayed on figures showing data or residuals versus distance, but were not used in the calculation of weights.
- Epicentral Locations and Travel Paths. For the development of the GMM for the Midcontinent region depicted on Figure 1.3-1 (see Sections 7.2 through 7-9), this project used only records with travel paths located entirely within the Midcontinent region. Additional recordings from the EarthScope Transportable Array (TA) were used for the quantification of anelastic attenuation in the Gulf Coast crustal region, as documented in Section 7.11.
- Components of Motion. This project used only horizontal data, in order to avoid the uncertainties associated with the conversion from vertical to horizontal. This option was not feasible in earlier studies (e.g., EPRI, 2004), which had access to few horizontal data.
- Site Conditions. This project used only data from rock sites in order to avoid the difficulty of having to quantify the effects of soil nonlinearity and of high soil kappa during the calculation of site adjustment factors. For many sites, the assignment to a rock site category was based on measured or estimated time-averaged shear-wave velocity of upper 30 m of the site (V_{S30}) values of 500 m/s or greater. For the remaining sites, the assignment to a rock site category was based on descriptions of the site geology.
- Record Quality. For data coming from the PEER NGA-East, this project generally used only records that had been assigned a quality level of "A" ("Good"). In addition, a few records with quality level "?" ("Accepted but might have problems") were retained, after visual examination of their processed time series. For data coming from the EPRI (2004) project, recordings obtained on dams or in other large structures were removed.

Data shown on the figures in this chapter represent data that were used in the analysis. The only exceptions are the data between 500 and 1,000 km that meet all other requirements, which are also shown. Unless indicated otherwise, all tables list or summarize data that were used in the analysis. The databases documented in Appendix A contain all data that were used, as well as additional data that were collected and tabulated as part of this project but were excluded from the analysis because they did not meet the criteria.

7.1.3 Overall Structure of GMM

The Updated GMM follows the EPRI (2004) approach of grouping the selected GMPEs into four clusters according to their technical characteristics, weighting the GMPEs within each cluster according to their consistency with the data, representing each cluster by three fitted GMMs, and calculating cluster weights on the basis of consistency with the data and other attributes of the GMMs within each cluster.

There are some differences in implementation, however. Some of these differences represent adjustments to the conditions encountered, while others represent methodological improvements. In particular, the set of selected GMPEs have changed because some of the GMPEs considered by EPRI (2004) are no longer supported by their developers and proponents, and because new GMPEs are available. The new GMPEs necessitated changes in the definition of Clusters 2 and 3 because the most salient grouping of the selected GMMs for these clusters was their difference in geometric spreading. Also, the calculation of consistency with the data was changed to a likelihood-based formulation, which is more flexible (e.g., it allows for consideration of single-station correlation in adjustment factors) and has a strong basis in theory. In addition, the characterization of within-cluster epistemic uncertainty was modified to sidestep some problems with unquantified correlations, to take advantage of the more abundant data in constraining the predictions at low magnitudes, and to account for uncertainty in magnitude scaling in a more direct manner.

7.1.4 Model for Aleatory Uncertainty

The EPRI (2006) model for aleatory uncertainty (sigma) was based on preliminary PEER NGA models for sigma from active tectonic regions (e.g., the Western United States), with adjustments that account for differences between active and stable tectonic regions. The Updated GMM incorporates nearly final PEER NGA-West 2 models, with the same adjustments. In that sense, the Updated GMM for aleatory uncertainty represents a straightforward update to the EPRI (2006) aleatory model, in which elements that have been superseded are replaced by their natural successors.

7.2 Development of Final Ground-Motion Database

The development of the Updated EPRI (2004, 2006) GMM relied in part on comparisons with earthquake ground motion recorded in CENA. As described in Section 6.1, a preliminary ground-motion database was developed for use in evaluating the need to update the EPRI (2004, 2006) GMM. The preliminary database was updated and refined for use in developing the Updated GMM. This section describes the development of the final database. The database files are documented in Appendix A.6 and provided in electronic form.

7.2.1 Ground-Motion Data Sources

The primary source of the final ground-motion database was the ground-motion database assembled by the PEER NGA-East Project. Development of the PEER NGA-East ground-motion database is described in Cramer et al. (2013). The August 2012 version of the PEER NGA-East database was obtained for development of the final project database. The data were obtained in the form of three Microsoft Excel files. File "NGAEastAsisFlatfileV3.0-2012-8-31.xlsx" contained the "flat file" of ground-motion data. The file contained 31,522 records of individual ground-motion components. Each earthquake in the database was assigned an earthquake identification number (EQID). For each earthquake, the following data were entered:

- EQID, earthquake name, date, time, location, magnitude, and focal mechanism (if available)
- recording station identification (station network and station code)
- recording-site V_{S30} (if available)
- station location (latitude and longitude)
- epicentral distance to earthquake
- recording component, recording quality
- record processing filter information
- peak ground acceleration (PGA)
- peak ground velocity (PGV)
- peak ground displacement (PGD)
- 5 percent damped pseudo-spectral accelerations (PSA) at 105 periods from 0.01 to 10 seconds

File "NGAEastEventTable2012-8-28.xlsx" contained information on the 94 earthquakes that contributed recordings to the flat file. The entries in this file repeated the earthquake information from the main flat file, along with additional available information on the earthquake location and mechanism. File "NGAEastStationCompTable2012-8-27.xlsx" contained additional information on the 1,466 stations represented in the PEER NGA-East database, including the components of recorded motion at each station, available descriptions of the site geology, and in some cases, information on the instrument location.

In addition to the ground-motion flat file and earthquake and station tables, the processed acceleration time series were obtained from the PEER NGA-East Project for 23,358 recordings. The recordings missing from this set include some of the more recent earthquakes. Some of these recordings were used to verify intermediate steps in the analytical calculation of site adjustments, but were not used directly in the final calculations.

The PEER NGA-East database did not include recordings from all the earthquakes that were used in the EPRI (2004) study. Review of the EPRI (2004) ground-motion database indicated that a limited number of additional recordings met the acceptance criteria for this study, namely, recorded horizontal components of motion at free-field instruments on rock sites from earthquakes with magnitude **M** 3.75 and greater. Data from five more earthquakes were added to the database. The source of these data was Appendix 2A of EPRI (1993). The tables in that

appendix provided information on the earthquakes, stations, record processing, and tabulated PGA and PSA at five periods. The remaining data in the EPRI (2004) database were not used due to instrument location (e.g., on dams or in large structures) or limited information (e.g., only the vertical component of motion was provided).

The third source of ground-motion data examined was the database contained in the Engineering Seismology Toolbox (www.seismotoolbox.ca) maintained by Dr. Gail Atkinson and her colleagues (Assatourians and Atkinson, 2010). Review of the toolbox database did not disclose any recordings meeting the acceptance criteria for this project that were not already in the PEER NGA-East database. However, the database did provide information on shear-wave velocity for a number of recording sites.

7.2.2 Ground-Motion Record Processing

In the broadest sense, record processing describes the process used to translate the recorded data at a site into the characterization of the level of ground shaking used in the assessment or development of GMMs. This process can be characterized by three steps:

1. Processing of the individual component waveforms to remove instrument response and identify the usable bandwidth.
2. Calculation of the appropriate ground-motion-intensity measures for each component.
3. Representation of the components of ground motion recorded at a site by a single ground-motion measure.

The following sections describe how each of these aspects of record processing was addressed in the project.

7.2.2.1 Waveform Processing

The PEER NGA-East Project performed processing of the individual waveforms of each component of motion present in the PEER NGA-East ground-motion database. As described in Cramer et al. (2013), the process involved reviewing the individual waveforms for obvious problems, instrument correction and initial filtering of original waveforms, generation of signal and pre-event noise Fourier spectra and selection of final filter corners, final band-pass filtering, and generation of acceleration, velocity, and displacement records. Each recording was assigned a quality code, typically either "A" or "?". For the most part, only data from recordings with quality level "A" ("Good") were retained for use in this project. The exceptions were a few records with quality level "?" ("Accepted but might have problems") at recording stations for which analytical site adjustments were made. The time series for recordings at these sites were visually examined for problems by the TI team, and those that appeared acceptable were retained. These recordings are indicated by the assigned quality level "?K" in the project ground-motion database (Appendix A.6). The NGA-East Project performed a number of checks and reviews of the waveform processing, both of the approach and software and of the resulting time series. This testing is described in Cramer et al. (2013).

EPRI (1993) did not provide details on the record processing used to produce the data in Appendix 2A. However, the filter corner frequencies used to process the recordings were reported and pseudo-spectral accelerations were provided for only those frequencies that fell

within the bandwidth used for processing. It was assumed that the data in Appendix 2A of EPRI (1993) were of similar quality to that in the PEER NGA-East database.

7.2.2.2 Calculation of Ground-Motion-Intensity Measures – Geometric Mean Horizontal Ground Motions

The PEER NGA-East record processing produced ground-motion intensity measures typically used in engineering practice, peak motions, and 5 percent damped pseudo-spectral accelerations. Pseudo-spectral accelerations were only reported in the PEER NGA-East flat file for spectral periods within the bandwidth used for record processing as identified by the high-pass and low-pass filter corners listed in the flat file.

The August 2012 version of the PEER NGA-East flat file provided ground-motion amplitudes for each component of motion. The EPRI (2004) GMM and the candidate CENA GMPEs reviewed in this project provide estimates of the average horizontal component of motion, which has been typically represented in the past by the geometric mean of the peak motions on the two horizontal components. Recently, Boore et al. (2006) and Boore (2010) introduced improved measures of the amplitude of horizontal ground motions that have come to replace the traditional geometric mean of the as-recorded components. However, as discussed by Boore (2010), the differences between these measures and the geometric mean are relatively small (at most about 7 percent). These small differences are not considered large enough to significantly affect relative comparisons of the CENA GMPEs with ground-motion data. Therefore, the geometric mean of the reported peak motions for each horizontal component was used in this study, as was done in the EPRI (2004) study.

The EPRI (2004) study provided GMPEs for PGA and PSA at frequencies of 25, 10, 5, 2.5, 1, and 0.5 Hz (spectral periods of 0.04, 0.1, 0.2, 0.4, 1, and 2 seconds, respectively). The geometric mean of the individual component motions for PGA and PSA at the six frequencies was computed for use in this project. Values were computed for only those frequencies that fell within the bandwidth of both components. These geometric mean values are reported in the project ground-motion database (Appendix A.6), along with the minimum bandwidth for the two components. The minimum bandwidth was defined by the maximum of the high-pass filter corners and the minimum of the low-pass filter corners for the two horizontal components. Those recordings for which only a single horizontal component was available were retained in the project database, as, on average, the motions should correspond to the geometric mean. The components used for each recording are identified in the project ground-motion database.

EPRI (2004) used vertical motions corrected to horizontal orientation in the evaluation of GMPEs. This was done because of the limited ground-motion data available at that time. The amount of available horizontal components of ground motion has been greatly expanded in the PEER NGA-East database. Therefore, for this project, it was decided to not introduce the additional uncertainty of vertical to horizontal corrections to the data. Only horizontal components of motion were used.

EPRI (2004) developed GMPEs for PGA and the PEER NGA database reports PGA for each recording. However, the data sampling rate and low-pass filter corners used in processing for many of the recordings preclude the use of spectral accelerations at 25 Hz, and in many cases at 10 Hz. This observation indicates that the PGA values in many cases would not accurately represent the high-frequency motions expected to be present at CEUS rock sites. Therefore, PGA

values were not used in the evaluation of the selected GMPEs in this project. The values are retained for information in the project database (Appendix A.6).

7.2.2.3 Representation of Multiple Recordings at a Site for Each Earthquake

For several sites contained in the PEER NGA-East database, there are multiple channels of horizontal recordings with different instrument types. The PEER NGA-East Project processed the waveforms for each of these channels separately and reported response spectral values for each channel. Due to the close spatial proximity of these instruments, the individual recordings cannot be considered independent ground-motion measures. Therefore, a single set of geometric mean ground motions was selected for each recording site for each earthquake. The ground-motion amplitude for the recording that had the widest bandwidth was typically selected as the set of ground-motion amplitudes for the site for an individual earthquake. However, there were some cases where the bandwidth for different instruments covered different frequency ranges. For example, one instrument might provide data for the frequency range of 2.5–25 Hz, and another instrument might provide data for the frequency range of 0.5–1 Hz. In such cases, the data from the two instruments were combined by selecting the spectral accelerations from one instrument for frequencies of 2.5–25 Hz and from the other instrument for frequencies of 0.5 and 1 Hz to provide a single set of ground-motion measures for the full frequency range of interest, 0.5 Hz to 25 Hz. The bandwidth reported in the project ground-motion database (Appendix A.6) reflects the combined bandwidth for the two instrument recordings. The reported PGA values were taken from the recording with the highest low-pass filter corner.

7.2.3 Assignment of Moment Magnitude

The PEER NGA-East database provided estimates of moment magnitude, **M**, for each earthquake in the database. These values were reviewed, along with additional information, in order to assign values of **M** to each earthquake. Table 7.2.3-1 lists the information gathered on moment magnitude for the 94 events contained in the PEER NGA-East database plus the 5 added from the EPRI (1993) database. This information was used to assign the moment magnitudes listed in the column of Table 7.2.3-1 labeled "Assigned Moment Magnitude." For those earthquakes where specific values of seismic moment, M_o, were available, moment magnitudes were computed from M_o (in dyne-cm) using the relationship of Hanks and Kanamori (1979):

$$\mathbf{M} = 2/3\log(M_o) - 10.7 \qquad (7.2.3\text{-}1)$$

For smaller earthquakes, values of **M** were based on conversions from other magnitude scales, such as those developed in NUREG-2115 (EPRI/DOE/NRC, 2012). Earthquakes with **M** less than 3.75 were not researched extensively as they were not used in the evaluation of the CENA GMPEs, and were not given assigned moment magnitudes.

7.2.4 Estimation of Rupture and Joyner-Boore Distance Measures

The PEER NGA-East database provides epicentral and hypocentral distances for the recordings. However, most of the GMPEs under consideration use either the closest distance to rupture (R_{Rup}) or the closest horizontal distance to the surface projection of the rupture (Joyner-Boore distance, R_{JB}) as the distance measure. Values of R_{Rup} and R_{JB} were estimated for the recordings using a modification of the simulation process developed in Appendix B of Chiou and Youngs (2008b). The process involves simulating rupture dimensions using the relationship between

seismic moment and rupture area, RA (km^2), for CENA earthquakes given in Somerville et al. (2001) and the definition of **M** given by Equation 7.2.3-1, yielding

$$\log(RA) = \mathbf{M} - 4.35$$
$$\sigma_{\log(RA)} = 0.24 \qquad (7.2.4\text{-}1)$$

The standard deviation of 0.24 is based on Wells and Coppersmith (1994). The length, L_R, and width, W_R, of the rupture are simulated using the following relationship for rupture aspect ratio developed by Chiou and Youngs (2008b) from the PEER NGA data set:

$$\log(AR = L_R / W_R) = (0.01552 - 0.00472F_{NM} - 0.01099F_{RV}) \times \max(\mathbf{M} - 4{,}0)^{3.097}$$
$$\sigma_{\log(AR)} = 0.16 \qquad (7.2.4\text{-}2)$$

In Equation 7.2.4-2, F_{NM} and F_{RV} are (0,1) indicator variables for normal faulting and reverse faulting, respectively. The simulated ruptures are placed on the hypocentral location of the earthquake using the earthquake focal mechanism information to specify orientation. If no information was available for the focal mechanism, the rupture strike was sampled from a uniform distribution for azimuth over 0–360 degrees, and the fault dip and rake were assigned based on the prevalent rupture style in the region. The vertical location of the simulated rupture with respect to the hypocenter was simulated using empirical distributions for the hypocenter location derived by Chiou and Youngs (2008b) from the PEER NGA set of earthquake rupture models. The observed and smoothed empirical distributions are shown on Figure 7.2.4-1. If the top of the simulated rupture plane extended above 0 depth, it was placed at 0 depth. The location of the hypocenter along strike was simulated using data from Mai et al. (2005) for earthquakes of magnitude $\leq$ **M** 6.5. This distribution is shown on Figure 7.2.4-2.

For each simulated rupture, the distances were computed to a grid of 700 points distributed evenly in azimuth around the epicenter over the distance range of 0 to 300 km. The process was repeated 101 times and the median distance to each site was obtained. Then the calculated distances for all the simulated ruptures were searched to identify the one realization that produced the minimum squared difference over all 700 points between the distances calculated for that simulation and the median distances. This rupture simulation was selected as the rupture model for the earthquake and was used to compute R_{Rup} and R_{JB} to the actual recording sites.

The modification introduced in the above approach is the use of a large grid of evenly spaced points to select the rupture simulation rather than the actual recording sites as was done by Chiou and Youngs (2008b). The use of the actual recording sites may result in a bias in the selected rupture location if there is a limited range of azimuths for the recording stations.

Figure 7.2.4-3 compares the simulated value of R_{JB} to the epicentral distances for the recordings in the database. Because of the small size of most of the earthquakes, the differences between epicentral distance and R_{JB} are generally small.

For three earthquakes, the values of R_{Rup} and R_{JB} were computed from available models of the rupture. The rupture model of Hartzell et al. (1994) was used for the November 25, 1988, Saguenay, Quebec, earthquake (EQID 5) and the rupture model of Chapman (2013) was used for

the August 23, 2011, Mineral, Virginia, earthquake (EQID 88). The values of R_{Rup} and R_{JB} computed in the PEER NGA Project for the December 23, 1985, Nahanni, Northwest Territories, main shock (EQID 70) were also used in this study.

7.2.5 Classification of Recording Station Site Conditions

The EPRI (2004) GMPEs were developed to provide estimates of ground motion on hard rock sites with shear-wave velocities of 2,800 m/s or greater, and this is the reference site condition for the update to the EPRI (2004, 2006) GMM. Evaluation of the selected GMPEs is therefore focused on comparisons of GMPEs that estimate ground motions for hard rock sites with empirical data recorded on hard rock sites. As the number of such sites in the ground-motion database is very limited, a larger set of ground-motion data records on rock sites can be used by adjusting these data to the target reference site condition. Ideally, this adjustment would be made based on differences in the velocity profiles at the recording stations compared to the reference site velocity profile, and this is the focus of the analytical site adjustments discussed in Section 7.3.1. However, the number of recording sites for which the velocity profile has been measured is limited. The alternative approach described in Section 7.3.2 is to use adjustments based on empirical site factors derived from the recorded ground-motion data. This is the general approach used in development of the PEER NGA GMPEs (Power et al., 2008) in which ground-motion scaling was based on V_{S30}. The PEER NGA Project developed correlations between V_{S30} and site geology such that estimates of V_{S30} were available for all sites in the PEER NGA ground-motion database.

Similar types of correlations have been developed for CENA recording sites by Silva et al. (2011), and they provide estimates of V_{S30} for many of the recording stations in the PEER NGA-East database. Shear-wave-velocity estimates are also available for some stations from the Engineering Seismology Toolbox (Assatourians and Atkinson, 2010). Figure 7.2.5-1 shows the distribution of available V_{S30} values for the recording stations. The data have been limited to stations with measured or estimated V_{S30} values of 500 m/s or greater. As indicated in Section 7.3, the lower limit of 500 m/s was used to remove the effects of significant soil nonlinearity from the estimation of site adjustment factors. There are no stations with measured or estimated shear-wave velocities at or near the target reference-rock shear-wave velocity of $\geq$2,800 m/s. A number of stations have estimated V_{S30} values at or near 2,000 m/s. The majority of stations have measured or estimated V_{S30} values in the range of 500 to 1,500 m/s.

However, there remain a large number of sites for which these estimates of V_{S30} have not been made. In order to include a larger amount of data into the GMPE evaluation, a simpler approach for site adjustment was used: site categorization. The use of site categories in GMPE development has a long history, with the simplest categorization being soil versus rock. Because the purpose of this project is to develop GMPEs for estimation of ground motions on rock sites, a classification scheme was developed focused on rock site categories. The PEER NGA-East database contained geologic descriptions for many of the recording stations. It is expected that, at least for sedimentary rocks, shear-wave velocity increases on average with increasing rock age. Therefore, the recording stations for which there were geologic descriptions were grouped into three rock classes:

- Class A – Cretaceous age and older rocks
- Class B – Tertiary age and younger rocks

- Class C – Unconsolidated sediments

Figure 7.2.5-2 shows the distribution of measured or estimated V_{S30} values for recording stations assigned to the three rock classes. There is a weak correlation between the assigned rock class and V_{S30}, with Class A containing more of the higher V_{S30} values. However, all the rock classes contain sites with a wide range of V_{S30} values.

As discussed in Section 7.3, the two approaches for evaluating site adjustments to the ground-motion data are to compute site adjustments analytically based on measured shear-wave-velocity profiles and to compute site adjustments empirically. The analytical approach is the more accurate approach, but results in a limited set of usable data. The empirical approach allows for the inclusion of more data at the expense of less precision in characterizing the site conditions. In order to utilize as much data as possible, the following site categorization scheme was employed and reviewed by a geologist.

CENA Rock Site Category Criteria

Rock Site Category	Criteria
Very Firm Rock	Class A, B, or C with $V_{S30} \geq 1{,}890$ m/s
Intermediate Rock	Class A, B, or C with $1{,}000 \leq V_{S30} < 1{,}890$ m/s or Class A with unknown V_{S30}
Soft Rock	Class A, B, or C with $500 \leq V_{S30} < 1{,}000$ m/s or Class B with unknown V_{S30}

The categorization scheme placed the most emphasis on the use of estimated or measured V_{S30}, using rock class only when V_{S30} values were not available for a site. The boundary between very firm rock and intermediate rock was placed at V_{S30} value of 1,890 m/s, as there were a number of sites with V_{S30} values just below 2,000 m/s. Very firm rock sites are those whose response is expected to be the closest to that of the reference hard rock site.

7.2.6 Distribution of Final Database

The earthquakes, stations, and ground-motion values in the final project database are listed in Appendix A.6. This database includes data for distances up to 1000 km. The analysis database used for evaluations of the selected GMPEs is the subset of the project database that includes recordings for distance of up to 500 km. Because, the selected GMPEs were developed for the Midcontinent region, recordings from the 2006 Gulf of Mexico earthquake (EQID 39) were excluded because of the distance from recording sites and the fact that the travel path from this earthquake is through the Gulf Coast attenuation region. Data from the 2011 Cormel, Texas earthquake (EQID 92) were also excluded because the earthquake was located within the Gulf Coast attenuation region.

Figure 7.2.6-1 shows the magnitude-distance distribution of the final ground-motion database developed for this project. Each panel shows the available date for the identified frequency color-coded by the site category defined in Section 7.2.5. Also shown on the figures are the boundaries of the magnitude-distance bins used in the evaluation of the selected GMPEs, as described in Section 7.4.3. Table 7.2.6-1 summarizes the number of earthquakes represented in each magnitude interval, and Table 7.2.6-2 summarizes the number of individual recordings in

each magnitude-distance bin. Similarly, Tables 7.2.6-3 and 7.2.6-4 summarize the number of stations (for all stations used and for the stations with available velocity profiles, respectively). The number of data varies with frequency because the useable bandwidth of each record was selected by the PEER NGA-East analysts on the basis of instrument characteristics and observed signal/noise ratios. As a consequence, the number of data for 25 Hz PSA is less than half the number available for the other frequencies. Note that the number of sites indicated to have measured V_{S30} differs slightly between Tables 7.2.6-3 and 7.2.6-4 due to the interpretation that values of V_{S30} listed in the Engineering Seismology Toolbox (Assatourians and Atkinson, 2010) were measured values unless indicated as inferred. Shear-wave-velocity profiles were not available for all these sites.

Figure 7.2.6-2 shows the spatial distribution of earthquakes in the final database with magnitudes $3.75 \leq \mathbf{M} < 4.75$, and Figure 7.2.6-3 shows the spatial distribution of earthquakes in the final database with magnitudes $4.75 \leq \mathbf{M}$. The earthquake locations are well distributed and span the entire CENA region. The earthquakes shown are those with rock site recordings at distances of 500 km and less. The color coding reflects the assignment of earthquakes to different regions for the testing of regional differences described in Section 7.4.2.

Figure 7.2.6-4a through 7.2.6-4f show the spatial distribution of rock site recording stations for the earthquakes with $3.75 \leq \mathbf{M} < 4.75$ and $R_{JB} \leq 500$ km that contribute data for the six frequencies. Figures 7.2.6-5a through 7.2.6-5f show the spatial distribution of rock site recording stations for the earthquakes with $\mathbf{M} \geq 4.75$ and $R_{JB} \leq 500$ km that contribute data for the six frequencies. The recording-site data are also generally well distributed across the entire CENA region. The exception is the recording-site data for 25 Hz, which are more heavily sampled in the northeastern portion of the study region.

7.3 Adjustment for Recording-Site Conditions

The purpose of this effort is to develop a procedure to adjust the recorded ground motions to the reference conditions for which the hard-rock GMPEs have been defined. The reference profile adopted for use in analytical site adjustments in this project is the same one used in the EPRI (1993), namely, a profile with shear-wave velocity of 2,830 m/s over the top 1.3 km and with kappa equal to 0.006 s. Further details on this reference profile are provided in Section 7.3.1.1 below. Note that the intended reference site condition for the Updated GMM is the same as that for the EPRI (2004) GMM, reference rock sites with shear-wave velocities of 2,800 m/s and greater.

This adjustment is desirable because nearly all the data described in Section 7.2 come from sites with shear-wave velocities different from those in the reference profile. If this adjustment is not performed, some of the site effects are double-counted, because the recordings used to develop the GMM are affected by site effects at the recording site, and then site effects are added again when modifying the rock-site hazard results for the effect of the local soil or rock column. On the other hand, the adjustment for site effects at the recording site carries uncertainty because of limitations in the data (e.g., most measured profiles extend only to approximately 30 m) and modeling uncertainty.

The adjustment is performed using two alternative approaches: an analytical approach and an empirical approach. Both approaches are used in Chapter 6 to test the applicability of the EPRI (2004) GMM in light of new data, and in this chapter to develop an updated GMM.

7.3.1 Analytical Adjustment for Recording-Site Condition

7.3.1.1 Characterization of the Profiles

The characterization of the profile at each recording station (and of the reference profile) consists of the following quantities:

- The depth-wise variation of the shear-wave velocity (V_S) and the density ρ.
- The anelastic attenuation through the soil and near-surface rock, characterized by parameter kappa.[1]

In defining these parameters, an effort was made to maintain consistency with the EPRI "screening, prioritization and implementation details" (SPID) procedure (EPRI, 2013b).

At the time this work was performed, a total of 54 recording-station profiles were available, from this project, from the USGS, and from PEER NGA-East[2] (see Table 7.3.1.1-1). For recording stations that had repeated measurements, the measurement that was received first was used. If estimates were available for the emplacement depth of the sensor, the portion of the profile above that depth was removed for the purposes of calculating amplification factors and V_{S30}.

These velocity profiles extend only to depths of 30–50 meters, and it becomes necessary to extend them to depths of one kilometer or more in order to quantify amplification factors at frequencies as low as 0.1 Hz. To this effect, the velocity profile templates in Appendix B of EPRI (2013b) were utilized. The templates are shown on Figure 7.3.1.1-1 and are included in tabular form in Appendix A. The following approach was used in this project for extending the profiles:[3]

1. Determine the two template profiles that bound the measured V_S at the bottom of the profile (denote them as template high and template low) and calculate the interpolation factor in $\ln[V_S]$ space using the V_S values at that depth, as follows:

$$\theta = \frac{\ln[V_S(\text{measured})] - \ln[V_S(\text{template low})]}{\ln[V_S(\text{template high})] - \ln[V_S(\text{template low})]} \qquad (7.3.1\text{-}1)$$

2. For each depth z below the bottom of the measured profile, interpolate between profiles, calculating the interpolated V_S as

[1] In terms of the original definition of kappa by Anderson and Hough (1984), the kappa used here corresponds to the value of kappa at zero epicentral distance, which is written sometimes as $\kappa(0)$ or κ_0. For the sake of brevity, this report will omit the 0.

[2] Some USGS and PEER NGA East station profiles were discarded earlier because they had $V_{S30} < 500$ m/s or they had no horizontal recordings in the PEER NGA-East flat file that met the selection criteria. Some of the station profiles listed in Table 7.3.1.1-1 were later discarded for the same reasons (see comments in table). In the end, 34 stations with measured Vs profiles were used in the calculations.

[3] The approach used in this project for extending the profiles is slightly different from the one recommended in EPRI (2013b), but is similar in concept and uses the same templates. Also, the approach used in this project does not preserve the templates' depth to layer boundaries exactly because some local interpolation over depth is used, but is accurate enough considering that the site-response approach employed is not sensitive to the exact depth to these boundaries because it uses integrated measures of the velocity.

$$V_S(z) = \exp\{\theta \ln[V_S(z)(\text{template high})] + (1-\theta)\ln[V_S(z)(\text{template low})]\} \quad (7.3.1\text{-}2)$$

3. Splice the interpolated profile to the measured profile.

In some instances, the templates were offset vertically in order to obtain profiles that are consistent with the local geology.

Figures 7.3.1.1-2 and 7.3.1.1-3 illustrate this process for station ET.SWET in Tennessee. Figure 7.3.1.1-2 depicts the profile measured by The University of Texas. Figure 7.3.1.1-3 depicts the top 1,000 m of the extended profile that is used for the calculation of amplification factors, as well as the template profiles.

The density ρ(z) is less variable than V_S. For depths at which no density information is available, the approach recommended by Boore (2007) for the estimation of density as a function of V_S is used.

For parameter kappa, this project used the approach recommended in the EPRI SPID (EPRI, 2013b), as follows:

- For rock (V_{S30} > 500 m/s) with at least 1,000 m of firm sedimentary rock (i.e., material between 500 and 2,000 m/s), use the Silva et al. (1998) equation for kappa as a function of V_{S30}, which (after conversion to natural logarithms and m/s) takes the form $\ln[\kappa(s)] = 3.9575 - 1.093\ln[V_{S30}(m/s)]$. This equation is close to the equation obtained by Van Houtte et al. (2011) using a much larger data set.
- For thinner rock, use 0.006 s plus the kappa associated with $Q = 40$ (calculated over the thickness of deposits with V_S < 2,000 m/s).
- For soils (V_{S30} < 500 m/s) with a depth to hard rock of 1,000 m or greater, use $k = 0.04$s (which is also the maximum kappa for all cases).[4]
- For thinner soils (V_{S30} < 500 m/s), use $\kappa(s) = 0.0000605 \times H(m) + 0.006$, where $H(m)$ is the thickness of the sedimentary column (V_S < 2,000 m/s) in meters.

Uncertainty in these parameters is specified as follows (also based on the recommendations of EPRI, 2013b):

- Uncertainty in V_S is characterized by a logarithmic standard deviation of 0.35 over the entire profile. This factor accounts both for uncertainty in velocity and uncertainty in the approach for the calculation of amplification factors. V_S is randomized using a two-point distribution and full depth-wise correlation, resulting in two profiles with V_S (z) equal to exp(–0.35) and exp(+0.35) times the base-case V_S (z).[5] The base-case profile is also run in the calculations,

[4] The analysis of Gulf Coast recordings at deep-soil sites presented in Section 7.11.1.1 indicates values of kappa greater than 0.04 s. There is no inconsistency between those results and the value of 0.04 s because all the stations considered in this chapter are outside the Gulf Coast.

[5] The uncertainty in both ln(Vs) and ln(kappa) is characterized by means of discrete distributions, each consisting of two equally weighted masses located at_base-case±1σ. This commonly used two-point approximation preserves the mean and standard deviation of each distribution being represented, and of linear functions thereof. The symmetry of the high and low curves relative to the base-case curves on Figures 7.3.2-1 through 7.3.2-6 indicates that the amplification is roughly linear in ln(Vs) and ln(kappa), thereby confirming the validity of these approximations. The

but is given no weight. Figure 7.3.1.1-4 depicts the base-case profile and the High-Vs and Low-Vs profiles obtained for the ET.SWET site.

- Uncertainty in the density ρ is not considered explicitly. The 0.35 logarithmic standard deviation in V_S also covers the much lower variation in density.
- Uncertainty in kappa is characterized by a logarithmic standard deviation of 0.4 and is taken as independent of V_S. Kappa is randomized using a two-point distribution, resulting in two profiles with kappa equal to exp(–0.4) and exp(+0.4) times the base-case kappa (the base-case kappa is also run in the calculations, but is given no weight).

Table 7.3.1.1-2 lists the reference profile.

7.3.1.2 Details of the Analytical Approach

The purpose of the analytical approach is to adjust the recorded horizontal spectral amplitudes to the reference site conditions, using information about the station's V_S profile. This project uses the Boore and Joyner (1997) quarter-wavelength approach to quantify the amplification ratio between the recording station and the reference profile. The adjustment process consists of four steps, as follows:

1. Calculation of amplification factors in terms of Fourier amplitude.
2. Calculation of Fourier amplitudes from the recorded horizontal response spectra.
3. Adjustment of the Fourier spectra to the reference conditions by dividing them by the (recording site)/reference Fourier-amplitude ratio.
4. Calculation of the adjusted reference-site spectral amplitudes.

Each of these steps is discussed below and then typical results are presented.

Calculation of Amplification Factors

Following Boore and Joyner (1997), the ratio of Fourier amplitudes between a real site and a hypothetical site with shear-wave velocity and density equal to those at the source is given by

$$A(f) = \sqrt{\frac{\rho_S \beta_S}{\overline{\rho}[z(f)]\overline{\beta}[z(f)]}} \exp(-\pi \kappa f) \qquad (7.3.1\text{-}3)$$

where β denotes shear-wave velocity, subscript S denotes properties at the source, and the quantities in the denominator represent time-weighted averages of the density and shear-wave velocity, as defined below.

The shear-wave travel time to a depth z is calculated as

functional forms of Equations 7.3.1-3 through 7.3.1-7 also suggest nearly linear dependence of ln-amplification on ln(Vs) and ln(kappa). This two-point approximation does not place any mass at the base-case value, so it is not essential to calculate amplification factors for the base-case profile and kappa. Nonetheless, it is useful to calculate amplification factors for the base case because the results from this calculation provide an indication of the central tendency of the calculated amplification factor, as well as a consistency check.

$$t(z) = \int_0^z \frac{du}{\beta(u)} \tag{7.3.1-4}$$

where u represents depth.

For a particular frequency f, the associated averaging depth z(f) is the depth z such that $f = [4t(z)]^{-1}$. The associated time-averaged shear-wave velocity is calculated as

$$\overline{\beta}[z(f)] = \frac{z(f)}{t[z(f)]} \tag{7.3.1-5}$$

Similarly, the associated time-averaged density is calculated as

$$\overline{\rho}[z(f)] = \frac{\int_0^{z(f)} \frac{\rho(u)du}{\beta(u)}}{t[z(f)]} \tag{7.3.1-6}$$

Applying Equation 7.3.1-3 to both the recording-site profile and the reference profile, one can obtain the amplification factor (recording site/reference), as follows:

$$A_{site/ref}(f) = \sqrt{\frac{\overline{\rho_{ref}}(f)\overline{\beta_{ref}}(f)}{\overline{\rho_{site}}(f)\overline{\beta_{site}}(f)}} \exp\left[-\pi(\kappa_{site} - \kappa_{ref})f\right] \tag{7.3.1-7}$$

where *ref* refers to the reference conditions and *site* refers to the recording-site conditions. The dependence on z is not shown explicitly in the above equation for the sake of clarity, but it is understood that the calculations involve the frequency-dependent averaging depth $z(f)$ and that the two averaging depths are different (i.e., $z_{ref}(f) \neq z_{site}(f)$).

The calculation of this amplification factor was performed for the 5 alternative profiles generated in Section 7.3.1.1 at each recording site (i.e., base-case profile and 4 profiles associated with randomized shear-wave velocity and kappa), resulting in 5 amplification factors as a function of frequency.

Note that this Fourier amplification factor is independent of the record (provided that soil linearity is maintained, which is the case for all the records considered). The amplification factor in terms of response spectra is different for different records at the same station because the motions have different frequency content as a result of differences in magnitude and distance.

Calculation of Recording-Site Fourier Spectrum

The Fourier amplitude spectrum of the recorded motion is calculated using the Inverse Random Vibration Theory (IRVT; see Gasparini and Vanmarcke, 1976, or Rathje et al., 2005), as

implemented by Kottke (2012).[6] Inputs to this calculation are the recording-site response-spectral ordinates from the horizontal flat file (see Section 7.2), and the ground-motion duration, which is calculated using the expression

$$T = 0.1R + 1/f_c \tag{7.3.1-8}$$

where R is distance and f_c is the corner frequency, which is calculated using a Brune model with 120 bar stress drop.[7] The coefficient of the distance-dependent term is double the value typically used (e.g., Herrmann, 1985) but agrees better with the durations computed from the available PEER NGA-East time histories.

The IRVT approach may not always resolve the high-frequency portion of the Fourier spectrum (i.e., in the region where spectral acceleration is approaching PGA). To overcome this limitation, Fourier spectra were also calculated from the PEER NGA-East time histories, and a procedure was developed to approximate the shape of the Fourier spectrum at high frequencies.

The calculations described above are performed for all recordings obtained at sites with profile information, for magnitudes greater than 3.75, and for distances less than 1,000 km. The number of resulting records is 335 (after data from stations with $V_{S30} < 500$ m/s are removed).

Adjustment of Recording-Site Fourier Spectrum to Obtain Reference-Site Fourier Spectrum

At each recording site, the recording-site Fourier spectrum for each record is divided by the (recording site)/reference amplification factor $A_{site/ref}(f)$ calculated with Equation 7.3.1-7, to obtain the Fourier spectra adjusted for site conditions. This calculation is performed for the 335 records selected above and for the five alternative amplification factors.

Calculation of Adjusted Response Spectra

Finally, the adjusted Fourier spectra are converted to adjusted spectral accelerations using the Random Vibration Theory (RVT; again using the implementation by Kottke, 2012). The duration given by Equation 7.3.1-8 is also used in this calculation. For each record, this calculation is performed separately for the five alternative amplification factors. The four results associated with the $\pm\sigma$ branches on shear-wave velocity and kappa are then used to calculate the logarithmic mean and standard deviation of the adjusted spectral acceleration.

Although the IRVT and RVT approaches are typically used with smooth spectra, this procedure also works well with the jagged spectra from individual records. The accuracy of this procedure is also commensurate with the accuracy of the quarter-wavelength approach. The reason for using IRVT and RVT, instead of adjusting the time histories in the time domain and then calculating response spectra for the adjusted motions, is that the quarter-wavelength approach does not provide the Fourier phase-angle information which would be required for the time-domain analysis.

[6] In the Kottke (2012) scripts, the maximum number of IRVT iterations was increased from 30 to 300.

7 The sensitivity of the IRVT and RVT calculations to duration is small. In particular, the sensitivity to stress drop is very weak for the magnitudes and distances of interest.

Typical Results

Figure 7.3.1.2-1 illustrates the calculation of the [recording site]/[reference site] Fourier amplification factor for the ET.SWET station for which the profiles are shown on Figures 7.3.1.1-1 and 7.3.1.1-2. The thin lines on the top portion of the figures indicate the amplification factors calculated using the five alternative combinations of V_S and kappa. The corresponding thick lines show the calculated logarithmic mean $\pm\sigma$ amplification factors. The red line on the bottom portion shows the logarithmic standard deviation of the amplification factor (referenced to the right vertical axis). Figures 7.3.1.2-2 and 7.3.1.2-3 show similar results for a softer station (NM.USIN, V_{S30} = 668 m/s) and for a harder one (CN.OTT, V_{S30} = 1692 m/s).

In general, the amplification is controlled by impedance at low and intermediate frequencies and by kappa at higher frequencies. The frequency at which the effect of kappa takes over depends on the recording-site kappa, which for most sites is controlled by the travel time to rock with V_S = 2000 m/s. The logarithmic standard deviation of the amplification factor has moderate values in the region controlled by impedance, but becomes much larger at higher frequencies as a result of the 40 percent uncertainty in the recording-site kappa.

Figures 7.3.1.2-4 through 7.3.1.2-6 illustrate the calculation of the adjusted spectra for some of the recordings obtained at these three stations. Each figure shows the spectrum of the unadjusted recording, the five adjusted spectra, and the calculated logarithmic mean $\pm\sigma$ spectra. Figures 7.3.1.2-4 and 7.3.1.2-5 show that the adjustment compensates for gross impedance and kappa effects, as one would expect, but it does not compensate for the resonance effect (which happens to be at 10 Hz for both sites). Similar figures for other recordings at the same stations also show a peak at 10 Hz, which one may be able to remove with an approach that takes resonances into account.

7.3.2 Empirical Adjustment for Recording-Site Condition

The empirical adjustment for recording-site conditions is based on analyzing the residuals of recorded ground motions compared to the predictions of a GMPE. The residuals are defined as the natural log of the ratio of observed PSA divided by predicted PSA. Figure 7.3.2-1 shows an example of the residuals computed for data from earthquakes of magnitude **M** 3.75 and larger using the EPRI (2004) Cluster 1 median model. The residuals are then analyzed to identify the effect of site categories on the value of the residuals. The assumption used is that the response for sites in the very firm rock category defined in Section 7.2.5 is similar to that for sites consisting of the reference rock condition. This assumption is necessary because the empirical database does not contain data from sites with shear-wave velocities at the reference rock condition.

The first step is to fit a base model to the residuals that does not include the effect of site classification. Model 1 provides an estimate of only C_0, the mean residual:

$$\ln(\text{Residual})_{\text{Model 1}} = C_0 + \varepsilon_{i,j} \qquad (7.3.2\text{-}1)$$

In Equation 7.3.2-1, the error term is designated $\varepsilon_{i,j}$ to indicate the jth recording for the ith earthquake. Because of the within-earthquake correlation of the residuals, linear mixed-effects regression was performed using the statistical package **R** (**R** Development Core Team, 2012).

A second model was defined that includes factors to account for differences between ground motions on the three rock categories. The residuals were analyzed using Model 2:

$$\ln(\text{Residual})_{\text{Model 2}} = C_0 + C_{IR}F_{IR} + C_{SR}F_{SR} + \varepsilon_{i,j} \qquad (7.3.2\text{-}2)$$

In Equation 7.3.2-2, F_{IR} and F_{SR} are indicator (dummy) variables that take on the value 1 for intermediate rock sites or soft rock sites, respectively, and are 0 otherwise. The formulation of Model 2 makes the very firm rock category the reference category. Coefficients C_{IR} and C_{SR} represent scale factors that define the average difference in ground motions for sites in the intermediate rock and soft rock categories, respectively, compared to sites in the very firm rock category.

Figure 7.3.2-2 shows the results of the analyses of the residuals applying Equations 7.3.2-1 and 7.3.2-2 to the residuals shown on Figure 7.3.2-1. The top left-hand plot shows the values of the coefficient C_0 obtained using Model 1, and the top right-hand plot shows the values of the coefficient C_0 obtained using Model 2. The vertical bars represent 90 percent confidence intervals on the fitted parameters. The results are shown for the analysis of the residuals in four magnitude-distance ranges. The bottom two plots on Figure 7.3.2-2 show the values of the site category scaling coefficients C_{IR} and C_{SR}. As one can see in the bottom left plot, the 90 percent confidence intervals for coefficient C_{IR} often include the value of 0, indicated lack of statistical significance. Applying the Akaike Information Criteria (AIC) test (Akaike, 1974) or the related Schwartz Bayesian Information Criteria (BIC) test (Schwartz, 1978) to these cases indicates that the use of Model 2 does not produce a statistically better fit to the residuals than Model 1 produces.

The 90 percent confidence intervals for coefficient C_{SR} in Model 2 typically do not include the value 0, indicating that the value for this coefficient is usually statistically significant. A third model incorporating only scaling for soft rock was tested.

$$\ln(\text{Residual})_{\text{Model 3}} = C_0 + C_{SR}F_{SR} + \varepsilon_{i,j} \qquad (7.3.2\text{-}3)$$

In this example, Model 3 was found to be an improvement over Model 2 in most cases (lower AIC and BIC scores). This result was typical of the results obtained when the procedure was applied to all the GMPEs for the development of the Updated GMM, indicating that the most statistically significant difference that could be obtained from analysis of the residuals is that the ground motions for the soft rock category of sites are different from those of the intermediate rock and very firm rock categories. Given this result, the empirically adjusted residuals for the *j*th recording of the *i*th earthquake are computed using the expression

$$\varepsilon_{ij}^{\text{empirically adjusted}} = \varepsilon_{ij} - C_{SR}F_{jk}^{SR} \qquad (7.3.2\text{-}4)$$

The parameter F_{jk}^{SR} takes on the value 1 if the *k*th site is in the soft rock category, and 0 otherwise. The values of C_{SR} used in the evaluations of the GMPEs were those computed for $\mathbf{M} \geq 4.75$ and $R_{JB} \leq 500$ km using Model 3 (Equation 7.3.2-3), as this is the magnitude-distance range of most interest for application of the Updated GMM.

7.3.3 Comparison of Analytical and Empirical Approaches

Although the two approaches to adjust for recording-site conditions are very different in terms of both the data and the models they use, it is useful to compare the two approaches in terms of their resulting amplification factors. To this effect, the logarithmic amplification factors from both approaches are shown as a function of V_{S30} on Figures 7.3.3-1 through 7.3.3-4. Each figure shows the analytically derived amplification factors as blue diamonds with $\pm\sigma$ error bars. These are shown only for magnitudes greater than 4.75 and distances shorter than 500 km. The factors for lower magnitudes or greater distances follow the same general trend but show more scatter. The empirically derived factors (averaged over all GMPEs) and their $\pm\sigma$ ranges are shown as red horizontal lines that extend between V_{S30} values of 500 and 1,000 m/s (soft rock). For greater values of V_{S30} (i.e., intermediate and hard rock), the amplification factor is unity, so it is shown as a single horizontal line.

The comparison for 1 Hz shows a good agreement between the two approaches. The comparisons for other frequencies show some differences, but these differences can be explained by the fact that there are few recordings from stations with V_{S30} greater than 2,000 m/s (hard rock). As a result, the empirical approach was not able to distinguish between intermediate and hard rock and, in addition, the empirical results for intermediate and hard rock (which are defined as equal to unity) are dominated by intermediate rock.

If one offsets the empirical factors so that the soft-rock factors agree with the analytical factors in the intermediate-rock range, one sees that they also agree in the soft-rock range. Therefore, an explanation for the differences between analytical and empirical adjustments is that the empirical adjustment cannot capture the amplification of intermediate rock relative to hard rock. The analytical approach, on the other hand, captures that effect by using measured profile data and explicit modeling of impedance and kappa effects.

Another consistency check is provided by the NGA amplification factors shown on Figure 7.3.3-5 for various frequencies (a distance of 100 km is used in this comparison to avoid nonlinear effects). These results indicate ratios of 1.6 to 2 (0.5 to 0.7 natural log units) between stations with V_{S30} values of 500 and 1,500 m/s, which is consistent with the results obtained here using the analytical and empirical approaches. As was the case for the empirical approach, these NGA results do not provide information about amplification factors between intermediate and hard rock.

7.4 Technical Bases for GMPEs and Development of Final Clusters

This section describes the technical bases for selection of GMPEs, their grouping into clusters, development of within-cluster weights, and evaluation of within-cluster epistemic uncertainty. In addition, the section discusses consideration of regional differences in ground motion within CENA. Following presentation of the technical bases, implementation of the approaches is described in Section 7.5.

7.4.1 Selection of GMPEs and Specification of Cluster Groupings

7.4.1.1 Candidate GMPEs

Section 6.2 presents evaluation GMPEs that are considered candidate GMPEs for this study. The selection of GMPEs from among the candidate GMPEs had two parallel elements: the identification of new candidate GMPEs and the decision as to which EPRI (2004) GMPEs have not been superseded, which retain technical validity, and, therefore, should be retained. Both elements were informed by literature reviews and interviews with Resource Experts performed by the TI Team and documented in Appendices B and C, and were complemented by internal TI Team discussions.

This effort to identify CEUS GMPEs that were developed since late 2003 (when the EPRI, 2004 technical work was completed) began in the fall of 2011, prior to formal initiation of this project. Informal discussions were conducted during a series of meetings and conference calls organized by the Project Manager. Following the initiation of the project, a formal process was defined and documented in accordance with guidance for a SSHAC Level 2 process. The formal process included literature reviews, interviews, and TI Team evaluation and integration.

The following six GMPEs were identified by the TI Team during this process. They are listed in alphabetical order, together with the abbreviations that will be used to refer to these models in the sections that follow.

- A08′ – Atkinson (2008) with the Atkinson and Boore (2011) modifications. The Atkinson (2008) GMPE is in essence the Boore and Atkinson (2008) NGA model, where the anelastic-attenuation term has been modified so it shows a long-distance decay similar to that of CEUS motions. Atkinson (2008) calls this approach "referenced empirical." This approach is similar in spirit to the hybrid empirical approach developed by Campbell (2003), although it does not go through the formal steps of using host and target stochastic models to adjust the GMPE, using instead recorded CENA ground motions for defining the adjustments. As described in Section 6.2.2, the published A08′ GMPE was altered slightly to remove the non-monotonic dependence on distance at low frequencies. Dr. Atkinson agreed with the alteration.
- AB06′ – Atkinson-Boore (2006) with the Atkinson and Boore (2011) modification. This is a GMPE derived from motions calculated using an extended-source stochastic model. The source characteristics were calibrated for California and then modified so they conform to CEUS source scaling of Somerville et al. (2001). The geometric and anelastic attenuation are based on Atkinson (2004a). Atkinson and Boore (2011) modified the model by making the stress parameters magnitude-dependent.
- PZT – Pezeshk et al. (2011). This is a GMPE developed using the hybrid empirical approach proposed by Campbell (2003). The authors use several 2008 PEER NGA GMPEs to define the host empirical models. The host and target stochastic models use constant stress and single-corner spectra. The geometric and anelastic attenuation model of Atkinson (2004a) is used for the target region. The functional form of the fitted GMPE is the same as that used by Atkinson and Boore (2006).
- SSCCSS, SSCVS, and SDCS – Silva et al. (2003). These three GMPEs were developed by Silva and colleagues using point-source stochastic models (with the alternative assumptions

of Single-Corner Constant Stress with Saturation, Single-Corner Variable Stress, and Double-Corner with Saturation, respectively). These GMPEs are very similar to those developed by the same authors in 2002 and used in EPRI (2004).

It is important to note that these four GMPEs are at their second generation of development, which provides additional assurance of their maturity and stability. It is generally accepted that the second generation of a model represents an improvement over the first generation, as the authors have the benefit of additional data and additional time understanding the model, along with its strengths and weaknesses. In the particular case of the A08′, AB06′, and PZT models, these second-generation models had the benefit of significant new earthquake data and (for A08′ and PZT) the availability of the PEER-NGA GMPEs.

In addition to being asked about new GMPEs, the Resource Experts that were contacted (see Appendix C) were asked to indicate which of the EPRI (2004) GMPEs have not been superseded, which retain technical validity, and which should be considered in conjunction with the new GMPEs. These questions were posed in general terms to all Resource Experts and in specific terms to experts who were authors of GMPEs used in EPRI (2004). The following GMPEs in each EPRI (2004) cluster were identified as valid by the TI Team, on the basis of input from the Resource Experts and other considerations:

- EPRI (2004) Cluster 1: Single-Corner Stochastic Models. Two versions of the Silva et al. (2002) single-corner GMPE, namely, the Single-Corner Constant Stress with Saturation (SSCCSS) and the Single-Corner Variable Stress (SSCVS), were identified as retaining technical validity. Furthermore, it was felt that it was important to retain these two alternative models for scaling at higher magnitudes as a way to represent epistemic uncertainty. The corresponding GMPEs in Silva et al. (2003), which are nearly identical to these 2002 versions, were considered instead of these two. In addition, the Frankel et al. (1996) and Toro et al. (1997) single-corner stochastic models were also considered to retain technical validity.
- EPRI (2004) Cluster 2: Double-Corner Stochastic Models. One version of the Silva et al. (2002) double-corner GMPE, namely, the Double-Corner Variable Stress (SDCVS), was identified as retaining technical validity. As was the case for the Silva et al. (2002) single-corner models, the nearly identical 2003 version was used instead.
- EPRI (2004) Cluster 3: Hybrid Empirical Models. The three hybrid empirical models in EPRI (2004) are considered to be superseded because they are no longer supported by their developers, who recommended the use of more recent GMPEs.
- EPRI (2004) Cluster 4: Finite Source/Green's Function Models. The one model in this cluster, namely, the Somerville et al. (2001), is still considered to be valid. In particular, this model has unique seismological features and no similar model has been developed for CENA that would supersede it. This model produces two slightly different GMPEs for rifted and non-rifted sources (the difference arises as a result of differences in the depth distributions). Both GMPEs were used.[8]

[8] When comparing GMPE predictions to data, the appropriate Somerville et al. (2001) GMPE was used, depending on whether the epicenter occurred in a zone identified as rifted or not, as indicated in Table 7.2.3-1. For the Updated EPRI (2004, 2006) GMM, separate GMPEs were developed for rifted and non-rifted sources.

The remaining seven GMPEs in EPRI (2004) are no longer supported by their developers or by the Resource Experts who are familiar with them, as discussed in Section 6.2.3. As a consequence of this input from the Resource Experts, supplemented by its own review and understanding of the technical literature and of the state of practice, the TI Team decided that these seven GMPEs should not be considered in the development of the Updated GMM.

7.4.1.2 Definition of GMPE Clusters

The project TI Team concluded that maintaining the EPRI (2004) strategy of grouping the alternative GMPEs into clusters of similar GMPEs and then assigning weights using a two-stage approach provides a rational mechanism for quantifying the central tendency and epistemic uncertainty in ground-motion amplitude. The rationale for defining these clusters is provided below.

The decision to maintain the structure of Clusters 1 and 4 is a natural one as the selected GMPEs maintain the same distinction in modeling approach, although the updated Cluster 1 contains a subset of the EPRI (2004) GMPEs. The definition of the other clusters is less obvious. After comparing the behavior of the various GMPEs not in Clusters 1 and 4, it was decided to define two additional clusters (which are called Clusters 2 and 3, but which are unrelated to Clusters 2 and 3 of EPRI [2004]) and to make geometric spreading within the first 100 km the defining characteristic for the unassigned GMPEs. The two reasons for the redefinition of Clusters 2 and 3 are as follows:

- Two of the new GMPEs do not fit within the EPRI (2004) definitions of Clusters 2 and 3. Most significantly, AB06′ was developed using a stochastic method but does not produce a two-corner spectrum, so it does not fit in Cluster 2 (and obviously not in Cluster 3). Also, A08′ was developed using an approach that shares some elements with the hybrid empirical approach, but also has significant differences.
- Comparisons of the predictions by the A08′, AB06′, PZT, and SDCS GMPEs indicated that the most natural clustering of these four GMPEs is one based on differences in geometric spreading. The TI Team initially defined Cluster 2 as AB06′ and SDCS and Cluster 3 as A08′ and PZT (notwithstanding the issue of lack of fit discussed above), but found that there were very large within-cluster differences, which would have led to problems when characterizing within-cluster epistemic uncertainty.

The resulting updated clusters and the assignment of GMPEs to these clusters are given in Table 7.4.1-1. This table also shows the abbreviated names for these GMPEs, which will be used throughout this chapter.

7.4.2 Consideration of Regional Differences

Questions were raised by Resource Experts during project review about the possibility of regional differences in ground motions related to differences in source characteristics. The principal example given was that the earthquakes that have occurred in central Arkansas and Oklahoma appear to have lower stress drops than other earthquakes occurring within the Midcontinent region of CENA. However, questions were also raised about differences for earthquakes in the northeastern United States/southeastern Canada. Figures 7.2.6-2 and 7.2.6-3, and Table 7.2.3-1 indicate the assignment of individual earthquakes to the three regions.

The issue of regionalization of ground motion was investigated by computing event terms for individual earthquakes using the residuals for the selected CENA GMPEs fit using the empirical site scaling Model 3 (Equation 7.3.2-3). The event terms, in essence, represent the average residual for each earthquake. Figures 7.4.2-1 through 7.4.2-9 show the event terms derived from fitting the residuals computed for each of the nine selected GMPEs. Each figure shows the event terms for the six structural frequencies analyzed: 0.5, 1, 2.5, 5, 10, and 25 Hz. The solid circles show the calculated event term for the individual earthquakes computed using linear mixed effects. The vertical lines denote approximate 90 percent confidence intervals for the event terms. The event terms for the central Arkansas and Oklahoma earthquakes are shown in blue, those for the northeastern United States/southeastern Canada earthquakes are in green, and those for the remaining CENA earthquakes are in red.

The statistical significance of differences between regions was tested by adding indicator variables for the central Arkansas and Oklahoma and Northeast earthquakes in the fit to the residuals, which allows for an average difference from the remaining CENA earthquakes. Tests were performed for three models. The first model considered only differences for the central Arkansas and Oklahoma earthquakes, and the residuals were fitted with the following modified form of Equation 7.3.2-3:

$$\ln(\text{Residual}) = C_0 + C_{SR}F_{SR} + C_{\text{OA Only}}F_{\text{OA}} + \varepsilon_{i,j} \qquad (7.4.2\text{-}1)$$

The second case considered only differences for the Northeast earthquakes, and the residuals were fitted with the following modified form of Equation 7.3.2-3:

$$\ln(\text{Residual}) = C_0 + C_{SR}F_{SR} + C_{\text{NE Only}}F_{\text{NE}} + \varepsilon_{i,j} \qquad (7.4.2\text{-}2)$$

The third case considered differences for both regions, and the residuals were fitted with the following modified form of Equation 7.3.2-3:

$$\ln(\text{Residual}) = C_0 + C_{SR}F_{SR} + C_{\text{OA Combined}}F_{\text{OA}} + C_{\text{NE Combined}}F_{\text{NE}} + \varepsilon_{i,j} \qquad (7.4.2\text{-}3)$$

In Equations 7.4.2-1, 7.4.2-2, and 7.4.2-3, the parameters F_{OA} and F_{NE} are indicator variables that take the value 1 for earthquakes in the indicated region and 0 otherwise. Table 7.2.3-1 lists the values of these indicator variables for each earthquake in the database. The results of these calculations are shown on Figures 7.4.2-10 and 7.4.2-11. Figure 7.4.2-10 shows the event terms (points) and their 90 percent confidence intervals (vertical bars) for the six frequencies for the nine selected GMPEs computed using residuals for earthquakes of $\mathbf{M} \geq 3.75$. Figure 7.4.2-11 shows the event terms computed using residuals for earthquakes of $\mathbf{M} \geq 4.75$. The top plot on each figure shows the coefficient for scaling only the central Arkansas and Oklahoma earthquakes relative to all other CENA earthquakes (Equation 7.4.2-1). The second plot from the top shows the coefficient for scaling only the Northeast earthquakes relative to all other CENA earthquakes (Equation 7.4.2-2). The bottom two plots show the coefficients for scaling the central Arkansas and Oklahoma earthquakes (third plot from top) the Northeast earthquakes (bottom plot) when both scalings are considered together (Equation 7.4.2-3). The coefficients computed using the residuals for earthquakes of $\mathbf{M} \geq 3.75$ (Figure 7.4.2-10) show differences at 25 Hz for both regions and at 10 Hz for central Oklahoma and Arkansas earthquakes. The 90 percent confidence intervals for the coefficients for these results are such that the differences are potentially statistically significant. The coefficients computed using the residuals for earthquakes

of $\mathbf{M} \geq 4.75$ (Figure 7.4.2-11) show smaller differences, and the 90 percent confidence intervals typically incorporate zero, indicating a lack of statistical significance.

The statistical significance of the differences was tested using the AIC and BIC measures. Table 7.4.2-1 lists which regionalization model produces the lowest AIC or BIC measures. Results are listed for both analyses based on the residuals for earthquakes of $\mathbf{M} \geq 4.75$ (top part of the table on each page) and the residuals for earthquakes of $\mathbf{M} \geq 3.75$ (bottom part of the table on each page). The BIC measure incorporates an adjustment for sample size and typically is less likely to produce a lower score for a model with more parameters for small sample sizes. The results indicate that the differences are significant and more clearly defined at magnitudes less than **M** 4.75 and at 25 Hz. The results are mixed, with some models suggesting that only the Northeast earthquakes have different 25 Hz motions, and other models suggesting that only the central Arkansas and Oklahoma have different 25 Hz motions, and still other models indicating both. However, as indicated by the data shown on Figures 7.2.6-4 and 7.2.6-5, there is limited data for 25 Hz and the majority of it comes from the northeastern region.

The central Arkansas and Oklahoma earthquakes occurred at shallower depths than the majority of the other CENA earthquakes. Some recent empirical GMPEs for active tectonic regions have included an effect of increasing ground motion with increasing depth (e.g., Abrahamson and Silva, 2008; Chiou and Youngs, 2008a). However, introducing a depth dependence on the event terms rather than regional differences did not lead to an improvement of the fit to the residuals from the final analysis database. Besides a depth effect, the differences in high frequency could be due to differences in general site conditions (e.g., site kappa) that are not captured by the broad rock site categorization used in this study.

The results of these comparisons do not lead to a conclusive indication that there are significant regional differences that should be incorporated into the analysis. Therefore, regional differences in the CENA ground-motion database were not included in the analysis of the selected GMPEs.

7.4.3 Approach for the Calculation of Within-Cluster Weights

7.4.3.1 Rationale and Mathematics of the Weighting Approach

This approach assigns weights to the GMPEs in a cluster based on each GMPE's consistency with the data. The approach is similar in spirit to that used in EPRI (2004), but more refined mathematically. It accounts for the following factors:

- Intra-event correlation. Records from the same earthquake are correlated because they share the same source characteristics. The presence of this positive correlation makes the data less informative than they would be if they were independent.
- Uncertainty in the soil correction and correlation from common site conditions. Records obtained at the same site are correlated in the sense that each particular site has a tendency to consistently over- or underpredict amplitudes, relative to a typical site. The presence of this positive correlation makes the data less informative than they would be if they were independent.
- Weights that depend on magnitude and distance, to account for the engineering importance and diagnostic power of data in the various magnitude-distance ranges.

- Sensitivity to sample size. Weights should be sharp if data are abundant, and should be less definitive (i.e., closer to uniform) if data are scarce.
- Incorporation of subjective weight to GMPEs within a cluster, in order to down-weight GMPEs that may be almost identical and do not represent independently developed models.
- The ability to combine in a consistent manner those weights calculated for different frequencies and those obtained using different modeling approaches or assumptions.

The calculation of weights for a particular frequency, cluster, and approach for adjusting to reference site conditions works with the ground-motion residuals for each GMPE. The residual associated with the *i*th GMPE, the *j*th earthquake, and the *k*th station is represented as ε_{ijk} and is calculated as

$$\varepsilon_{ijk} = \ln[\text{Ampl}_{ijk}]_{\text{observed}} - \ln[\mu_{ijk}] \tag{7.4.3-1}$$

where $\mu_{ijk} = \mu_i(M_j, R_{jk})$ is the amplitude predicted by the *i*th GMPE for an event with magnitude M_j and distance R_{jk}.

The approach used in this project works with the likelihood of the observed residuals given GMPE *i*, which is closely related to the inverse sum of squared residuals used with the EPRI (2004) approach, but which provides more flexibility to include effects such as the uncertainty in site correction, and has a stronger basis in theory (as discussed by Scherbaum et al., 2009). The development of this approach is provided below.

Assume first (for the sake of explanation) that the recordings are all obtained at sites with properties identical to the reference site, so that no site adjustment is necessary and there is, thus, no uncertainty in the value of the adjustment factor. In this hypothetical case, one can write

$$\varepsilon_{ijk} = \ln[\text{Ampl}_{ijk}]_{\text{observed}} - \ln[\mu_{ijk}] = \delta B_j + \delta W_{jk} \tag{7.4.3-2}$$

where δB_j represents inter-event variation (with standard deviation τ) and δW_{jk} represents intra-event station-to-station variation (with standard deviation ϕ). Because all recordings are obtained at real sites, with characteristics different from those at the reference site, the uncertainty in the site adjustment must be considered, obtaining

$$\varepsilon_{ijk} = \ln[\text{Ampl}_{ijk}]_{\text{adjusted observation}} - \ln[\mu_{ijk}] = \delta B_j + \delta W_{jk} + \delta C_{jk} \tag{7.4.3-3}$$

where δC_{jk} represents uncertainty in the value of the ln[Adjustment Factor] to reference rock for earthquake *j* and station *k* (with standard deviation $\sigma_{C,jk}$, which was computed as described in Section 7.3).[9]

[9] Note that the standard deviation of δC_{jk} for a given station is, in general, different for different earthquakes. Consider, for instance, a frequency of 25 Hz and recordings from a nearby earthquake and a very distant one. The 25 Hz spectral acceleration is more sensitive to kappa for the nearby earthquake than for the distance one, resulting in a

To calculate the standard deviation of each epsilon term, one can use the values of τ and ϕ adopted by this project, which are documented in Section 7.10, and the site-adjustment standard deviation $\sigma_{C,jk}$, which was computed for each recording in Section 7.3. Furthermore, epsilon values from the same earthquake are correlated because they share a common δB_j term. Using the information in Equation 7.4.3-3, one can calculate the equation for the covariance between any two residuals as follows:

$$Cov[\varepsilon_{ijk}, \varepsilon_{irs}] = \tau^2 \delta_{jr} + \phi^2 \delta_{jr} \delta_{ks} + \sigma_{C,jk} \sigma_{C,rs} \delta_{ks} \qquad (7.4.3\text{-}4)$$

where δ_{xy} is the Kronecker delta (equal to 1 if the two indices are equal, equal to 0 if they are different).

In words, the covariance matrix between two epsilons is the sum of three terms. The first term is equal to τ^2 if both residuals are associated with the same earthquake, and zero otherwise; the second term is equal to ϕ^2 between a residual and itself (same earthquake, same station), and zero otherwise; and the third term is equal to $\sigma_{C,jk}\sigma_{C,rs}$ if both residuals are associated with recordings at the same station, and zero otherwise.

For brevity in notation, all the residuals associated with one GMPE are arranged into a column vector $\boldsymbol{\varepsilon}_i$, and all the associated covariances are arranged into a square covariance matrix $\boldsymbol{\Sigma}_{\varepsilon}$.

Using the epsilon vector for the *i*th GMPE, and using the standard assumption of joint normality of the residuals, the likelihood function of the observations given the GMPE takes the form

$$L(\boldsymbol{\varepsilon}_i) = \exp\left(-\frac{1}{2}\boldsymbol{\varepsilon}_i^{\,T}\boldsymbol{\Sigma}_{\varepsilon}^{\,-1}\boldsymbol{\varepsilon}_i\right) \qquad (7.4.3\text{-}5)$$

where constant terms have been omitted if they do not depend on the data or on the specific GMPE. Using the likelihood functions for all GMPEs in the cluster, one can compute the weight for each GMPE as

$$w_i = \frac{L(\boldsymbol{\varepsilon}_i)}{\sum_i L(\boldsymbol{\varepsilon}_i)} \qquad (7.4.3\text{-}6)$$

This exponential form in the likelihood has a behavior similar to that of the EPRI (2004) approach, in that larger, squared residuals lead to lower weights. The two approaches differ in behavior in the following ways:

- The likelihood-based approach uses a negative-exponential functional form rather than reciprocals of sums of squares.

higher standard deviation for the nearby earthquake. A related issue is whether the δC_{jk}'s for two recordings at the same station should be treated as fully correlated. This project assumes full correlation.

- The covariance matrix contains scale information (i.e., residuals smaller than the corresponding standard deviation incur a low penalty, regardless of the size of other residuals).
- Within-event correlation is handled in a manner that is more efficient statistically (similar to the random-effect formulation of Abrahamson and Youngs (1992).
- The record-specific values of σ_C are easily incorporated.

In Cluster 1, the weights obtained for the two Silva et al. (2003) GMPEs are halved and then all the weights are renormalized. Effectively, the two Silva et al. (2003) GMPEs are counted as one because they have many elements in common.

In practice, some magnitude-distance combinations are more important than others depending on engineering significance and diagnostic power. To adjust the importance of the data as a function of magnitude and distance, the data for each frequency are first partitioned into six magnitude-distance bins, and the weights (Equations 7.4.3-5 and 7.4.3-6) are calculated separately for each bin. Finally, the results are combined according to bin importance and sample size, as described below.

The first step in adjusting for each bin's importance is to assign an importance factor t to each bin. Different importance factors are assigned for high and low frequencies below, with the factors for low frequencies given in parentheses:

Distance Range	**M** 3.75 to 4.75[10]	**M** 4.75 and greater
Rjb 0 to 70 km	1/4 (1/4)	**1 (1)**
Rjb 70 to 150 km	1/12 (1/4)	1/3 (1)
Rjb 150 to 500 km	1/24 (1/12)	1/6 (1)

The second step is to make an adjustment for sample size in each bin because the low-magnitude and large-distance bins may contain many more data than the more important bins, which may have the undesirable effect of controlling the calculation of weights (despite having a lower importance factor). This adjustment is made by multiplying each bin's importance factor t_{MR} by the quantity $\max(n'_{>4.75,0-70} / n'_{MR}, 1)$, resulting in $t'_{MR} = t_{MR} \times \max(n'_{>4.75,0-70} / n'_{MR}, 1)$, where n'_{MR} is the equivalent sample size in an arbitrary magnitude-distance bin and $n'_{>4.75,0-70}$ is the equivalent sample size in the most important bin (i.e., **M** > 4.75, R < 70 km). The equivalent sample size is the number of residuals in the bin, reduced by the effect of correlation, and is given by the equation

$$n'_{MR} = \frac{1}{n_{MR}} \mathrm{Tr}(\Sigma_{MR}) \mathbf{1}^T \Sigma_{MR}^{-1} \mathbf{1} \qquad (7.4.3\text{-}7)$$

[10] As a sensitivity test, the TI Team considered the effect of giving zero weight to the **M** 3.75–4.75 data. The effect of this change was found to be small.

where Σ_{MR} is the covariance matrix of the residuals contained in an arbitrary magnitude-distance (MR) bin, Tr( ) denotes the trace of this matrix, n_{MR} is the number of residuals in the bin, and **1** is a unit column vector of size n_{MR}.

Thus, if a bin contains data with an effective sample size greater than the effective sample size of the **M** > 4.75, R < 70 km bin, its initial importance factor t_{MR} is reduced to a smaller factor t'_{MR}, so that more abundant data from lower-magnitude or longer-distance bins do not overwhelm the data from the latter bin—which is of greater engineering interest.

To combine the weights for all bins, the weights for each bin are raised to the power t'_{MR}, multiplied over all the bins, and then normalized so the weights for all GMPEs sum to unity. As a result, the combined weight for the *i*th GMPE is given by

$$w_i = \alpha \prod_{MR} w_{i,MR}^{\ t'_{MR}} \tag{7.4.3-8}$$

where α is a normalizing constant so that the weights for all GMPEs in the cluster sum to unity.

In the above calculation, raising weights to a power smaller than unity is equivalent to reducing the sample size in the bin, effectively making the residuals in the bin less influential for the purposes of calculating weights. The multiplication of weights from different bins is also consistent with the way likelihoods from independent data are combined.[11]

Weights are first calculated separately for the different frequencies. Then the weights for high frequencies (5, 10, and 25 Hz) are combined into one weight and the weights for low frequencies (0.5, 1, and 2.5 Hz) are combined into another using the approach described below. The steps for combining the high-frequency weights are as follows:

- Multiply the 25 Hz, 10 Hz, and 5 Hz weights for each GMPE.
- Raise each weight to a power of 0.446.
- Normalize the weights.

The steps for combining the low-frequency weights are identical. The power of 0.446 accounts for the correlation between spectral accelerations at these three frequencies, and is calculated using the correlation coefficients of Baker and Jayaram (2008)[12] and similar arguments of equivalent sample size.

All the manipulations of weights described so far use multiplication, together with exponentiation, to adjust for importance or correlation. As indicated earlier, this is consistent with the way likelihoods from different data sets are combined. The next step is done arithmetically because it involves alternative interpretations or adjustments of the same data set.

[11] By simply multiplying bin weights, one is effectively ignoring that there is some correlation between the residuals in separate bins. Consideration of this correlation would be difficult and its effect is likely small.

[12] The correlation coefficients by Baker and Jayaram (2008) are modified to account for WUS-CEUS differences in frequency content by assuming that the contours in their Figure 4b remain parallel to each other between 10 Hz and 25 Hz.

The next combination step consists of averaging (using equal weights) the GMPE weights obtained with the analytical and empirical adjustments for site conditions. The TI Team gives equal weights to the two approaches. The analytical approach makes use of more information about selected recording sites in the context of a mechanical model of site response; however, this information is available for only a fraction of the recording sites. In contrast, the empirical approach can make use of many more recordings, though with less precise site adjustments. Using both approaches produces final results that are more robust.

The highest and lowest within-cluster weights resulting from these calculations sometimes differ by more than one order of magnitude. Given the limitation of the data—in terms of the number of records, their magnitudes and distances, etc.—the TI Team judged that these large differences did not appropriately reflect the relative ability of the GMPEs to predict future ground motions. The TI Team adopted the condition that no GMPE should receive a within-cluster weight greater than 2/3 (the two Silva et al. [2003] GMPEs in Cluster 1 are counted as one GMPE for the purpose of this condition). This condition was enforced by raising all the weights to a power (less than unity) chosen such that the maximum weight (after normalizing) is equal to 2/3.

Raising all the weights to a power is equivalent to reducing the effective sample size of the data, which is consistent with the likelihood-based approach adopted in this study for the calculation of weights. It also has the advantage that it preserves the hierarchy of the weights.

Implementation and results of the approach described above for calculating within-cluster weights is described in Section 7.5.

7.4.4 Development of Within-Cluster Epistemic Uncertainty

The EPRI (2004) study developed a representation of the within-cluster epistemic uncertainty by combining three sources of uncertainty. The first factor was model-to-model variability of the weighted models within a cluster. The model-to-model standard error, $\sigma_{\text{model-to-model}}$, is computed using Equation 7.4.4-1:

$$\sigma(m,r,f)_{\text{model-to-model}} = \left\{ \sum_i w_i \times \left(\ln[z_i(m,r,f)/\hat{z}(m,r,f)] \right)^2 \Big/ \sum_i w_i \right\}^{1/2} \qquad (7.4.4\text{-}1)$$

where $z_i(m,r,f)$ is the median ground-motion prediction for the ith GMPE, and $\hat{z}(m,r,f)$ is the weighted mean log ground-motion prediction for the models in the cluster obtained by

$$\hat{z}(m,r,f) = \sum_i w_i \times \ln[z_i(m,r,f)] \Big/ \sum_i w_i \qquad (7.4.4\text{-}2)$$

The calculation of $\sigma_{\text{model-to-model}}$ was conducted for distances up to 1000 km in order to develop uncertainty models for the full distance range of interest.

The second source was an assessment of the parametric uncertainty in the parameters used in the development of the individual models. This uncertainty was separated into a source part and a path part, and separate parametric uncertainty analyses were used to assess σ_{source} and σ_{path}. An example of the parametric source uncertainty is uncertainty in the median stress drop (stress parameter) used in the stochastic single-corner point-source models, and an example of the parametric path uncertainty is uncertainty in the Q model used in assessing distance attenuation.

The third source of uncertainty was the standard error from fitting the cluster median ground motions with an algebraic function form. The composite epistemic uncertainty for the cluster median model was then obtained in EPRI (2004) by summing the variances, assuming all the sources of uncertainty are independent.

$$\sigma(m,r,f)_{\text{clustermedian-2004}} = \left\{ \begin{matrix} \sigma^2(m,r,f)_{\text{model-to-model}} + \sigma^2(m,r,f)_{\text{source}} + \\ \sigma^2(m,r,f)_{\text{path}} + \sigma^2(m,r,f)_{\text{median fit}} \end{matrix} \right\}^{1/2} \qquad (7.4.4\text{-}3)$$

For this study, the above approach was modified somewhat as explained below.

The first minor change was that the concept of independent source and path parametric uncertainties was not used. One issue with this approach is that assessments of source and path terms are often dependent upon each other, requiring that a joint distribution for the variability be defined that properly accounts for correlations. Also, some of the selected GMPEs do not lend themselves readily to assessment of parametric uncertainties. For example, the Atkinson (2008) referenced empirical model uses fits of residuals for CENA ground-motion data from the Boore and Atkinson (2008) active tectonic region GMPE to produce a CENA GMPE. Representing the epistemic uncertainty in this model should be based on the uncertainty in the Boore and Atkinson (2008) GMPE and the statistical uncertainty in the fitting of the residuals. Defining parametric uncertainty for finite fault simulation models is also difficult. EPRI (2004) applied the single-corner stochastic model source uncertainty to more complicated models as a surrogate estimate, but that becomes more problematic as the complexity of the underlying ground-motion prediction approach expands.

Secondly, the greatly expanded CENA ground-motion database available for use provides the ability to make an assessment of how well median ground-motion estimates are constrained by data. This uncertainty was assessed by calculating the standard error in the distance-dependent mean model residual, using the adjusted residuals for $\mathbf{M} > 3.75$, and taking correlation into account by means of the covariance matrix introduced in Section 7.4.3. The mean residual is taken as constant for distances less than 10 km, piece-wise linear (in log-distance–log-amplitude space) with hinges at 10, 70, and 150 km, and linear (in distance–log-amplitude space) between 150 and 500 km (see Figure 7.4.4-1). This form conforms to the general shape of the distance attenuation functions used by the various GMPEs.

The linear trend with log distance using hinge points at 10, 70, and 150 km conforms to the distance range where geometric spreading controls the amplitude of ground motions. At distances beyond 150 km, anelastic attenuation becomes a controlling factor, and ground-motion amplitude decays proportional to distance. A maximum-likelihood problem is formulated where the mean residual has the functional form described above and the covariance between residuals is given by Equation 7.4.3-4. Solving the maximum-likelihood problem and calculating the partial derivatives of the log-likelihood function, one obtains the standard error of the coefficients p_1 through p_4. The calculation is performed for both the analytically adjusted and empirically adjusted residuals, and the resulting variances are averaged, yielding $\sigma_{\text{data constraint}}$ at the hinge points These hinge-point values of $\sigma_{\text{data constraint}}$ are then interpolated piece-wise to calculate the values of $\sigma_{\text{data constraint}}$ at other distances. The assessment of the coefficients p_1 through p_4 is based on the analysis of the residuals for data in the distance range of 0–500 km, the distance range used to develop the GMPE weights. This trend is extrapolated to a distance of 1,000 km in order to develop the GMM for the distance range needed for application.

The values of $\sigma_{\text{data constraint}}$ are based on data primarily from earthquakes of about **M** 5 and smaller, while the primary application will be to assess ground motions for earthquakes of **M** 5 and larger. The ground-motion amplitudes for earthquakes of magnitudes larger than the observed data are constrained by the magnitude scaling forms of the various GMPEs. To address the epistemic uncertainty at larger magnitudes, additional epistemic uncertainty associated with magnitude scaling is introduced by considering how the various selected GMPEs scale with magnitude. The process involves computing the standard deviation of the ratio of the predicted ground motions at large magnitudes divided by the prediction at **M** 5. This standard deviation, termed $\sigma_{\text{magnitude scaling}}$, is by definition 0 at **M** 5 and typically increases with magnitude. The values of $\sigma_{\text{magnitude scaling}}$, are computed without consideration of the relative weights assigned to the GMPEs in each cluster. The values of $\sigma_{\text{data constraint}}$ and $\sigma_{\text{magnitude scaling}}$ are then combined (variances are summed) to define a combined data and modeling epistemic-uncertainty standard deviation. The result is increasing epistemic uncertainty in the median ground motions with increasing magnitude, reflecting the lack of empirical data from large-magnitude CENA earthquakes. Details on this process are provided in Section 7.7.

The fourth minor change was to ignore the contribution of the standard error in fitting the cluster medians. As will be shown below in Section 7.6.2, the cluster median ground motions are well fitted by the chosen algebraic forms such that the standard error of the fit has a negligible contribution to the overall uncertainty.

The model-to-model variability was retained as it remains an important source of epistemic uncertainty. The overall cluster median epistemic uncertainty was taken to be the envelope of the model-to-model standard deviation, $\sigma_{\text{model-to-model}}$, and the data- and model-based estimate of the standard deviation of the median, $\sigma_{\text{data constraint}}$ and $\sigma_{\text{magnitude scaling}}$:

$$\sigma(m,r,f)_{\text{clustermedian-ln(PSA)}} = \max\left\{\sigma^2(m,r,f)_{\text{model-to-model}}, \sigma^2(m,r,f)_{\text{data constraint}} + \sigma^2(m,r,f)_{\text{magnitude scaling}}\right\}^{1/2} \quad (7.4.4\text{-}4)$$

The reason for taking the envelope (instead of the sum) of the two variances is that they represent different manifestations of the same epistemic uncertainty.

7.4.5 Development of Cluster Weights

Following EPRI (2004), the approach for the calculation of cluster weights takes into account consistency with the data, as well as other more subjective factors. The portion of the weights that measure consistency with the data is calculated using the residuals between the adjusted recordings and the median GMPEs from the various clusters, following the same approach described in Section 7.4.3 for within-cluster weights.

For the subjective assessments, EPRI (2004) developed a somewhat mechanistic approach that scored the ground-motion clusters on the basis of the adherence to seismological principles and consideration of uncertainty. The ultimate result was nearly equal weights being assigned to the four clusters. Reflection on the discussions in EPRI (2004) by the TI Team led to the assessment that the purpose of the subjective portion of the weights should be to evaluate each cluster's robustness and ability to extrapolate properly from the available recordings to the magnitude-distance combinations of engineering interest. Therefore, this attribute was directly assessed by

the TI Team for this project. The weights resulting from this assessment are denoted as *confidence weights*.

The starting point for the assessment was that all four clusters have roughly equal weight. All clusters contain models and modeling approaches that have been employed for a number of years to assess earthquake ground motions and are judged to be credible models by the TI Team and by the technical community at large, as confirmed by the feedback from Resource Experts. Cluster 4 contains the most explicit modeling of the physical process, but contains only one implementation. Cluster 1 contains the simplest models, but these models have been shown to adequately model ground motions for engineering application and this cluster contains multiple alternative GMPEs. These relative attributes counter balance each other such that there is no compelling reason to favor one cluster over the other. The GMPEs in Clusters 2 and 3 have some advantage over those in Clusters 1 and 4 in that they include more recent GMPEs, which have had the benefit of more CEUS data and more technical insights drawn from recent work and from analyses of larger-magnitude data in active crustal regions. Because of this attribute, Clusters 2 and 3 are slightly favored over Clusters 1 and 4 in terms of the confidence in their robustness and ability to extrapolate properly to larger magnitudes. Accordingly, the assigned confidence weights are 0.2 to Clusters 1 and 4, and 0.3 to Clusters 2 and 3. Section 7.9 provides details on the development of the cluster weights.

7.5 Calculation of Within-Cluster Weights

7.5.1 Calculation of Within-Cluster Weights Based on Analytical Site Adjustments

The calculation of within-cluster weights based on analytical site adjustments follows the approach described in Section 7.4.3. The first step was to apply the approach described in Section 7.3.1 to all recordings in the analytical database ($R_{JB} \leq 500$ km) obtained at stations for which profile data were available, to obtain the adjusted spectral amplitudes. Stations with $V_{S30} <$ 500 m/s were excluded, as there is higher uncertainty regarding the adjustment for these sites. The next step is to compute the residuals using each of the selected GMPEs. Figures 7.5.1-1a through 7.5.1-9b show the resulting residuals for the nine selected models. The residuals are plotted against Joyner-Boore distance, but the specified distance metric used by each model (i.e., either rupture distance or Joyner-Boore distance) was used to compute the residuals. For the SEL GMPE, earthquakes were categorized as occurring inside or outside rifted zones, and the appropriate rift or non-rift version of the model was used to compute the residuals. The assignment of the individual earthquakes in the project database to rifted or non-rifted crust is indicated in Table 7.2.3-1. Part (a) of each figure shows the residuals for the magnitude range $3.75 \leq \mathbf{M} < 4.75$, and part (b) shows the residuals for $\mathbf{M} \geq 4.75$. The data are plotted using the rock categories defined for the empirical approach (see Section 7.3.2), even though the analytical approach does not use those categories.

Note that most GMPEs show a tendency to overpredict the motions (indicated by negative residuals) for $3.75 \leq \mathbf{M} < 4.75$ and for low frequencies at distances less than 100 km.

Using the formulation developed in Section 7.4.3, the likelihood value for each GMPE was computed for the six magnitude-distance bins. The covariance matrix is constructed in the manner described in Section 7.4.3 using the assigned values of τ and ϕ for CENA earthquake

ground-motion data developed in Section 7.10, and the uncertainty in the site-adjustment factor that was calculated for each recording and each frequency using the approach described in Section 7.3.1.

Likelihood values were computed for the nine selected GMPEs for the six structural frequencies and the six magnitude-distance bins. The relative likelihoods were then normalized to produce relative weights for the GMPEs within the clusters defined in Section 7.4.1 and using the approach introduced in Section 7.4.3. Intermediate and final results from the calculation of within-cluster weights are given in Section 7.5.3.

7.5.2 Calculation of Within-Cluster Weights Based on Empirical Site Adjustments

The calculation of within-cluster weights based on empirical site adjustments followed the general procedure described in Section 7.5 using analytical site corrections. The first step was to compute the residuals for the rock site database described in Section 7.2 using each of the selected GMPEs. Figures 7.5.2-1a through 7.5.2-9b show the resulting residuals for nine selected models. The residuals are plotted against Joyner-Boore distance, but the specified distance metric used by each model (i.e., either rupture distance or Joyner-Boore distance) was used to compute the residuals. For the Somerville et al. (2001) models, earthquakes were again categorized as occurring inside or outside rifted zones, and the appropriate rift or non-rift version of the model was used to compute the residuals. Part (a) of each figure shows the residuals for the magnitude range $3.75 \leq \mathbf{M} < 4.75$, and part (b) shows the residuals for $\mathbf{M} \geq 4.75$.

The residuals for the magnitude range $3.75 \leq \mathbf{M} < 4.75$ typically show more of a trend with distance and greater offset from 0 than those for $\mathbf{M} \geq 4.75$. This is not surprising given that many of the GMPEs were not developed to predict ground motions for earthquakes less than about **M** 5, and the Somerville et al. (2001) GMPE (SEL) was based on simulations for earthquakes of **M** 6 and greater.

As discussed in Section 7.3.1, the empirical site correction that was found to generally produce an improved fit to residuals was Model 3 (Equation 7.2.2-3), in which a scale factor is found for only the soft rock site category and the intermediate and hard rock sites are considered one group. Figures 7.5.2-10a, 7.5.2-10b, and 7.5.2-10c show the resulting values of C_{SR} obtained for each of the selected GMPEs. Values are shown for four different magnitude-distance ranges of the data. The results show consistent estimates of the soft rock category scaling factor C_{SR} among the selected GMPEs.

Using the formulation developed in Section 7.4.3, the likelihood value for each GMPE was computed for the six magnitude-distance bins. The empirically adjusted residual for the *j*th recording of the *i*th earthquake was computed using the following expression:

$$\varepsilon_{ij}^{\text{empirically adjusted}} = \varepsilon_{ij} - C_{SR} F_{jk}^{SR} \qquad (7.5.2\text{-}1)$$

The parameter F_{jk}^{SR} takes on the value 1 if the *k*th site is in the soft rock category, and 0 otherwise. The values of C_{SR} for data in the range of $\mathbf{M} \geq 4.75$ and $R \leq 500$ km were used for the empirical site adjustments, as this is the magnitude range given the greatest weight. As indicated on Figure 7.5.2-10 the values for other magnitude-distance ranges are similar. Table 7.5.2-1 lists the values of C_{SR} obtained for each GMPE that were used for the empirical site adjustments.

The covariance matrix (Equation 7.4.3-4) is constructed in a manner similar to that described in Section 7.5.1, using the assigned values of τ and ϕ for CENA earthquake ground-motion data developed in Section 7.10. The variance estimate for the site adjustment factor for the kth site was set equal to the square of the standard error of estimation for C_{SR} if the site is in the soft rock category, and 0 otherwise.

Likelihood values were computed for the nine selected GMPEs for the six structural frequencies and the six magnitude-distance bins. The relative likelihoods within the clusters were then normalized to produce relative weights for the GMPEs within the clusters using the approach introduced in Section 7.4.3. Intermediate and final results from the calculation of within-cluster weights are given in Section 7.5.3.

7.5.3 Results for Within-Cluster Weights

As indicated in Section 7.4.3, the calculation of weights for the GMPEs in each cluster involves the following steps:

1. Calculation of GMPE weights for each magnitude-distance bin. This is done separately for each magnitude-distance bin, each frequency, and each adjustment approach.
2. Multiplicative combination of weights for the various magnitude-distance bins, taking into account their importance factors and effective sample sizes, obtaining GMPE weights for each frequency. This is done separately for each frequency and each adjustment approach.
3. Multiplicative combination of weights for the various high and low frequencies, taking their correlation into account, obtaining GMPE weights for high frequency and low frequency. This is done separately for high and low frequencies and each adjustment approach.
4. Arithmetic averaging of weights for the two adjustment approaches, obtaining GMPE weights for high frequency and low frequency. This is done separately for high and low frequencies.
5. Modification ("moderation") of the within-cluster weights to avoid very lopsided weights due to the limited available data.

Tables 7.5.3-1 through 7.5.3-12 show the calculation of the weights by bin for each frequency and the combination of bin weights (i.e., the first two steps) for Cluster 1 and for both the analytical and empirical site-adjustment approaches. The weights shown for each magnitude-distance bin are the weights after they have been raised to the exponent shown. Note that this exponent accounts for the importance of the bin and for its sample size (so that a less-important bin with a large equivalent sample size will not dominate results). Table 7.5.3-13 shows the combination of weights for the various frequencies, and the combination of weights from the two site-adjustment approaches (steps 3 and 4), also for Cluster 1. Tables 7.5.3-14 through 7.5.3-39 show similar calculations for Clusters 2 and 3.

Finally, Table 7.5.3-40 shows the "raw" within-cluster weights obtained in the steps above, as well as the "moderated" weights obtained by introducing the condition that no weight can exceed 2/3. This is done by raising the weights to an appropriate power and then normalizing.

Because Cluster 4 contains only the Somerville et al. (2001) GMPE, though in two different variants, this GMPE gets unit weight within Cluster 4.

7.6 Cluster Median GM Models for the Midcontinent

Following the approach of EPRI (2004), the weights assigned to the individual GMPEs within each cluster were used to calculate weighed mean values of ln(PSA) for a range of magnitudes and distances. These median values were then fitted with an algebraic form to produce the median GMPE for each cluster.

7.6.1 Conversion from Rupture to Joyner-Boore Distance

The first step in the process was to convert all selected GMPEs to a common distance measure. The AB08′ and PZT models use R_{Rup} as the distance metric, while the rest use R_{JB}. To simplify application, all the cluster median GMPEs were developed in terms of R_{JB} distance. In order to produce estimates for a given value of R_{JB} using the AB08′ and PZT models, ruptures were simulated for a distribution of fault depths, and the weighted average of the ln(PSA) values based on the resulting R_{Rup} values was used as the GMPE estimate for the given value of R_{JB}. This process was used in the EPRI (2004) study to produce the R_{JB} distance version of the hard rock FEL GMPE used to develop the EPRI (2004) GMM, and also used in this study. The simulations used an equally weighted mixture of vertical and 40 degree dipping reverse fault ruptures. The 40-degree dip represents the approximate average dip for reverse faulting earthquakes in the summary published by Sibson and Xie (1998). The rupture area as a function of magnitude was defined using Equation 7.2.4-1, based on the area–seismic moment relationship for CENA earthquakes developed by Somerville et al. (2001). The rupture depth was specified by simulating a hypocenter focal depth from a focal depth distribution and then placing the hypocenter at a point 2/3 from the top of the rupture. The resulting magnitude-dependent rupture depth distributions were trimmed to remove ruptures that extended outside the depth range 0–30 km, and then renormalized.

The focal depth distribution was developed using the well-located earthquake data set from the NUREG-2115 earthquake catalog. Figure 7.6.1-1 shows the distributions of focal depth for four magnitude intervals:

- $3 \leq \mathbf{M} < 4$
- $4 \leq \mathbf{M} < 5$
- $\mathbf{M} \geq 5$
- $\mathbf{M} \geq 4$

The distributions have similar shapes. The distribution for $\mathbf{M} \geq 4$ was used in the simulations as it is closer to the magnitude range of interest and has sufficient data to define the distribution shape.

7.6.2 Calculation of Cluster Median GMMs

The cluster median values of PGA and PSA were computed for **M** 5, 5.5, 6, 6.5, 7, 7.5, and 8 earthquakes at distances from 1 km to 1,000 km evenly spaced at 100 points per decade of log R_{JB}, with added points at specific distance hinge points in the GMPEs (e.g., 70 km and 130 km). Figures 7.6.2-1, 7.6.2-2, and 7.6.2-3 show the results of developing the median ground motions for Clusters 1, 2, and 3, respectively. Each figure has parts (a) through (g) for the six structural frequencies (0.5, 1, 2.5, 5, 10, and 25 Hz) and PGA. The high-frequency within-cluster weights

were used for PGA. Shown on each plot are the motions predicted by the component GMPEs and the resulting weighted median motion. Plots are provided for **M** 5, 6, 7, and 8.

The mean values of ln(PSA) and ln(PGA) for Clusters 1, 2, and 3 were then fit with algebraic forms. The GMPE for Cluster 4 was left unchanged from EPRI (2004), because only a single model, the SEL model, is in the cluster. Two forms were used for the other clusters. The values of ln(PSA) and ln(PGA) for Clusters 1 and 3 were fit with the following form:

$$\begin{aligned}\ln(PSA) = {} & C_1 + C_2\mathbf{M} + C_3\mathbf{M}^2 + (C_4 + C_5\mathbf{M}) \times R_1 + \\ & (C_6 + C_7\mathbf{M}) \times R_2 \; + \; (C_8 + C_9\mathbf{M}) \times R_3 \; + (C_{10} + C_{11}\mathbf{M}) \times R' \\ & R' = \sqrt{R_{JB}^2 + \{\exp(C_{12} + C_{13}\mathbf{M})\}^2} \\ & R_1 = \min[\ln(R'), \ln(C_{14})] \\ & R_2 = \max\{\min[\ln(R'/C_{14}), \ln(C_{15}/C_{14})], 0\} \\ & R_2 = \max\{\ln(R'/C_{15}), 0\}\end{aligned} \tag{7.6.2-1}$$

This form has the flexibility to represent the tri-linear distance attenuation shapes with distance breakpoints at C_{14} and C_{15}.

The values of ln(PSA) and ln(PGA) for Cluster 2 were fit with the following form:

$$\begin{aligned}\ln(PSA) = {} & C_1 + C_2\mathbf{M} + C_3\mathbf{M}^2 + C_4\mathbf{M}^3 + \\ & [C_5 + C_6 \times \min(\mathbf{M}, C_{14}) \; + C_7 \times \max(\mathbf{M} - C_{14}, 0)] \times \ln(R') + \\ & [C_8 + C_9 \times \min(\mathbf{M}, C_{14}) \; + C_{10} \times \max(\mathbf{M} - C_{14}, 0)] \times R' \\ & R' = R_{JB} + \exp\{C_{11} + C_{12}\mathbf{M} + C_{13}\mathbf{M}^2\}\end{aligned} \tag{7.6.2-2}$$

This form was needed to capture a break in magnitude scaling that occurs at magnitude C_{14}.

Figures 7.6.2-4, 7.6.2-5, and 7.6.2-6 show the fits of the above forms to the values of ln(PSA) and ln(PGA) for Clusters 1, 2, and 3, respectively. As can be seen, the functional forms provide a close match to the median ground-motion values. The resulting coefficients are provided in Appendix G.

7.7 Overall Epistemic Uncertainty for Each Cluster and Calculation of High and Low GMMs for the Midcontinent

EPRI (2004) represented the epistemic uncertainty in the median ground motions for the individual clusters by three alternative models that define a discrete distribution for median ground motions. Utilizing the discrete distribution suggested by Keefer and Bodily (1983), models were defined for the median (50th percentile) with weight 0.63, and for the 5th and 95th percentiles, each with weight 0.185. The 5th and 95th percentiles were set at ±1.645 standard deviations from the median (mean log) model, consistent with the normal distribution. The

approach used by EPRI (2004) GMM is followed in developing the epistemic uncertainty distribution for median ground motions in the Updated GMM.

7.7.1 Development of Within-Cluster Epistemic Uncertainty

As discussed in Section 7.4.4, the epistemic uncertainty in the median ground motions for a cluster is represented by a standard deviation of the natural log of ground-motion amplitude, $\sigma(m,r,f)_{\text{clustermedian-ln(PSA)}}$. The value of $\sigma(m,r,f)_{\text{clustermedian-ln(PSA)}}$ is taken as the maximum of the model-to-model variability among the ground-motion amplitudes given by the GMPEs that make up the cluster, $\sigma(m,r,f)_{\text{model-model}}$, and a cluster-independent uncertainty that is composed of a data constraint and a magnitude scaling uncertainty. The development of these uncertainty estimates is described below.

7.7.1.1 Model-to-Model Variability

The model-to-model variability, $\sigma_{\text{model-to-model}}$, is computed using Equations 7.4.4-1 and 7.4.4-2. Figures 7.7.1-1, 7.7.1-2, and 7.7.1-3 show the resulting values for Clusters 1, 2, and 3, respectively. Each figure shows the values of $\sigma_{\text{model-to-model}}$ for **M** 5, 6, 7, and 8 earthquakes for the six structural frequencies and PGA. The "raw" values shown by the dashed line indicate the values computed at each specific distance. As indicated, these values have abrupt changes reflecting details of the relative behavior of the GMPEs as a function of distance. This is particularly the case for Clusters 2 and 3, which contain two models each. When the predicted ground-motion attenuation curves for the models cross, the computed value of $\sigma_{\text{model-to-model}}$ goes to zero. Following the approach used in EPRI (2004), these values were smoothed over distance using a Gaussian smoothing operator on $\ln(R_{JB})$:

$$\sigma(m,r_j,f)_{\text{model-model}} = \sum_i w_i \times \sigma(m,r_i,f)_{\text{model-model}} \Big/ \sum_i w_i$$

$$w_i = \exp\left\{-\frac{\ln(r_i/r_j)^2}{2h^2}\right\} \qquad (7.7.1\text{-}1)$$

A smoothing parameter of h equal to 1 was used for Clusters 1 and 3. For Cluster 2, h was increased to 1.5 to account for the greater variability in $\sigma_{\text{model-to-model}}$. The resulting smoothed values of $\sigma_{\text{model-to-model}}$ are shown by the solid curves color coded by magnitude on Figures 7.7.1-1, 7.7.1-2, and 7.7.1-3. Cluster 4 contains only one GMPE. As a result, $\sigma_{\text{model-to-model}}$ is zero.

7.7.1.2 Cluster-Independent Within-Cluster Epistemic Uncertainty

As discussed in Section 7.4.4, the cluster-independent estimate of epistemic uncertainty contains two components. The first component is denoted as the data constraint uncertainty, $\sigma(m,r,f)_{\text{data constraint}}$. The value of $\sigma(m,r,f)_{\text{data constraint}}$ indicates the degree to which the amount of available ground-motion data can constrain the estimates of median ground motions. This uncertainty was assessed by calculating the standard error in the distance-dependent mean model residual, using the adjusted residuals for **M** > 3.75 and taking correlation into account by means of the covariance matrix introduced in Section 7.4.3. The mean residual is taken as constant for distances less than 10 km, piece-wise linear (in log-distance–log-amplitude space) with hinges at

10, 70, and 150 km, and linear (in distance–log-amplitude space) between 150 km and 500 km as shown on Figure 7.4.4-1. The maximum-likelihood formulation for the mean residual. given the covariance between residuals defined by Equation 7.4.3-4. is then solved. The solution provides an estimate of the standard error of the coefficients p_1 through p_4. The calculation was performed for both the analytically adjusted and empirically adjusted residuals, and the resulting variances of the coefficients were averaged. The resulting values for the parameters of $\sigma_{\text{data constraint.}}$ are given in Table 7.7.1-1.

Although the available ground-motion database assembled by the PEER NGA-East Project is much larger than was available for the EPRI (2004) study, the data are primarily from earthquakes of magnitude about **M** 5 and smaller. Therefore, $\sigma(m,r,f)_{\text{data constraint}}$ is considered to apply to this magnitude range. The approach taken to estimate the uncertainty in ground-motion estimation at larger magnitudes was to evaluate the variability in ground-motion-magnitude scaling across the suite of selected GMPEs considered appropriate for estimating CENA ground motions. A magnitude scaling factor, *MSF*, was defined as follows:

$$MSF(\mathbf{M}) = PSA(\mathbf{M}) / PSA(\mathbf{M} = 5) \tag{7.7.1-2}$$

Figures 7.7.1-4a through 7.7.1-4g show the range in *MSF*(**M**) for the nine selected GMPEs that were used to develop the median GMMs presented in Section 7.6. Each plot shows values of *MSF*(**M**) for one of the seven ground-motion measures at six values of R_{JB} ranging from 1 to 500 km.

The values of *MSF*(**M**) shown on Figures 7.7.1-4a through 7.7.1-4g for the Somerville et al. (2001) GMPE (denoted SEL) were computed by extrapolating the model down to **M** 5. This extrapolation is considered appropriate because the magnitude scaling of ln(PSA) for the SEL model is nearly linear over the full magnitude range, as shown on the figures. An alternative approach would be to develop magnitude scaling factors relative to **M** 6 for the SEL model and then use the scale factor between **M** 6.5 and **M** 6 to establish the scaling from **M** 5 to **M** 6. This alternative approach would produce values of ln[*MSF*(**M** = 8)] that are within 5 percent of the values shown for the SEL model on Figures 7.7.1-4a through 7.7.1-4g. Therefore, this more involved process was not used.

The variability in magnitude scaling was quantified by computing the standard deviation in the natural log of *MSF*(**M**) using the following relationship:

$$\sigma_{\ln(MSF)} = \left\{ \sum_i w_i \times \left[\ln(MSF_i(m,r,f) - \overline{\ln(MSF(m,r,f)}) \right]^2 \Big/ \sum_i w_i \right\}^{1/2}$$

$$\overline{\ln(MSF(m,r,f)} = \sum_i w_i \times \ln(MSF_i(m,r,f) \Big/ \sum_i w_i \tag{7.7.1-3}$$

In Equation 7.7.1-3, $MSF_i(m,r,f)$ is the magnitude scaling factor for the *i*th GMPE. The weights applied in Equation 7.7.1-3 are the confidence weights assigned to the four clusters in Section 7.9.3. Consistent with the development of the within-cluster weights, the two Silva et al. (2003) models in Cluster 1 receive 1/2 weight each. Also, the alternative rift and non-rift Somerville et al. (2001) models in Cluster 4 receive 1/2 weight each.

Figure 7.7.1-5 shows the resulting values of $\sigma_{\ln(MSF)}$ computed from the magnitude scaling factors shown on Figures 7.7.1-4a through 7.7.1-4g. Each plot shows the values of $\sigma_{\ln(MSF)}$ computed for the seven ground-motion measures at one value of R_{JB}. The results show that the variability in magnitude scaling is similar across the seven ground-motion measures. To first order, the values of $\sigma_{\ln(MSF)}$ can be approximated by a linear relationship with magnitude of the form

$$\sigma_{\ln(MSF)}(\mathbf{M}) = \sigma_{\ln(MSF)}(\mathbf{M}=8) \times \frac{\mathbf{M}-5}{3} \qquad (7.7.1\text{-}4)$$

The dashed lines in each of the plots on Figure 7.7.1-5 show the results of fitting Equation 7.7.1-4 to the values of $\sigma_{\ln(MSF)}$ for all seven ground-motion measures. The resulting values of $\sigma_{\ln(MSF)}(\mathbf{M}=8)$ are listed in the second column of Table 7.7.1-2 (i.e., "Total Across All Nine GMPEs"). The results show that in the distance range of 20–70 km, $\sigma_{\ln(MSF)}(\mathbf{M}=8)$ is relatively constant at a value of about 0.36. Outside of this distance range, the magnitude scaling variability increases. This increase is attributed to interplay between basic magnitude scaling and its interaction with modeling of geometric spreading and anelastic attenuation.

The use of confidence weights in applying Equation (7.7.1-3) is considered appropriate as these weights reflect the assessment of the degree to which the GMPEs in each cluster represent the current state of knowledge on scaling of ground motions. However, the use of equal weights applied to all models would result in values of $\sigma_{\ln(MSF)}$ that are generally within 5 percent of those shown on Figure 7.7.1-5.

The magnitude scaling variability shown on Figure 7.7.1-5 and listed in the second column of Table 7.7.1-2 is the computed total variability across all the selected models. Within the framework of the update to the EPRI (2004) GMM, the total epistemic uncertainty is composed of a within-cluster component and a cluster-to-cluster component. The magnitude of the cluster-to-cluster uncertainty in magnitude scaling was computed using Equation 7.7.1-3 and the four cluster median models. The results are shown on Figure 7.7.1-6, and the values of $\sigma_{\ln(MSF)}(\mathbf{M}=8)$ are tabulated in the third column of Table 7.7.1-2 (i.e., "Across Cluster 1-4 Medians"). The results show that the cluster-to-cluster magnitude scaling uncertainty is nearly the same as the total magnitude scaling uncertainty.

Assuming that the total variance in magnitude scaling is made up of within-cluster and cluster-to-cluster variance components, then the magnitude of the within-cluster magnitude scaling uncertainty can be computed by subtracting the cluster-to-cluster variance from the total variance. The fourth column of Table 7.7.1-2 (i.e., "Computed Residual Intra-cluster") lists the resulting residual $\sigma_{\ln(MSF)}(\mathbf{M}=8)$ that could be treated as within-cluster magnitude scaling uncertainty in order to have the combined model represent the total magnitude scaling uncertainty. As indicated, the values are relatively small. The fifth column shows the ratio of the cluster-to-cluster variance to the total variance in magnitude scaling (i.e., residual inter-cluster values of $\sigma_{\ln(MSF)}(\mathbf{M}=8)$ to the total $\sigma_{\ln(MSF)}(\mathbf{M}=8)$ values). The ratios are generally well above 0.5, indicating that the cluster-to-cluster variance can represent most of the variance in magnitude scaling.

The results presented in Table 7.7.1-2 apply to the cases where all four cluster models are used for ground-motion estimation. However, in the EPRI (2004) model, Cluster 4, which was based on the Somerville et al. (2001) model, was not used for estimating ground motions for sources where there is a significant hazard contribution from earthquakes of magnitude less than **M** 6. For these sources, only Clusters 1 through 3 were used. The Cluster 4 model was not used because the Somerville et al. (2001) model was developed from ground-motion simulations for **M** 6 and larger earthquakes. In order to evaluate the magnitude scaling uncertainty for cases where the Somerville et al. (2001) GMPE is not used, the above calculations of $\sigma_{\ln(MSF)}$ were repeated. Figure 7.7.1-7 shows the total $\sigma_{\ln(MSF)}$ computed for the eight GMPEs that make up Clusters 1, 2, and 3. Figure 7.7.1-8 shows the cluster-to-cluster $\sigma_{\ln(MSF)}$ computed using the median models for Clusters 1, 2, and 3. The resulting values of $\sigma_{\ln(MSF)}(\mathbf{M}=8)$ are listed in Table 7.7.1-3. The magnitude scaling variability is somewhat lower than that computed using all the selected GMPEs (Figure 7.7.1-5). The cluster-to-cluster variance is a somewhat smaller fraction of the total variance, as indicated by the fifth column of Table 7.7.1-3, but still generally remains equal to at least one-half of the total variance.

The results presented above indicate that a reasonable approximation to the total uncertainty in magnitude scaling to be included in the Updated GMM is given by Equation 7.7.1-4, with the value of $\sigma_{\ln(MSF)}(\mathbf{M}=8)$ set equal to 0.36. The larger variability seen at very small and large distances represents the interaction of magnitude scaling with distance scaling and is captured by the differences in model-to-model variability and cluster-to-cluster variability at these distances. The within-cluster variance in magnitude scaling is assumed to be one-half of the total variance in magnitude scaling. Examination of the results in Tables 7.7.1-2 and 7.7.1-3 indicates that this is a conservative, but not unreasonable, assumption. Using this assumption, the within-cluster $\sigma_{\ln(MSF)}$ is given by Equation 7.7.1-4, with $\sigma_{\ln(MSF)}(\mathbf{M}=8)$ equal to $\sqrt{0.5}\times 0.36$, or 0.25.

The total cluster-independent within-cluster epistemic uncertainty is set equal to the sum of the variance from the data constraint uncertainty (Table 7.7.1-1) and the magnitude scaling variance defined by Equation (7.7.1-4) with $\sigma_{\ln(MSF)}(\mathbf{M}=8)$ equal to 0.25. Figure 7.7.1-9 shows the resulting values of cluster-independent within-cluster epistemic standard deviation.

As discussed in Section 7.4.4, the within-cluster epistemic standard deviation is specified to be the maximum of the model-to-model standard deviation and the cluster-independent within-cluster epistemic standard deviation. Figures 7.7.1-10, 7.7.1-11, and 7.7.1-12 show the resulting envelope of the smoothed model-to-model standard deviations (Figures 7.7.1-1 through 7.7.1-3) and the cluster-independent standard deviation (Figure 7.7.1-9). The values on Figures 7.7.1-10 through 7.7.1-12 are used to develop the epistemic uncertainty models for the median ground motions for Clusters 1, 2, and 3, respectively. As will be discussed below, the values for Cluster 2 were capped at a distance of 500 km in order to produce appropriate behavior in the resulting GMPEs. Figure 7.7.1-13 shows the within-cluster epistemic uncertainty applied to Cluster 4. As there is only one model in this cluster, the values are the same as the cluster-independent epistemic uncertainty shown on Figure 7.7.1-9.

7.7.2 Development of GMPEs to Represent Within-Cluster Epistemic Uncertainty

Following the procedure used in EPRI (2004), the epistemic uncertainty in median CENA ground motions is represented by the three-point discrete distribution proposed by Keefer and Bodily (1983): one value at the median with a weight of 0.63, the other two values at the 5th percentile and 95th percentiles of the uncertainty distribution, each weighted 0.185. For a normal distribution, the 5th and 95th percentiles occur at −1.645 and +1.645 standard deviations respectively. The envelope values of the standard deviation of the median shown on Figures 7.7.1-10 through 7.7.1-13 were used to compute 5th percentile and 95th percentile ground motions relative to the median GMMs developed in Section 7.6.2. Ground-motion values were computed for the same set of magnitudes and distances that were used to develop the median GMPEs. These ground-motion values were then fitted with the same functional forms used for the cluster median GMPEs. The ground-motion values for Cluster 4 were fitted with the functional form used by Somerville et al. (2001). Figures 7.7.2-1a, 7.7.2-2a, 7.7.2-3a, 7.7.2-4a, and 7.7.2-5a show the 5th percentile GMPEs, and 7.7.2-1b, 7.7.2-2b, 7.7.2-3b, 7.7.2-4b, and 7.7.2-5b show the corresponding 95th percentile GMPEs. Two sets of models are produced for Cluster 4, one for rift earthquakes and one for non-rift earthquakes, consistent with the median models developed by Somerville et al. (2001). As was the case for the median models, the selected functional forms provide a close match to the ground-motion values.

The initial values of epistemic standard deviation for Cluster 2 became very large at large distances. As a consequence, the resulting 95th percentile model displayed unrealistic behavior (upward curvature) at distances greater than 500 km. Therefore, the value of epistemic standard deviation for Cluster 2 was capped at the value computed for a distance of 500 km, as shown on Figure 7.7.1-11. The distance range used for fitting the 5th percentile and 95th percentile models for Cluster 2 was also extended beyond 1,000 km in order to force the fitted parameters to produce the desired behavior of a monotonic trend of amplitude with distance. In addition, the use of −1.645 standard deviations to produce the 5th percentile GMPEs for Cluster 2 produced a tendency for predicted ground motions for **M** 8 that were lower than those for **M** 7 at short distances for some frequencies. Given that this type of behavior is very rarely implemented in GMPEs, the predictions for magnitudes greater than 7 were altered to produce monotonic increases in ground motions with increasing magnitude at all distances and frequencies for the 5th percentile GMPEs for Cluster 2.

The resulting coefficients of the GMPEs are listed in Appendix G.

7.8 Adjustments from Epicentral Distance to Joyner-Boore Distance

For computation efficiency in hazard calculations for distributed seismicity sources, EPRI (2004) provided relationships that allow the use of an epicentral distance measure in PSHA calculations. The process used in EPRI (2004) was repeated for the Updated GMM.

7.8.1 Distance Adjustment

The adjustments from epicentral distance to the Joyner-Boore distance measure are developed for each ground-motion cluster as follows. At a given epicentral distance from a hypothetical site, a set of randomly oriented ruptures is simulated for **M** 5, 6, 7, and 8 earthquakes. The magnitude-dependent rupture area is computed using Equation 7.2.4-1, based on Somerville et al. (2001). A seismogenic crustal thickness of 25 km is used, together with the focal depth

distribution developed in Section 7.6.1. An equal mixture of vertical strike-slip and 40-degree-dipping reverse faults is simulated. For each simulated rupture, the R_{JB} is calculated. Using this value of R_{JB} and the earthquake magnitude, the predicted ground motion is obtained using the cluster median GMPE. The process is repeated for a large number of simulations. The geometric mean (mean log) ground motion is then computed for the set of simulated ruptures. Finally, the cluster median GMPE is inverted to obtain the value of R_{JB} that would give the same ground-motion level as the median for all the simulations. The process is then repeated for a range of epicentral distances for each magnitude.

Figures 7.8.1-1a through 7.8.1-5g show the resulting values of R_{JB} plotted versus epicentral distance for the four cluster models and seven ground-motion measures. Two sets of simulations were performed. One set assumed that the ruptures are centered on the epicenters. These results are shown by the red symbols on the figures. The second set assumes that the ruptures are randomly located on the epicenters with a uniform distribution along the rupture length. These results are shown by the blue symbols. Finally, the following equation was fitted to the simulated distances to provide an algebraic relationship to use in hazard calculations:

$$
\begin{aligned}
R_{JB} &= R_{Epicentral} \times \left[1 - 1/\cosh\{R_{Adj}\}\right] \\
R_{Adj} &= C_1 + C_2(\mathbf{M} - 6) + C_3 \ln(R') \\
R' &= \sqrt{R_{Epicentral}^2 + H^2} \\
H &= \exp\{C_4 + C_5(\mathbf{M} - 6)\}
\end{aligned}
\qquad (7.8.1\text{-}1)
$$

The solid curves on Figures 7.8.1-1a through 7.8.1-4g show the results of fitting Equation 7.8.1-1 to the simulated data. The fitted model provides a reasonably good fit to the simulated data. The poorest fits are at very close distances for large magnitudes. In these cases, the model fit tends to give distances that are slightly smaller than the simulated data, but the differences are not large and these situations (large-magnitude earthquakes at close distances) typically do not have a large contribution to the hazard for the type of sources that would be modeled in a PSHA using epicentral distance. The coefficients of Equation 7.8.1-1 for each cluster median model are provided in Appendix G.

7.8.2 Additional Aleatory Variability

The random orientation of ruptures at a given epicentral distance also introduces additional aleatory variability in the ground motions that may be produced at a site. This additional aleatory variability was obtained by computing the standard deviation of the log of the ground-motion estimates used to derive the distance adjustments described in Section 7.8.1. Figures 7.8.2-1a through 7.8.2-4g show the resulting values of additional aleatory variability plotted versus epicentral distance for the four cluster models and seven ground-motion measures. Again, results are shown for centered ruptures and randomly located ruptures. The following equation was fitted to the simulated additional aleatory variability values to provide an algebraic relationship to use in hazard calculations:

$$\sigma_{Additional} = \frac{F_1\left[1 - 1/\cosh\left\{\min\left(F_2 + F_3 R_{Epicentral}, 50\right)\right\}\right]}{\cosh\left[\min\left\{F_4 \ln(R'/F_5), 50\right\}\right]}$$

$$R' = \sqrt{R_{Epicentral}^2 + F_5^2}$$

$$F_1 = \exp\left\{C_1 + C_2(\mathbf{M} - 6) + C_3(\mathbf{M} - 6)^2\right\}$$

$$F_2 = \exp\left\{C_4 + C_5(\mathbf{M} - 6)\right\} \qquad (7.8.2\text{-}1)$$

$$F_3 = \exp\left\{C_6 + C_7(\mathbf{M} - 6)\right\}$$

$$F_4 = \exp\left\{C_8 + C_9(\mathbf{M} - 6)\right\}$$

$$F_5 = \exp\left\{C_{10} + C_{11}(\mathbf{M} - 6)\right\}$$

The solid curves on Figures 7.8.2-1a through 7.8.2-4g show the results of fitting Equation 7.8.2-1 to the simulated data. The fitted model provides a reasonably good fit to the simulated data. The coefficients of Equation 7.8.2-1 for each cluster median model are provided in Appendix G.

The additional aleatory variability calculated using Equation 7.8.2-1 is to be combined with the aleatory variability model developed in Section 7.10 by summing variances.

7.9 Cluster Weights

As indicated in Section 7.4.5, the cluster weights are calculated on the basis of consistency of the cluster medians with the data (after adjusting the data to reference site conditions) and on the TI Team's judgment regarding the robustness of the GMPEs underlying each cluster as extrapolators for magnitude and distance ranges of engineering interest for which data are not available (Confidence Weights).

7.9.1 Calculation of Data-Consistency Cluster Weights Based on Analytical Site Adjustments

The first step in these calculations was to compute the residuals between the analytically adjusted spectral accelerations obtained using the approach in Section 7.3.1 and the cluster median GMPEs. For Cluster 4, earthquakes were categorized as occurring inside or outside rifted zones, and the appropriate rift or non-rift version of the model was used to compute each residual. Figures 7.9.1-1a through 7.9.1-4b show the resulting residuals for the four clusters using the analytically adjusted data. Part (a) of each figure shows the residuals for the magnitude range $3.75 \leq \mathbf{M} < 4.75$, and part (b) shows the residuals for $\mathbf{M} \geq 4.75$. The data are plotted using the rock categories defined for the empirical approach (see Section 7.2.5), even though the analytical approach does not use those categories.

The covariance matrix is constructed in a similar manner to that described in Section 7.4.3, using the assigned values of τ and ϕ for CENA earthquake ground-motion data developed in Section

7.10. The uncertainty in the site-adjustment factor, which was also calculated in Section 7.3.1, is also considered in constructing this matrix.

The calculation of data-consistency weights uses the same general likelihood-based approach that was introduced in Section 7.4.3. The resulting weights for each magnitude-distance bin and each frequency are given in Section 7.9.3.

7.9.2 Calculation of Data-Consistency Cluster Weights Based on Empirical Site Adjustments

The calculation of cluster weights based on empirical site adjustments followed the procedure for calculation of within-cluster weights described in Section 7.5.2. The first step was to compute the residuals for the rock site database using the cluster median GMPEs. For the Cluster 4 GMPE, earthquakes were categorized as occurring inside or outside rifted zones, and the appropriate rift or non-rift version of the model was used to compute the residuals. Figures 7.9.2-1a through 7.9.2-4b show the resulting residuals for the four clusters. Part (a) of each figure shows the residuals for the magnitude range $3.75 \leq \mathbf{M} < 4.75$, and part (b) shows the residuals for $\mathbf{M} \geq 4.75$. As was the case for the individual GMPEs, the residuals for the magnitude range $3.75 \leq \mathbf{M} < 4.75$ typically show more of a trend with distance and greater offset from 0 than those for $\mathbf{M} \geq 4.75$.

As was done for the individual GMPEs, the empirical site correction was based on the use of Model 3 (Equation 7.2.2-3), in which a scale factor is found for only the soft rock site category and the intermediate and hard rock sites are considered one group. Figures 7.9.2-5a and 7.9.2-5b show the resulting values of C_{SR} obtained for each of the cluster median GMPEs. Values are shown for four different magnitude-distance ranges of the data. The results show consistent estimates of the soft rock category scaling factor C_{SR} among the cluster median models.

Using the formulation developed in Section 7.4.3, the likelihood value for each cluster median GMPE was computed for the six magnitude-distance bins. The empirically adjusted residual for the jth recording of the ith earthquake was computed using Equation 7.5.2-1. The values of C_{SR} for data in the range of $\mathbf{M} \geq 4.75$ and $R \leq 500$ km were used, as this is the magnitude range given the greatest weight, although the values for other magnitude-distance ranges are similar.

The variance matrix is constructed in a manner similar to that described in Section 7.4.3, using the assigned values of τ and ϕ for CENA earthquake ground-motion data developed in Section 7.10. The variance estimate for the site adjustment factor was set equal to the standard error of estimation for C_{SR} for the kth site if it is in the soft rock category, and 0 otherwise. Likelihood values were computed for the four cluster median GMPEs for the six structural frequencies and six magnitude-distance bins. The resulting weights for each magnitude-distance bin and each frequency are given in Section 7.9.3.

7.9.3 Results for Cluster Weights

The initial steps in the calculation of data-consistency cluster weights proceed in a manner similar to the within-cluster weights in Section 7.5.3. One difference with the approach followed for within-cluster weights is that the data-consistency weights for high frequency and low frequency are combined arithmetically using equal weights. There are two reasons for this additional step, as follows:

- Using the same weights for all frequencies makes the PSHA calculations simpler because there is only one ground-motion logic tree for all frequencies.
- Using the same weights avoids the possibility of uniform-hazard spectra with unrealistic shape discontinuities between 2.5 and 5 Hz.

Tables 7.9-1 through 7.9-12 show the calculation of weights by magnitude-distance bin, and the combination of these weights for all frequencies and for both the analytical and empirical approaches to adjust for site conditions. Table 7.9-13 shows the combination of these results across frequency and across both approaches for site adjustment. Table 7.9-13 shows that Clusters 2 and 3, which contain new GMPEs, get a majority of the data-consistency weight.

The choice of equal weights for high and low frequencies is a natural one, given that the entire frequency range between 0.1 and 100 Hz must be considered in defining the GMRS. In this instance, this choice has the beneficial effect of balancing the weights between Clusters 2 and 3, which may have been quite different if one frequency range had been given a significantly higher weight.

The interpretation of the data-consistency weights for Cluster 4 is not straightforward, as the SEL GMPE is considered applicable to magnitudes $\geq$ **M** 6 and nearly all data come from earthquakes with lower magnitudes. Despite this, Cluster 4 receives an intermediate weight. Because the data-consistency weights are not the major contributor to the final Cluster weight, this issue is not considered serious. In addition, the approach for the calculation of Cluster 4 weights in this project is identical to the approach followed in EPRI (2004).

Table 7.9-14 shows the combination of the data-consistency and confidence weights. As was done in EPRI (2004), data consistency was given 25 percent weight. In the judgment of the TI Team, the data available to the project do not justify a greater weight. Although much more data are available to the project than were available to the EPRI (2004) study, the data from **M** > 5 earthquakes at distances less than 100 km is still limited. In particular, these data provide little information about the GMPEs ability to predict motions at higher magnitudes.

The assignment of slightly higher confidence weights to Clusters 2 and 3 was based on the considerations: (1) Clusters 2 and 3 include more recent GMPEs, which have had the benefit of more CEUS data and more technical insights drawn from recent work and from larger-magnitude data in active crustal regions, and are all in their second generation of development; and (2) Clusters 1 and 4 are judged to be credible models by the TI Team and by the technical community at large, as confirmed by the feedback from Resource Experts.

The introduction of confidence weights achieves the following two related objectives:

- It tends to produce more reliable results because it transfers weight to Clusters 1 and 4, which are judged to be credible models by the TI Team and by the technical community at large, as confirmed by the feedback from Resource Experts.
- It gives weight to GMPEs that make different assumptions regarding magnitude scaling, thereby causing a realistic increase in the epistemic uncertainty.

Another desirable consequence of applying these confidence weights is that the end result yields approximately 2/3 weight to GMPEs with 1/R geometric spreading and 1/3 weight to those with $1/R^{1.3}$ geometric spreading. This is a reasonable outcome given the current state of uncertainty

regarding geometric spreading, in which there is significant uncertainty but there is a moderate preference for 1/R models.[13]

7.10 Updated EPRI (2006) Aleatory Variability Model

7.10.1 Approach for Specification of Aleatory Variability Model

The EPRI (2004) study developed a model for aleatory variability to accompany the model for median ground motions. The EPRI (2004) aleatory model was based on the range of aleatory models associated with the GMPEs considered in that study. The aleatory models used ranged from values of 0.55 to 0.62 in natural log units developed by Atkinson and Boore (1995), based on empirical data, to values of 0.75 to 0.95 developed by Silva et al. (2002), based on parametric variability and modeling misfit to empirical data. The EPRI (2004) aleatory model included an additional component of variability at small distances to apply to those GMPEs that use Joyner-Boore distance, R_{JB}. The additional aleatory variability was due to the range in possible rupture distances, R_{Rup}, for a given value of R_{JB}. Following the approach used by EPRI (1993), the additional aleatory variability was based on calculations of the variability in ground motions at a given R_{JB} using a focal depth distribution and assuming that ground motions scale with $1/R_{Rup}$.

EPRI (2006) performed an extensive evaluation of the basis for assessing aleatory variability for CEUS GMMs. As described in EPRI (2006), most modern GMPEs based on the analysis of empirical data separate aleatory variability into two main components: intra-event variability, which measures the scatter in ground-motion amplitudes recorded during a single earthquake, and inter-event variability, which measures the scatter in the average level of ground motion from earthquake to earthquake among different earthquakes. This separation is performed to properly account for the correlation in ground motions obtained from a single earthquake (e.g., see Abrahamson and Youngs, 1992). Using current convention, the standard deviation of the inter-event component of aleatory variability is labeled tau (τ), and the standard deviation of the intra-event component is labeled phi (ϕ). These two components of variability have been found to be independent, such that the total aleatory variability standard deviation, sigma (σ), is given by

$$\sigma = \sqrt{\tau^2 + \phi^2} \qquad (7.10.1\text{-}1)$$

EPRI (2006) evaluated these two components of aleatory variability individually using a variety of data sets. The study produced the following conclusions:

- The inter-event variability for CEUS earthquakes is slightly larger than that for earthquakes in active tectonic regions. The difference was modeled by increasing the inter-event standard deviation τ by a value of 0.03 units in natural log of ground-motion amplitude.
- The intra-event variability for CEUS earthquakes is similar or slightly smaller than that for earthquakes in active tectonic regions. The basis for slightly smaller variability was that a more homogeneous crustal structure is expected for the reference hard rock condition for the

[13] Upon further study, and with the benefit of additional data not available at present, this issue of 1/R versus $1/R^{1.3}$ geometric spreading may turn out to be explained by regional differences in wave propagation. With the current knowledge, potential differences in geometric spreading can be treated only as epistemic uncertainty.

EPRI (2004) GMPEs. The favored model (weight 0.7) was that the intra-event variability for CEUS earthquakes is similar to that for active tectonic regions. The alternative model (weight 0.3) is that the intra-event standard deviation ϕ should be decreased by 0.03 units in natural log of ground-motion amplitude.

- CEUS ground motions contain greater high-frequency energy than do ground motions in active tectonic regions. Therefore, the reduction in aleatory variability at frequencies above 10 Hz seen in ground motions in active tectonic regions may not be appropriate for CEUS ground motions. As a result, EPRI (2006) used the observed variability at 10 Hz for active tectonic regions to represent the variability in CEUS ground motions for both 10 Hz and 25 Hz.
- There was not a strong basis for increasing the intra-event variability at small distances when using the R_{JB} distance measure. The preferred model (weight 0.6) was that there is no increase in standard deviation at small values of R_{Rup}. A second model (weight 0.3) included a small additional component of aleatory variability with a standard deviation of 0.12 at R_{JB} values of 10 km or less, and a third model (weight 0.1) included a somewhat larger additional aleatory variability with standard deviation of 0.23 at R_{JB} values of 10 km or less. The additional aleatory variability at small values of R_{JB} proposed by EPRI (2006) is smaller than that developed in EPRI (2004) based on modeling ground motions with $1/R_{Rup}$ scaling.

The conclusion that aleatory variability for CEUS ground motions should be similar to that for ground motions in active tectonic regions reached by EPRI (2006) is generally consistent with Campbell (2003), who added a small amount to the aleatory variability models for GMPEs in active tectonic regions to produce an aleatory variability model for CENA ground motions. Tavakoli and Pezeshk (2005) used an average of aleatory variability values from WNA GMPEs to define the aleatory variability for Eastern North America (ENA) ground motions. Pezeshk et al. (2011) used an average of the aleatory variability values found by the 2008 NGA models to represent the aleatory variability of ENA ground motions. Pezeshk et al. (2011) included the variance in their fitting to the adjusted ground-motion predictions as part of the aleatory variability, but indicated that this additional model fitting variability did not have a physical basis and could perhaps be neglected in application. EPRI (2004) instead considered the standard deviation from fitting the model predictions by algebraic forms as part of epistemic uncertainty, rather than aleatory variability. As described in Section 7.4.4, the standard deviation of fitting the median ground-motion estimates for each cluster is also considered part of epistemic uncertainty, but is neglected because its inclusion has a negligible effect on the estimates of within-cluster epistemic uncertainty. Recently, Atkinson (2013) also concluded that aleatory variability in CENA ground motions should be similar to that for earthquake motions in active tectonic regions based on evaluation of empirical ground-motion data. Atkinson et al. (2012) have implemented this concept in proposed GMMs for use in developing the next set of seismic hazard maps for Canada.

Based on the above considerations, the conclusion of the EPRI (2006) study that aleatory variability for ground motions in the CEUS should be similar to that for ground motions in active tectonic regions is interpreted by the TI Team to be representative of the interpretations of the scientific community. Therefore, the approach used by EPRI (2006) to develop an aleatory variability model for CEUS ground motions was used in this study.

7.10.2 Updated Aleatory Variability Model

The EPRI (2006) aleatory variability model was based on preliminary models from the NGA project (Power et al., 2008). The final NGA GMPEs were published in 2008. Table 7.10.2-1 compares the values of the aleatory variability components used in EPRI (2004) with the average of the values for the four NGA models that separate aleatory variability into inter-event and intra-event components (i.e., Abrahamson and Silva, 2008; Boore and Atkinson, 2008; Campbell and Bozorgnia, 2008; Chiou and Youngs, 2008a). The aleatory variability for the Idriss (2008) model was not included because the estimates were not derived using this separation of inter-event and intra-event components. The values listed for τ for the EPRI (2006) study have been reduced by 0.03 units from those reported in Table 6-3 to remove the increase for CEUS models implemented by EPRI (2006). Values are not listed for 25 Hz because they were not used by EPRI (2006), as discussed in the previous section.

One important difference between the preliminary and published NGA results was the reintroduction of magnitude dependence in aleatory variability in several of the GMPEs. Magnitude-dependent aleatory variability has been an attribute of many GMPEs for active tectonic regions (e.g., Youngs et al., 1995) and was considered a part of the alternative models for aleatory variability by EPRI (2004).

The published 2008 NGA aleatory variability components are similar to or slightly lower than the preliminary values used by EPRI (2006). The averages of the published 2008 NGA values of τ for **M** 5 and **M** 7 are 0.04 to 0.1 units smaller, respectively, than those used by EPRI (2006), and the values for ϕ are the same as or 0.05 units smaller than the values used by EPRI (2006).

Currently, the PEER NGA-West 2 Project (Bozorgnia et al., 2012) is updating the 2008 NGA GMPEs utilizing a greatly expanded database of strong ground-motion recordings and additional ground-motion simulation studies. Although the final updated models were not available for this study, preliminary results indicated some small increases in the components of aleatory variability from those published in 2008. In addition, the preliminary results for some of the models suggest slightly weaker magnitude dependence. In order to incorporate this information in the updated aleatory variability model for CEUS ground motions, the preliminary results from the PEER NGA-West 2 Project were used to scale the 2008 NGA aleatory variability components to produce the values on the right-hand side of Table 7.10.2-1. The updated aleatory models include breakpoints in the magnitude dependence of aleatory variability components at **M** 5, 6, and 7. Averaging the values for the three magnitudes indicates that the values of τ are 0.07 units smaller to 0.04 units larger than used by EPRI (2006), and the values of ϕ are 0.01 units smaller to 0.03 units larger than the values used by EPRI (2006).

The preliminary PEER NGA-West 2 values of total aleatory variability fell approximately into two groups separated by about 0.1 units (natural log of ground-motion amplitude). A sensitivity test was performed to evaluate the need for including this difference as two alternative sets of values, rather than using the composite average value. The sensitivity test involved computing seismic hazard for a site in a uniform source zone with a radius of 200 km, in which earthquakes occur following a truncated exponential recurrence model with a rate of one event per year of **M** 3 and larger, a *b*-value of 1, and a maximum magnitude of **M** 7.5. Hazard analyses were performed using total standard deviation values of 0.55 and 0.65 using a preliminary version of the Cluster 1 GMPE. The resulting hazard curves were averaged to produce a mean hazard curve

assuming equal weights on the two estimates of σ, consistent with the groupings of the PEER NGA-West 2 aleatory variability estimates. The resulting mean hazard is shown by the red solid curve on Figure 7.10.2-1. The hazard analysis was then repeated using the variance averaged value of the two standard deviations, 0.602. The resulting hazard is shown by the black dashed curve. The results of the two analyses are very close, with the hazard computed using the variance average sigma of 0.602 being slightly lower than the mean hazard computed using the two alternative values of 0.55 and 0.65 by less than 1 percent for frequencies of exceedance of 10^{-6} and greater, and by about 5 percent at 10^{-7}. Therefore, it was concluded that the difference in the grouping of the aleatory variability models could be adequately represented by an average value for the purpose of computing mean hazard.

The updated aleatory variability model for CEUS ground motions is given in Table 7.10.2-2. Following the approach used in EPRI (2006), the values derived from the models for active tectonic regions are adjusted for application to CEUS ground motions by increasing the inter-event standard deviation τ by 0.03 units. In addition, the values of τ and ϕ at high frequency (between PGA and 10 Hz) are set equal to the value at 10 Hz to account for the increased high-frequency content of CEUS ground motions. The EPRI (2006) model included a lower-weighted alternative for a reduction to the intra-event variability ϕ of 0.03 units. The effect of this alternative on the total σ is small and it was not included in the Updated GMM.

Figure 7.10.2-2 compares values of total aleatory σ computed using Equation 7.10.1-1 for the EPRI (2006) and updated models. For motions at 2.5 Hz and higher, the updated aleatory variability model has higher values of total σ than the EPRI (2006) model for **M** 5 earthquakes, and lower values for **M** 6 and 7 earthquakes. At 1 Hz, the values of σ are comparable in the two models and at 0.5 Hz, the Updated GMM has slightly higher σ than the EPRI (2006) model.

The updated aleatory variability model includes values for frequencies of 0.25 and 40 Hz. These are provided to aid in the development of ground-motion estimates for a broad frequency range. The values at 0.25 Hz were developed in the same manner as those for the other frequencies, and those for 40 Hz were assumed to be the same as those for 10 Hz.

Similar to EPRI (2006), the favored model (weight 0.6) is that there is no increase in aleatory variability at small values of R_{JB}. The alternative models developed by EPRI (2006) were represented by a single alternative model (weight 0.4) such that there is an additional aleatory variability component, σ_{Rjb}, with a maximum standard deviation of 0.16.[14] The value of σ_{Rjb} is given by

$$\sigma_{Rjb} = \begin{cases} 0.16 & \text{for } R_{JB} \le 10\,\text{km} \\ 0.16\left(1 - \dfrac{\ln(R_{JB}/10)}{\ln(20/10)}\right) & \text{for } 10\,\text{km} < R_{JB} < 20\,\text{km} \\ 0 & \text{for } R_{JB} \ge 20\,\text{km} \end{cases} \qquad (7.10.2\text{-}1)$$

[14] A branch with 0.4 weight and a coefficient of 0.16 in Eq. 7.10.2-1 is equivalent to the more cumbersome model given in EPRI (2006), which consists of two branches with weights of 0.3 and 0.1 and coefficients of 0.12 and 0.23, respectively. This equivalency can be demonstrated using the formulation in Appendix I of EPRI (2004) and typical values of the hazard-curve slope.

The value of σ_{Rjb} is to be combined with the total σ computed from Table 7.10.2-1 by summing variances such that the total standard deviation is given by

$$\sigma = \sqrt{\tau^2 + \phi^2 + \sigma_{Rjb}^2} \qquad (7.10.2\text{-}2)$$

7.11 Development of Alternate Set of Median GMPEs for the Gulf Coast

7.11.1 Basis for Defining Gulf Coast Region

Salvador (1991a) describes the Gulf of Mexico basin as a roughly circular structural basin, filled in the central part with approximately 15 km of Triassic to Holocene sedimentary rocks. The central part of the basin is occupied by the Gulf of Mexico, with maximum water depths of 3,750 meters. The floor of the Gulf rises steeply to the east and south, along the Florida and Campeche Escarpments: to the west and north, it rises more gradually to the coast, forming a well-defined continental rise, slope, and shelf. A broad coastal plain forms the northern part of the basin in Texas, Arkansas, Louisiana, Mississippi, Alabama, Georgia, and Florida, and the basement rocks in those regions were involved in the structural development of Gulf of Mexico. Geophysical surveys indicate that the deep central part of the basin is underlain by oceanic crust, whereas the U.S. Gulf Coastal Plain and the Florida Platform are underlain by either thick continental crust or thinned "transitional" crust. The transitional (rifted or extended) crust occurs beneath the coastal areas of the Gulf Coast states. The landward margins of the Gulf of Mexico basin in the United States are marked by the Marathon and Llano Precambrian uplifts in southern Texas; the Paleozoic Ouachita orogenic belt in north-central Texas, Oklahoma, and Arkansas; the Mississippi Embayment; and the southern reaches of the Paleozoic Appalachian orogenic belt.

Very few permanent seismographic stations exist in the Gulf Coastal Plain. However, on the basis of several early deployments of temporary seismic arrays, the region was known to differ, in terms of regional Lg-phase attenuation, from large regions of cratonic North America. In a previous study for EPRI, Gupta et al. (1989) developed a regionalization of Q models for North America. Their data set consisted of short-period, three-component recordings from the Long-Range Seismic Measurements (LRSM) and Regional Seismic Test Network (RSTN) seismic stations. Gupta et al. (1989) separated the Q values into eight distinct geophysical regions, based on Bouguer gravity contours interpreted to delineate regions with differing crustal structure/compositional characteristics. EPRI (1993) defined 16 velocity structure regions in the CEUS and correlated them with five of the Q regions defined by Gupta et al. (1989). Four of the five Q models were quite similar, with the exception of Region 8, which consisted of the coastal areas of Texas, Loüisiana, Mississippi, Alabama, southern Georgia, and the entire state of Florida. That region exhibited much lower Q than the other four models. Recently, new data have become available that can shed more light on these earlier findings.

The observation of strong attenuation in the Gulf Coast region is linked to major differences in the structure and lithology of the region compared to the cratonic platform and Ouachita orogenic belt to the north. The southern part of the Gulf Coastal Plain is underlain by thinned continental crust that was affected by early Mesozoic extensional tectonics associated with the formation of the Gulf of Mexico (Salvador, 1991a; EPRI/DOE/NRC, 2012). This crustal thinning can be expected to have some impact on the propagation of the Lg phase. Lg is a crust-guided phase that is sensitive to lateral changes in crustal structure and is typically the largest-amplitude phase observed on seismograms at regional distances in regions underlain by thick

continental crust (Kennett, 1986). The transition between thick North American continental crust and thin oceanic crust of the Gulf of Mexico occurs in the southern Gulf Coastal Plain area. An additional factor affecting attenuation in this region is the presence of an extremely thick Mesozoic and Cenozoic sedimentary section in the region affected by crustal extension. Near the coastline in Texas, Louisiana, and Mississippi, the sedimentary section reaches a thickness in excess of 10 km (Salvador, 1991b). Shear-wave velocities in the upper crust in this region are much lower than in regions of the Midcontinent, due to the thick section of sedimentary rock (Mooney et al., 2012).

The geographic extent of the Gulf Coast attenuation region of interest here includes the northern and eastern margin of the Gulf of Mexico structural basin in the United States that is underlain by basement that experienced thinning by extension during the early Mesozoic. Examination of the region suggested by Mooney et al. (2012) as a Gulf Coast crustal region indicated that it closely corresponded to the area encompassed by three seismotectonic zones defined by EPRI/DOE/NRC (2012), specifically:

- ECC-GC (extended continental crust–Gulf Coast region)
- GHEX (Gulf Coast highly extended continental crust)
- RR (Reelfoot Rift)

These seismotectonic zones were based on the structure of the basement rock beneath the thick Mesozoic-Cenozoic Gulf Coastal Plain sedimentary sequence. Accordingly, the union of these three seismotectonic zones was used to define a Gulf Coast crustal region for the assessment of differences in path effects, and data from seismic stations in this region were used for analysis.

7.11.1.1 Evaluation of Regional Path/Source Effects from Recent Earthquake Recordings

The EarthScope Transportable Array (TA) was located in the Central United States in 2010 and 2011, as shown on Figure 7.11.1-1. The array comprised over 200 broadband stations spaced on a 70 km grid extending from the Gulf Coast to the Canadian border. To advance eastward, the westernmost column of stations along a north-south line was moved eastward to form a new column of stations on the eastern edge of the array. Each station remained at a given location for approximately two years. Several felt earthquakes occurred in Arkansas, Oklahoma, and Texas during the time the TA was in these regions. The seismicity and high seismic station density provided an opportunity to examine Lg wave propagation in the Gulf Coast region using a new, high-quality data set.

The objective of the analysis of the TA data was to quantify Q in the basement rocks of the upper crust in the Gulf Coast region, taking into account the large thickness of Cretaceous-Cenozoic sediments in the coastal areas. Figure 7.11.1-2 shows the epicenters of the 16 earthquakes that provided data for analysis, and the boundary of the Gulf Coast region in the vicinity of the epicenters. As indicated above, the defined Gulf Coast region is taken to be the union of the ECC-AM, GHEX, and RR seismotectonic zones defined in EPRI/DOE/NRC (2012). Table 7.11.1-1 lists the dates, hypocenters, and moment magnitudes of the 16 earthquakes, derived by Herrmann (2013).

Data Processing

The raw broadband data from the 16 earthquakes in Table 7.11.1-1 recorded at TA stations within 1,000 km of the earthquake epicenters were downloaded from the IRIS Data Management Center website (http://www.iris.edu/hq/), along with the files containing instrument displacement response represented as Laplace transform poles and zeros in SAC format. The data segments for each station were 600 seconds long, beginning 20 seconds prior to the earthquake origin time. The three-component recordings for each station were corrected to ground acceleration.

The focus of the analysis was the attenuation of the Lg phase on the horizontal components. The analysis involved computation of the Fourier transform of a windowed time segment containing the maximum amplitude of the Lg phase, and required development of models for the prediction of the Lg-phase arrival time and signal duration at a given epicentral distance.

The Lg-phase arrival times from the February 28, 2011, Arkansas earthquake were picked at approximately 250 stations within 600 km of the source, and the travel times were regressed on epicentral distance using a linear model (Figure 7.11.1-3). The model for the prediction of Lg-phase onset time is

$$T_{Lg} = T_0 + {}^{r}/_{3.53}, \qquad (7.11.1\text{-}1)$$

where T_{Lg} is the arrival time of the initial onset of the Lg phase, T_0 is the earthquake origin time, and r is epicentral distance in kilometers.

The duration of the window for Fourier analysis of the Lg phase was defined by examination of the integral of the squared acceleration time series. The duration of the Lg window, t_d, was defined according to the following:

$$\int_{T_{Lg}}^{T_{Lg}+t_d} a^2\,dt = 0.7 \int_{T_{Lg}}^{T_{Lg}+100} a^2\,dt, \qquad (7.11.1\text{-}2)$$

where a is the ground acceleration. The Lg signal duration is defined as the time at which the integral of the squared acceleration time series (starting at time T_{Lg}) reaches 70 percent of its value at T_{Lg} + 100 seconds. A duration versus distance relationship was determined using the data from the February 28, 2011, Arkansas earthquake. Figure 7.11.1-4 shows the estimates of t_d according to Equation 7.11.1-2, plotted versus epicentral distance. A straight line was fitted to those data by linear regression, with the following result:

$$t_d = 8.71 + 0.026\,r. \qquad (7.11.1\text{-}3)$$

The standard errors for the slope and intercept are 0.0018 and 1.126, respectively. Equations 7.11.1-1 and 7.11.1-3 define the Lg window used for Fourier analysis of the Lg wave at all the stations involved in this study.

The mean values of the Fourier acceleration amplitudes were calculated for each of 12 frequency intervals, or bins: (0.2–0.3, 0.3–0.4, 0.4–0.6, 0.6–0.8, 0.8–1.2, 1.2–1.6, 1.6–2.4, 2.4–3.2, 3.2–4.8, 4.8–6.4, 6.4–9.6, and 9.6–12.8 Hz). The center frequencies of each bin were 0.25, 0.35, 0.5, 0.7, 1.0, 1.4, 2.0, 2.8, 4.0, 5.6, 8.0, and 11.2 Hz. The geometric mean of the amplitudes of the two horizontal components at each station was calculated for each frequency bin and used for analysis.

Figure 7.11.1-5 shows an example of the data recorded at two stations approximately 500 km from the epicenter of the February 28, 2011, earthquake in central Arkansas. Station P37A is in

northern Missouri and Station 441A is in southern Louisiana. Note the difference in amplitude with the station near the Gulf Coast, which exhibits extreme attenuation of high-frequency energy, compared to the station to the north in the cratonic platform.

Regression Model

The objective was to quantify the Lg quality factor for the basement beneath the Gulf Coast region. Several different regression models were examined, which led to the conclusion that the attenuation observed at the various stations in the Gulf Coast region is highly correlated with the thickness of the Cretaceous and younger sedimentary section beneath the stations. Stations near the coastline, where the depth to the basement is approximately 12 km (Salvador, 1991b), exhibit extremely strong attenuation in comparison to stations near the margin of the Gulf coastal plain, where the sedimentary section is thin. To obtain a useful first approximation, the total attenuation observed in the Gulf Coast region can be considered to involve two components. The first component is dependent on the travel time of the wave energy through the basement. This time is proportional to the source-receiver distance. The second component is proportional to the time the wave energy spends in the sedimentary section, and is proportional to the thickness of the sediments in the vicinity of the station. This behavior suggested the following form for a regression model to estimate Q, the Lg quality factor for the basement beneath the Gulf Coast region:

$$Ln\left[\frac{A_{ij}(f)}{S_i(f)G(r_{ij})}\right] = R_j(f) - \frac{\pi r_{ij} f}{QV}, \qquad (7.11.1\text{-}4)$$

where

$A_{ij}(f)$ = Fourier acceleration amplitude (geometric mean of the two horizontal components)

$S_i(f)$ = earthquake source amplitude spectrum

$G(r_{ij})$ = geometric spreading (independent of frequency f)

$R_j(f)$ = receiver (site) amplitude term

r_{ij} = epicentral distance, from ith earthquake to the jth receiver station

V = Lg velocity (3.53 kilometers per second [km/s])

In Equation 7.11.1-4, the source spectrum for each earthquake and the geometric spreading are assumed to be known. The unknowns to be determined are Q in the basement and Rj, a receiver (site response) term for each of the j stations. This formulation separates, to a large degree, the two components of attenuation and concentrates the attenuation due to the sedimentary sequence beneath the receiver station in the first term on the right-hand side of Equation 7.11.1-4 (the Rj terms), whereas attenuation in the basement between the source and the receiver is represented by the second term on the right, which involves Q and distance. The source spectra were modeled according to Brune (1970) with unit radiation pattern, crustal density of 2,700 kilograms per cubic meter (kg/m^3), shear-wave velocity at the source of 3.53 km/s, and two alternative values for stress drop: 10 MPa and 5 MPa. The estimates of Q are quite insensitive to the two choices of stress drop. The seismic moments assumed for the earthquakes are those determined by Herrmann (2013), with corresponding moment magnitudes listed in Table 7.11.1-1.

Two geometric spreading models were examined to assess sensitivity of the estimates of Q to uncertainty concerning geometric spreading at near-source distances. Because the great majority of the data are at distances exceeding 120 km, uncertainty concerning geometric spreading to a distance of 120 km has virtually no impact on estimates of Q, but instead impacts the estimates of the receiver (site response) terms (Rj).

Geometric Spreading Model 1:

$$G(r) = r^{-1.3}, r \leq 60\ km,$$

$$G(r) = 60^{-1.3}, 60 \leq r \leq 120\ km,$$

$$G(r) = 60^{-1.3}\left(\frac{r}{120}\right)^{-0.5}, r > 120\ km.$$

Geometric Spreading Model 2:

$$G(r) = r^{-1.0}, r \leq 60\ km,$$

$$G(r) = 60^{-1.0}, 60 \leq r \leq 120\ km,$$

$$G(r) = 60^{-1.0}\left(\frac{r}{120}\right)^{-0.5}, r > 120\ km.$$

Results

Table 7.11.1-2 lists the estimates of Q for the 12 frequency bands examined, along with the regression standard errors of estimate, for both geometric spreading models, and an assumed stress drop of 10 MPa. Note that the estimates of Q are not sensitive to the choice of geometric spreading model. Figure 7.11.1-6 shows Q versus frequency (Geometric Spreading Model 1). The filled circles show the values in Table 7.11.1-2, computed assuming a stress drop of 10 MPa. The open circles show values assuming a stress drop of 5 MPa. Note that results are insensitive to the assumed stress drop. The solid line is a least-squares fit to the data in Table 7.11.1-2 (Geometric Spreading Model 1), stress drop 10 MPa. The result is

$$\log Q = (2.562 \pm 0.014) + (0.624 \pm 0.025) \log f$$

or

$$Q = 365 f^{0.624}.$$

The corresponding result for a stress drop of 5 MPa is

$$\log Q = (2.575 \pm 0.015) + (0.615 \pm 0.026) \log f$$

or

$$Q = 376 f^{0.615}.$$

Figure 7.11.1-7 shows the mean site response for stations in the Gulf Coast region south of latitude 33N, using Geometric Spreading Model 1. The mean values plotted on Figure 7.11.1-7 were computed according to

$$mean\ site\ response = exp\left(\frac{1}{n}\sum_{i=1}^{n} R_i\right), \qquad (7.11.1\text{-}5)$$

where n is the total number of receivers south of latitude 33N, for a given frequency. The dashed and dotted lines on Figure 7.11.1-7 show the mean ± standard error estimates of the site terms.

Figure 7.11.1-8 shows the mean receiver (site) terms for stations in the Gulf Coast region south of latitude 33N, using Geometric Spreading Model 1, plotted to illustrate the linear relationship between the receiver (site) terms and frequency. The values plotted on Figure 7.11.1-8 were computed according to

$$mean\ receiver\ (site)term = \frac{1}{n}\sum_{i=1}^{n} R_i, \qquad (7.11.1\text{-}6)$$

where, again, n is the total number of receivers south of latitude 33N, for a given frequency. The dotted line shows a linear regression fit to mean receiver (site) terms, implying a κ_0 value of 0.096 ± 0.010 seconds.

Figures 7.11.1-9 and 7.11.1-10 are analogous to Figures 7.11.1-7 and 7.11.1-8, but are based on Geometric Spreading Model 2. The Q estimates are insensitive to the choice of spreading model, but the amplitudes of the receiver (site) term spectra are sensitive to the choice of spreading model. Note, however, that the slope of the mean receiver (site) terms versus frequency are independent of the assumed geometric spreading, implying $\kappa_0 = 0.096$ seconds for the average condition in the Gulf Coast region south of latitude 33N.

Figures 7.11.1-11 through 7.11.1-14 show the regression residuals and the site terms for the 12 frequency bands plotted in map view. The geographic extent of the Gulf Coast region is indicated by a solid line. Note that as frequency increases, the receiver (site) terms become smaller (less positive), particularly near the coast, where the thickness of the sedimentary section is greatest. The negative receiver terms at 4 Hz occur in a region where the depth to the base of the marine sedimentary sequence exceeds 6 km (Salvador, 1991b). At frequencies greater than 4 Hz, recordings from many of the stations near the coast could not be used in the regression because of low signal-to-noise ratios due to extreme attenuation. Consequently, those stations do not appear on Figure 7.11.1-14 for 5.6 Hz and higher.

Figure 7.11.1-15 shows the boundary of the Gulf Coast crustal region where the differences in Q from the Midcontinent region are to be applied. The region is defined as the union of the ECC-AM, GHEX, and RR seismotectonic zones defined in EPRI/DOE/NRC (2012). The region covered by these seismotectonic zones more closely corresponds to the area of the Gulf Coast suggested by the analysis of Mooney et al. (2012) and the evaluations by the TI Team presented above than to the Gulf Coast region defined in EPRI (1993) and used by EPRI (2004).

7.11.2 Modification of Midcontinent GMM for Application to Gulf Coast Crustal Region

This section documents the process of modifying the Midcontinent GMM developed in Sections 7.2 through 7.9 so that one can compute ground-motion amplitudes for earthquake paths that travel primarily through Gulf Coast crust. This modification is done by accounting for differences in anelastic attenuation between the Midcontinent and the Gulf Coast, using the Gulf Coast Q model developed in Section 7.11.1 and following an approach analogous to the one followed in EPRI (2004).

Ideally, one should develop the GMM for hard rock in the Gulf Coast region by following an approach parallel to the approach followed in Sections 7.1 through 7.10. However, the data and models available at present do not permit this approach.

The results in Section 7.11.1 contain other useful insights regarding ground motions in the Gulf Coast region, particularly insights about the effects of the thick sedimentary column beneath sites in the region, which may lead to values of kappa much greater than those considered in Section 7.3.1. These effects are not considered as part of the modifications introduced in this section, because it is understood that those effects are to be introduced on a site-specific basis as part of the site-response analysis. Therefore, the bottom of the site column used in the site-response analysis should correspond to a horizon with a shear-wave velocity of ≥2,800 m/s.[15]

7.11.2.1 Q Models for the Midcontinent and Gulf Coast

The two widely used Q models for the CEUS Midcontinent are the models of Silva et al. (2002) and Atkinson (2004a). The Silva et al. (2002) model is used by the Silva et al. (2003) GMPEs in Clusters 1 and 2 and was used in EPRI (2004) as the "host" Q model for the Midcontinent in the EPRI (2004) Midcontinent-to-Gulf Coast conversion. The Atkinson (2004a) model is used by the AB06′ and PZT GMPEs in Cluster 3. The FEL and TEL GMPEs use earlier Q models. The A08′ and SEL GMPEs do not explicitly use Q models of this kind.

The Silva et al. (2002) and Atkinson (2004a) Q models are shown on Figure 7.11.2-1.[16] These two models differ substantially in their values at low and high frequencies and in the spectral shapes that they generate if used with the same source spectrum. Also shown is the harmonic average of these two Q models.[17]

Also shown on Figure 7.11.2-1 is the Q model for the Gulf Coast region developed in Section 7.11.1 using TA data; this model will be used as the "target"[18] Q model for the Gulf Coast in the Midcontinent-to-Gulf Coast conversion. For the sake of reference, the figure also shows the EPRI (1993) Gulf Coast Q model, which was the target Q model for the Gulf Coast in the EPRI (2004) conversion.

The harmonic average of the two Midcontinent models will be used as the "host" Q model for the Midcontinent in the Midcontinent-to-Gulf Coast conversion performed below. This model represents a compromise between the Silva et al. (2002) and Atkinson (2004a) models and shows a modest dependence on frequency. One important property of this harmonic-average Q model is

---

[15] This interface between the rock GMM and the site response is somewhat different from what was done in EPRI (1993) and EPRI (2004), where some differences in impedance were included in the derivation of the Gulf Coast model. The approach followed here is preferable because it is less likely to lead to double-counting of impedance effects.

[16] The Atkinson (2004a) Q model was fit using a crustal shear-wave velocity of 3.7 km/s, while the other two Q models used in this section were fit with 3.5 km/s. In order to predict the same anelastic attenuation with 3,500 m/s, the Atkinson (2004a) Q model was modified from $893f^{0.32}$ to $944f^{0.32}$. This modified model will be used throughout this section.

[17] Using the harmonic-average Q is equivalent to computing the Fourier amplitude using both Midcontinent Q models and then calculating their logarithmic average.

[18] The terms *host* and *target* are used in the context of Campbell's (2003) hybrid empirical method.

that it predicts a higher anelastic attenuation in the Gulf Coast than in the Midcontinent for all frequencies below 100 Hz, as one would expect.

Note that, although Q models are usually derived mainly on the basis of data between 1 and 10 or 20 Hz, they are plotted here (and used in calculations) for much higher frequencies. In addition, Q often has a minimum near 1 Hz (e.g., Atkinson, 2004a; Zandieh and Pezeshk, 2010). Thus, it may be inappropriate to extrapolate relations of the form $Q(f) = Q_0 f^{\eta}$ below 1 Hz. To alleviate this issue, the Midcontinent and Gulf Coast Q models will be treated as flat for frequencies below 1 Hz.

Note also that the difference between the host and target Q models was much greater in EPRI (2004) than it is in this project (i.e., the difference between the dotted lines on Figure 7.11.2-1 is much greater than the difference between the solid lines). Therefore, the difference between Midcontinent and Gulf Coast GMPEs at long distances is expected to be smaller.

7.11.2.2 Details of the Midcontinent to Gulf Coast Conversion

EPRI (2004) used Campbell's (2003) hybrid empirical method (HEM) to perform the Midcontinent to Gulf Coast conversion. This project uses the IRVT approach introduced by Al Atik et al. (2012), which represents a modern variant of the HEM. Although the IRVT approach was introduced to make kappa adjustments, it can also be used for Q adjustments. IRVT has the advantage that there is no need for the definition of complete target and host RVT models, because the IRVT approach back-calculates the implicit host model and then applies the prescribed differences between host and target.

The calculations for one Midcontinent GMPE (e.g., the Cluster 1 median curve) and one magnitude-distance combination proceed as follows:

1. Calculate the Midcontinent response spectrum at 0.5, 1, 2.5, 5, 10, 25, and 100 Hz (PGA) using the corresponding GMPEs for these frequencies. Interpolate lineally in log-log space between frequencies and extrapolate between 0.5 Hz and 0.1 Hz, assuming that spectral acceleration in this range is proportional to 1/period.
2. Convert the Midcontinent response spectrum to Midcontinent Fourier spectrum using IRVT, as implemented by Kottke (2012).[19]
3. Convert the Midcontinent Fourier spectrum to a Gulf Coast Fourier spectrum. This is done by multiplying the Fourier spectrum by the frequency-dependent Q adjustment:

$$\exp\left\{-\frac{\pi f R}{\beta}\left[\frac{1}{Q_{Gulf}}-\frac{1}{Q_{Midcontinent}}\right]\right\} \qquad (7.11.2\text{-}1)$$

   where β is the crustal shear-wave velocity (taken as 3.5 km/s).
4. Convert the Gulf Coast Fourier spectrum to the Gulf Coast response spectrum using RVT and read the spectral accelerations at 0.5, 1, 2.5, 5, 10, 25, and 100 Hz for further processing. Again, Kottke's (2012) implementation of RVT is used.

[19] In the Kottke (2012) scripts, the maximum number of IRVT iterations was increased from 30 to 300.

5. If necessary, make the following three consistency adjustments to the Gulf Coast spectral accelerations at 25 and 100 Hz and at low frequencies: (1) reduce Sa(100) in the Gulf Coast, if necessary, so that Sa(25)/Sa(100) in the Gulf Coast is greater than or equal to its value in the Midcontinent; (2) make Sa(25) and Sa(100) the same in the Gulf Coast and the Midcontinent if Sa(25) is greater in the Gulf Coast than in the Midcontinent; and (3) reduce Sa(0.5), if necessary, so that Sa(0.5)/Sa(1) in the Gulf Coast is smaller than or equal to its value in the Midcontinent.

For each Midcontinent Cluster median, high, and low GMPE, these calculations are performed for **M** between 5 and 8, with an increment of 0.25 **M** units, and for 68 distances between 1 and 1,000 km. The 871 "data" points for each frequency are then fit using the same functional forms used in Sections 7.6 and 7.7. These calculations are performed for all four clusters. For Cluster 4, they are done separately for rifted and non-rifted conditions. The resulting coefficients of the Gulf Coast GMPEs are listed in Appendix G.

7.11.2.3 Results

Figures 7.11.2-2 through 7.11.2-36 compare the Gulf Coast and Midcontinent GMPEs for all clusters and branches. As anticipated, the amplitudes are similar at short distances, but the Gulf Coast amplitudes are lower at longer distances.

7.12 Comparison with EPRI (2004, 2006) GMM and Other Models

7.12.1 Comparison with EPRI (2004, 2006) GMM

Figures 7.12.1-1 through 7.12.1-7 compare the Updated GMM developed in this project for the Midcontinent to the corresponding EPRI (2004) GMM. Results are shown as spectral acceleration versus distance for multiple magnitudes. These comparisons consider all curves in all clusters and use line thickness to convey each curve's weight by making thickness proportional to weight. For $\mathbf{M} < 6$ (i.e., the left panel), Cluster 4 is not shown and the weights have been normalized, in accordance with the recommended use of Cluster 4 in both the Updated and EPRI (2004) GMMs. It is worth noting that Clusters 2 and 3 have changed substantially in their definition and composition, so that within-cluster comparisons between the Updated GMM and the EPRI (2004) GMM is meaningful only for Clusters 1 and 4.

Figures 7.12.1-1 through 7.12.1-7 indicate that the Updated GMM is somewhat lower than EPRI (2004) GMM when the two models are taken as a whole, but these differences are moderate, given the broad uncertainty range spanned by both GMMs. The greater differences occur at low frequencies. At short distances, these differences are largely due to the single-corner Cluster 1 having a lower weight in the Updated GMM than in the EPRI (2004) GMM. At long distances, these differences are due to EPRI (2004) Cluster 3 being much higher than the other models. For PGA, the updated Cluster 2 95th percentile curve predicts higher amplitudes than other curves in the 10–200 km range, but the bulk of the curves are consistent between the two GMMs.

Figures 7.12.1-8 through 7.12.1-14 show similar comparisons, but showing arithmetic-mean and fractile curves[20] for both GMMs. These results are useful in assessing overall epistemic uncertainty and trends. These figures confirm the general trends observed above.

Figures 7.12.1-15 through 7.12.1-21 show results as spectral acceleration versus magnitude for multiple distances, also in the form of arithmetic-mean and fractile curves. In a manner consistent with the guidance in EPRI (2004) and in Appendix G, Cluster 4 is used only for magnitudes 6 and greater, causing discontinuities at **M** 6.[21] Results are consistent with those shown earlier. In both GMMs, there is a tendency for increased epistemic uncertainty with increasing magnitude. For PGA at 20 km, the mean and 84th percentile curves are nearly identical for both GMMs. For low frequencies, the EPRI (2004) GMM has higher upper-tail curves, consistent with earlier observations.

Finally, Figures 7.12.1-22 through 7.12.1-27 show results as spectra for multiple combinations of magnitude and distance, also in the form of arithmetic-mean and fractile curves. The results are consistent with those shown earlier. The overall impression from these figures is that both GMMs encompass broad uncertainty ranges, and this is consistent with the present state of knowledge regarding ground motions in the CEUS. In addition, there is a substantial overlap between these ranges, indicating that the Updated GMM does not represent a radical departure from the EPRI (2004) GMM. The observed differences are the result of possessing and using substantially more data and having acquired additional insights from other regions over a period of nearly 10 years.

Comparison between the models for the aleatory uncertainty is provided on Figure 7.10-2, which compares the updated model (magnitude-dependent) with the EPRI (2006) model (magnitude-independent). For frequencies of 1 Hz and greater, the updated model contains somewhat higher values of the standard deviation for **M** 5, slightly lower or comparable values for **M** 6, and lower values for **M** 7. For 0.5 Hz, the updated model contains slightly higher values for all magnitudes.

7.12.2 Comparison with Atkinson et al. (2012)

Atkinson et al. (2012) have proposed a set of GMMs for use in the next generation of Canada seismic hazard maps. The models were developed by combining the predictions of a set of five GMPEs. The models used by Atkinson et al. (2012) are the A08′, AB06′, PZT, SDCS, and SSCVS GMPEs used in this study. The mean log ground motions and the associated standard deviation among the model predictions were computed and adjusted by judgment. The results were used to construct three ground-motion relationships: a low model, a central model, and a high model. The ground-motion relationships are presented in the form of tables of values as a function of magnitude and epicentral distance. The models provide estimates of PGA and PSA at a number of frequencies for sites with a V_{S30} of 760 m/s. The suggested weights to be applied to

[20] These arithmetic-mean and fractile curves are calculated by summing over the 12 GMPEs in each GMM (for each magnitude-distance combination), considering their respective weights. The aleatory uncertainty does not enter these calculations. It is also worth noting that the arithmetic-mean curve reflects both central tendency and epistemic uncertainty, because the epistemic uncertainty has a high skewness and because it is calculated arithmetically and not logarithmically.

[21] These discontinuities do not cause discontinuity in the hazard curves, because hazard is an integrated quantity and integration has the effect of smoothing the result.

the low, central, and high models are 0.2, 0.5, and 0.3, respectively (G. Atkinson, pers. comm., 2013).

The ground-motion tables in Atkinson et al. (2012) were used to develop comparisons with the predictions of the updated GMPEs developed in this study. The values in the tables were converted from epicentral to Joyner-Boore distance and from V_{S30} 760 m/s to hard rock using the relationships given in Atkinson et al. (2012). Figures 7.12.2-1 through 7.12.2-5 compare these adjusted predictions from Atkinson et al. (2012) with the ground-motion values obtained using the updated model for PGA, and PSA at 10, 5, 1, and 0.5 Hz. Shown for each study are the arithmetic mean ground motions and the range of ground motions for **M** 5.5 and **M** 7.5 earthquakes. The comparisons show good agreement between the mean ground motions. This is not surprising because the two studies are using common GMPEs, although with different weighting schemes.

The range in ground-motion predictions is larger for the model developed in this study than for the Atkinson et al. (2012) models. This is to be expected because the GMM developed in this study contains many more alternative estimates (9 to 12), while the Atkinson et al. (2012) model represents the uncertainty by only 3 alternatives. The comparisons do show that the two representations of the center and range of CENA ground-motion estimates are consistent.

Atkinson et al. (2012) also developed a companion assessment of aleatory variability. They developed a single model to apply to all seismic sources in Canada, both CENA and WNA sources. Figure 7.12.2-6 compares their aleatory model with the updated model developed in Section 7.10. The Atkinson et al. (2012) aleatory variability values are significantly lower than those developed in this project.

7.12.3 Comparison with NGA for WNA

Figure 7.12.3-1 compares the mean ground motions produced by the updated model developed in this study to those produced by the 2008 NGA GMPEs. Shown on each plot are the arithmetic mean ground motions for **M** 5.5 and **M** 7.5 earthquakes. The NGA values are the average of those produced by Abrahamson and Silva (2008), Boore and Atkinson (2008), Campbell and Bozorgnia (2008), and Chiou and Youngs (2008a) for strike-slip and reverse earthquakes. Footwall motions were used for the reverse earthquakes. The NGA values were computed for a V_{S30} of 760 m/s and then adjusted to hard rock conditions using factors derived from the ratios of ground motions produced by the Atkinson and Boore (2006) GMPEs for hard rock and V_{S30} equal to 760 m/s.

The comparisons show that the updated CEUS model developed in this study produces higher motions than the NGA GMPEs for 10 Hz PSA, and comparable levels of motion for 1 Hz PSA. The higher 10 Hz motions may be attributed to higher stress drops for CEUS earthquakes compared to those in active tectonic regions, such as WNA. For 1 Hz PSA, differences in stress drop would not lead to significant differences in ground motion. In addition, the crustal amplification may be somewhat higher at 1 Hz in WNA than in CENA.

7.13 Sensitivity Analyses

In response to feedback received following presentation of an earlier version of the Updated GMM, the TI Team performed a number of sensitivity calculations to investigate the effect of a

number of alternative assumptions. Results from these sensitivity analyses were presented at the February 13, 2013, briefing in the form of comparisons between the base-case and sensitivity cluster GMPEs, cluster weights, and fractile comparisons. These results are described below. Graphical results are not included here in order to avoid confusion, because the final base-case model is now different from the one considered for these sensitivity analyses.

7.13.1 Effect of Giving Zero Weight to Data with M < 4.75

This sensitivity analysis considered the effect of setting to zero the weights for the $3.75 \leq \mathbf{M} < 4.75$ magnitude-distance bins.[22] Calculations with this alternative set of weights were carried through all the steps, obtaining alternative low, median, and high curves for Clusters 1, 2, and 3, and alternative cluster weights.

The most significant effects of this alternative were increases of roughly 20 percent or less in the Cluster 1 GMPEs at distances less than 10 km, some reductions at these distances and for high magnitudes in Cluster 3, and changes in cluster weights (with Cluster 2 gaining 0.12 and Cluster 3 losing 0.15). The effect of these changes is to cause the 95th-percentile curve for PGA and 25 Hz to grow by approximately a factor of two, for magnitudes 6 and greater and distances of 10 to 100 km. This change is brought about mainly by changes in the weight assigned to Cluster 2.[23] The effect on the arithmetic-mean and 84th percentile curves, and for other frequencies, is much smaller. Because only the 95th percentile curve is affected, the effect of this difference on hazard is probably small.

7.13.2 Effect of Down-Weighting Oklahoma-Arkansas Data

Earlier versions of the GMM gave 50 percent weight to the assumption that earthquakes in Oklahoma and Arkansas were not representative of earthquakes in the Midcontinent. The within-cluster weights and the cluster weights were calculated separately with and without these earthquakes, and the weights were averaged. Although this assumption was later discarded by the TI Team, it is useful to summarize the effect of whether or not one gives full weight to these earthquakes.

Results indicate that down-weighting the Oklahoma and Arkansas earthquakes causes an increase of roughly 20 percent or less in the Cluster 1 GMPEs at distances less than 10 km, and some reductions at these distances and for high magnitudes in Cluster 3 (both similar to what was observed in the previous sensitivity case), and small changes in cluster weights (with Cluster 1 losing 0.01 and Cluster 2 gaining 0.01). The effect on the arithmetic-mean and percentile curves is also similar to that observed in the previous sensitivity test. To an even greater degree than the previous sensitivity test, the effect of this assumption on hazard is likely very small.

---

[22] The base-case weights used for these sensitivities were nearly identical to those obtained in Sections 7.5.3 and 7.9.3.

[23] Because the number of hazard curves used to represent the epistemic uncertainty is relatively small, upper fractile calculated from these curves can be somewhat unstable. This is particularly clear in the second sensitivity test, where small changes in the cluster GMPEs, combined with very small changes in the cluster weights, yield a factor of two change in the 95th-percentile curve, while the accompanying change in hazard is likely insignificant.

7.13.3 Effect of Considering Only 10 Hz and 1 Hz Weights for Within-Cluster Weights

Instead of combining the weights from high frequencies (i.e., 25, 10, and 5 Hz) and low frequencies (i.e., 2.5, 1, and 0.5 Hz), this sensitivity test considered only 10 Hz and 1 Hz as representative frequencies and used them in the calculation of within-cluster weights and data-consistency cluster weights.

The main effect of this alternative is to raise the high Cluster 1 GMPE by approximately 20 percent for 10 Hz. The effect on cluster weights is moderate (with Clusters 1 and 2 gaining 0.02 and Cluster 3 losing 0.04). The effect on the arithmetic-mean and percentile curves is again similar to that observed in the previous two sensitivity tests. As indicated earlier, the effect of these differences on hazard is likely very small.

7.13.4 Effect of Alternative Approach for Calculation of Within-Cluster Weights

This sensitivity test investigated the effect of not imposing the 2/3 cap to the within-cluster weights. The main effects of not applying this cap occur for low frequencies and increase more or less uniformly for distances greater than 70 km. The GMPEs decrease by factors of approximately 2 at 500 km for the Cluster 1 95th percentile, and increase by a similar factor for Cluster 2 5th percentile. Also, the Cluster 2 95th-percentile curve decreases by up to 1/3 for large magnitudes. The cluster weights are unchanged. The effect on the arithmetic-mean and percentile curves is again similar to that observed in the previous sensitivity tests, but in the opposite direction (i.e., lower hazard if the weights are not capped). As indicated earlier, the effect of these differences on hazard is likely small.

7.14 Discussion of Updated GMM

In the view of the TI Team, the Updated GMM captures the center, body, and range (CBR) of technically defensible interpretations (TDI) for the following reasons:

Process. A SSHAC Level 2 process has been followed, with a number of SSHAC Level 3 enhancements, while keeping the same overall framework and approach as the Level 3 EPRI (2004) GMM project.

Ground-Motion Data. The Updated GMM is based on a database of recordings that was significantly larger than any that were available during the development of the EPRI (2004) GMM. These new data include recordings from important earthquakes such as those in Mineral, Virginia, Val des Bois, Quebec, Mount Carmel, Illinois, and others. Another important difference with EPRI (2004) and earlier studies is that this project relied entirely on horizontal ground-motion data, thereby avoiding the uncertainty introduced by having to convert vertical data to horizontal using conversion factors that are not well known and may depend on magnitude, distance, depth, amplitude, and site conditions. In addition, some of the data used in EPRI (2004) do not meet the more stringent criteria used in this project because they were recorded by instruments that are located on dams or in other large structures.

Station Data. Station data have been collected and used to adjust recorded motions to reference site conditions using two alternative approaches. This marks an important step because many of the available data were obtained at stations softer than the reference conditions. The use of two alternative adjustments procedures makes the result more robust. Adjustments for differences in

rock site recording conditions were not made as part of the development of the EPRI (2004) GMM.

Engagement of Resource and Proponent Experts. This project engaged Resource and Proponent Experts in CEUS ground motions beyond the normal SSHAC Level 2 guidance, including a feedback workshop. These interactions ensure that the updated GMM captures the profession's current state of knowledge regarding data, models, and methods, particularly the gains that have been made during the nearly 10 years that have elapsed since the EPRI (2004) work was performed.

Candidate GMPEs. The TI Team's reviews of the literature and interactions with Resource and Proponent Experts led to the conclusion that seven GMPEs that were evaluated and represented in the EPRI (2004) GMM should be excluded from the Updated GMM—six of them because they are no longer endorsed by their developers, and the seventh because of its limited range of applicability. Furthermore, the three new GMPEs that were identified and that the TI Team decided to include are in their second generation of development, which adds to the TI Team's confidence in them.

Aleatory Uncertainty. The EPRI (2006) model for aleatory uncertainty was based on preliminary PEER NGA models for sigma from the WUS, with adjustments that account for differences between west and east. The updated model incorporates nearly final PEER NGA-West 2 models, with the same adjustments.

Comparisons with Other Studies. The epistemic uncertainty in the updated model is comparable to the range proposed by Atkinson et al. (2012) for the Canadian seismic hazard maps, which adds to the TI Team's confidence that the updated model has captured the CBR of TDI.

PPRP and Observer Feedback. The TI Team's assessment has incorporated extensive feedback from PPRP Members and Observers. As a particular example, considering the limitations of currently available relevant data, additional uncertainty in magnitude scaling was added in response to a PPRP comment to ensure that the goal of representing the CBR of TDI was met.

7.15 Hazard Input Document

7.15.1 Overview

The Hazard Input Document (HID) contained in Appendix G of this report provides instructions on how to implement and apply the Updated GMM developed in this project. The material in that appendix, together with the computer files referenced therein (and provided as an electronic attachment), defines the functional form and numerical coefficients of the GMM in sufficient detail that the GMM can be coded by a knowledgeable practitioner, even one with no direct involvement with this project. The HID also provides guidance for the hazard analysts who may use the GMM to make decisions on selecting GMPEs for a particular combination of source and site.

By design, the HID contains all the information required for a future user to implement the model within a PSHA, but it does not include the technical basis or justification for the elements of the model. Therefore, the HID contains no arguments or data in support of the model, and no cross-references to portions of the report where these arguments and data are provided. The only

purpose of the HID is to ensure that the expert assessments made by the TI Team are captured fully and accurately and delivered for use by the hazard analyst for a PSHA at a specific site. For the EPRI (2004, 2006) GMM Review Project, this HID was used by the hazard analyst to carry out hazard calculations at seven demonstration sites, as summarized in Chapter 8.

7.15.2 Contents of the Hazard Input Document

The HID in Appendix G contains the following information:

- Weights, functional forms, and coefficients for the GMPEs that define the median amplitude and its epistemic uncertainty in the Updated GMM.
- Functional forms and coefficients for the conversion from epicentral distance to Joyner-Boore distance, and associated aleatory uncertainty in amplitude, to be employed when using point sources to represent earthquakes in area sources.
- Guidance on calculating aleatory uncertainty in ground-motion amplitude for given magnitude, distance, and frequency.
- Range of applicability of the Updated GMM.
- Definition of the Gulf Coast crustal region and guidance on the use of the Updated GMM when the source-to-site path is partially or wholly contained within the Gulf Coast region.
- Guidance on when to include Cluster 4 in the hazard calculations and on how to construct the
- PSHA logic tree when both area sources and RLME sources contribute to seismic hazard.

Table 7.2.3-1 (page 1 of 7)
Moment Magnitudes for Earthquake in Ground-Motion Database

EQID	Earthquake	Date	Moment Magnitude Information	Assigned Moment Magnitude (M)	Rift Code[1]	NE Code[2]	OA Code[3]
1	Charlevoix, QC	1925/03/01	**M** 6.3, Bent (1992); **M** 6.43, Johnston (1996)	6.36 Not used, no rock recordings with $R_{JB} \leq 500$ km	1	1	0
2	Grand Banks, NL	1929/11/18	**M** 7.1, Bent (1995); **M** 7.25, Johnston (1996)	7.18 Not used, no rock recordings with $R_{JB} \leq 500$ km	0	1	0
3	Timiskaming, QC	1935/11/01	**M** 6.1, Bent (1996a); **M** 6.21, Johnston (1996)	6.15 Not used, no rock recordings with $R_{JB} \leq 500$ km	1	1	0
4	Cornwall Massena, ON	1944/09/05	**M** 5.8, Bent (1996b); **M** 5.79, Johnston (1996)	5.79 Not used, no rock recordings with $R_{JB} \leq 500$ km	1	1	0
5	Saguenay, QC	1988/11/25	**M** 5.85, Johnston (1996)	5.85	1	1	0
6	La Malbaie, QC	1997/08/20	**M** 3.25, Cramer et al. (2103), E(**M**) 3.27, NUREG-2115[1]	Not used **M** < 3.75	1	1	0
7	La Malbaie, QC	1997/10/28	**M** 4.29, Du et al (2003)	4.29	1	1	0
8	Cap-Rouge, QC	1997/11/06	**M** 4.38, SLU[2]; **M** 4.5, Du et al (2003)	4.44	1	1	0
9	Cote-Nord, QC	1999/03/16	**M** 4.43, Du et al (2003); **M** 4.5, Lamontagne et al. (2004)	4.47	1	1	0
10	Kipawa, QC	2000/01/01	**M** 4.61, Du et al (2003); **M** 4.7, Ma and Eaton (2007); **M** 4.57, Atkinson (2004a, 2004b)	4.63	1	1	0

Table 7.2.3-1 (page 2 of 7)
Moment Magnitudes for Earthquake in Ground-Motion Database

EQID	Earthquake	Date	Moment Magnitude Information	Assigned Moment Magnitude (M)	Rift Code[1]	NE Code[2]	OA Code[3]
11	La Malbaie, QC	2000/06/15	**M** 3.29, Atkinson (2004a, 2004b)	Not used **M** < 3.75	1	1	0
12	Laurentide, QC	2000/07/12	**M** 3.65, Atkinson (2004a, 2004b)	Not used **M** < 3.75	1	1	0
13	Laurentide QC aftershock	2000/07/12	**M** 3.11, Atkinson (2004a, 2004b)	Not used **M** < 3.75	1	1	0
14	Ashtabula, OH	2001/01/26	**M** 3.88, Du et al. (2003)	3.88	0	1	0
15	Enola, AR	2001/05/04	**M** 4.37, SLU	4.37	0	0	1
16	Au Sable Forks, NY	2002/04/20	**M** 4.97, SLU; **M** 5.0, Boore et al. (2010)	5.0	1	1	0
17	Lac Laratelle, QC	2002/06/05	**M** 3.67, SLU	Not used **M** < 3.75	0	1	0
18	Caborn, IN	2002/06/18	**M** 4.60, SLU	4.6	0	0	0
19	Boyd, NE	2002/11/03	**M** 4.18, SLU	4.18	0	1	0
20	Charleston, SC	2002/11/11	**M** 4.03, SLU	4.03	1	0	0
21	Ft Payne, AL	2003/04/29	**M** 4.8, LDSN[3]; **M** 4.62 SLU	4.7	0	0	0
22	Blytheville, AR	2003/04/30	**M** 3.67, Cramer et al. (2013)	Not used **M** < 3.75	1	0	0
23	Bardwell, KY	2003/06/06	**M** 4.02, SLU	4.02	1	0	0
24	La Malbaie, QC	2003/06/13	**M** 3.37, SLU	Not used **M** < 3.75	1	1	0
25	Bark Lake, QC	2003/10/12	**M** 4.0, NEDB[4]	4.0	0	1	0
26	Jefferson, VA	2003/12/09	**M** 4.25, Kim and Chapman (2005)	4.25	0	0	0
27	St Teresa, MX	2004/04/06	**M** 4.31, Cramer et al. (2013)	Not used, no recordings	--	--	--
28	La Baie, QC	2004/05/04	**M** 2.86, Cramer et al. (2013)	Not used **M** < 3.75	1	1	0
29	Prairie Center, IL	2004/06/28	**M** 4.18, SLU; **M** 4.2 LDSN	4.19	0	0	0

Table 7.2.3-1 (page 3 of 7)
Moment Magnitudes for Earthquake in Ground-Motion Database

EQID	Earthquake	Date	Moment Magnitude Information	Assigned Moment Magnitude (M)	Rift Code[1]	NE Code[2]	OA Code[3]
30	Port Hope, ON	2004/08/04	**M** 3.1, Kim et al. (2006); **M** 3.19, SLU	Not used **M** < 3.75	0	1	0
31	Milligan Ridge, AR	2005/02/10	**M** 4.14, SLU	4.14	1	0	0
32	Riviere Du Loup, QC	2005/03/06	**M** 4.60, SLU; **M** 4.7, Boore et al. (2010)	4.65	1	1	0
33	Shady Grove, AR	2005/05/01	**M** 4.35, SLU	4.25	1	0	0
34	Miston, TN	2005/06/02	**M** 4.01, SLU	4.01	1	0	0
35	Thurso, ON	2006/02/25	**M** 3.7, Ma and Eaton (2007), **M** 3.65, SLU	Not used **M** < 3.75	1	1	0
36	Hawkesbury, ON	2006/02/26	**M** 2.9, Cramer et al. (2013)	Not used **M** < 3.75	1	1	0
37	Baie Saint Paul, QC	2006/04/07	**M** 3.80, SLU	3.8	1	1	0
38	Ridgely, TN	2006/09/07	**M** 3.41, Cramer et al. (2013)	Not used **M** < 3.75	1	0	0
39	Gulf of Mexico	2006/09/10	**M** 5.8,USGSMT; **M** 5.9, GCMT	5.85 Not used (propagation paths through Gulf region)	0	0	0
40	Acadia, ME	2006/10/03	**M** 3.90, SLU	3.9	0	1	0
41	Marston, MO	2006/10/18	**M** 3.47, Cramer et al. (2013)	Not used **M** < 3.75	1	0	0
42	Marvin, VA mine collapse	2006/11/02		Non-earthquake	--	--	--
43	Skeggs, VA mine collapse	2006/11/23		Non-earthquake	--	--	--
44	Cobourg, ON	2007/07/19	**M** 2.82, Cramer et al. (2013)	Not used **M** < 3.75	0	1	0
45	Baie Saint Paul, QC	2008/01/03	**M** 2.95, Cramer et al. (2013)	Not used **M** < 3.75	1	1	0

Table 7.2.3-1 (page 4 of 7)
Moment Magnitudes for Earthquake in Ground-Motion Database

EQID	Earthquake	Date	Moment Magnitude Information	Assigned Moment Magnitude (M)	Rift Code[1]	NE Code[2]	OA Code[3]
46	Mt Carmel, IL	2008/04/18	**M** 5.26, SLU	5.26	0	0	0
47	Mt Carmel, IL aftershock	2008/04/18	**M** 4.64, SLU	4.64	0	0	0
48	Mt Carmel, IL aftershock	2008/04/21	**M** 4.03, SLU	4.03	0	0	0
49	Mt Carmel, IL aftershock	2008/04/25	**M** 3.75, SLU	3.75	0	0	0
50	Buckingham, QC	2008/06/11	**M** 2.96, Cramer et al. (2013)	Not used **M** < 3.75	1	1	0
51	Riviere du Loup, QC	2008/11/15	**M** 3.60, SLU	Not used **M** < 3.75	1	1	0
52	Pine Forest, SC	2008/12/16	**M** 3.41, Cramer et al. (2013)	Not used **M** < 3.75	1	0	0
53	Rosehill, SC	2009/01/29	**M** 2.2, Cramer et al. (2013)	Not used **M** < 3.75	1	0	0
54	Palmetto, SC	2009/05/06	**M** 2.2, Cramer et al. (2013)	Not used **M** < 3.75	1	0	0
55	Constance Bay, ON	2009/05/08	**M** 2.9, Cramer et al. (2013)	Not used **M** < 3.75	1	1	0
56	Jones, OK	2010/01/15	**M** 3.84, SLU	3.84	0	0	1
57	Lincoln, OK	2010/02/27	**M** 4.18, SLU	4.18	0	0	1
58	Whiting, MO	2010/03/02	**M** 3.40, SLU	Not used **M** < 3.75	1	0	0
59	Lebanon, IL	2010/05/21	**M** 2.5, Cramer et al. (2013)	Not used **M** < 3.75	0	0	0
60	Val-des-Bois, QC	2010/06/23	**M** 5.07, SLU	5.07	1	1	0
61	St. Flavien, QC	2010/07/23	E(**M**) 3.6 based on M_N 4.1, NUREG-2115	Not used **M** < 3.75	1	1	0
62	Bhuj, India	2001/01/26	**M** 7.6, Cramer et al. (2013)	7.6 Not used, usable frequency and rock site classification unclear	--	--	--

Table 7.2.3-1 (page 5 of 7)
Moment Magnitudes for Earthquake in Ground-Motion Database

EQID	Earthquake	Date	Moment Magnitude Information	Assigned Moment Magnitude (M)	Rift Code[1]	NE Code[2]	OA Code[3]
63	Mont Laurier, QC	1990/10/19	**M** 4.56, Johnston (1996)	4.56	0	1	0
64	Montgomery, MD	2010/07/16	**M** 3.42, SLU	Not used **M** < 3.75	0	0	0
65	Gazli, USSR	1976/05/17	PEER NGA-West[5]	6.8 Not used, no rock recordings	--	--	--
66	Slaughterville, OK	2010/10/13	SLU	4.36	0	0	1
67	Guy, AR	2010/10/15	SLU	3.86	0	0	1
68	Concord, NH	2010 /09/26	**M** 2.80 Cramer et al. (2013)	Not used **M** < 3.75	0	1	0
69	Nahanni, NWT foreshock	1985/11/09	**M** 4.4 Cramer et al. (2013)	4.4	0	0	0
70	Nahanni, NWT	1985/12/23	PEER NGA-West	6.76	0	0	0
71	Nahanni, NWT aftershock	1985/12/23	**M** 5.1 Cramer et al. (2013)	5.1	0	0	0
72	Nahanni, NWT aftershock	1985/12/25	**M** 5.2 Cramer et al. (2013)	5.2	0	0	0
73	Arcadia, OK	2010/11/24	**M** 3.96, SLU	3.96	0	0	1
74	Bethel Acres, OK	2010/12/12	**M** 3.23, SLU	Not used **M** < 3.75	0	0	1
75	Greentown, IN	2010/12/30	**M** 3.85, SLU	3.85	0	0	0
76	Guy, AR	2010/11/20	**M** 3.90, SLU	3.9	0	0	1
77	Greenbrier, AR	2011/02/17	**M** 4.0 Cramer et al. (2013)	Not used, no recordings	0	0	1
78	Greenbrier, AR	2011/02/18	**M** 4.0 Cramer et al. (2013)	Not used, no recordings	0	0	1
79	Greenbrier, AR	2011/02/18	**M** 4.3 Cramer et al. (2013)	Not used, no recordings	0	0	1
80	Greenbrier, AR	2011/02/28	**M** 4.67, SLU	4.67	0	0	1
81	Sullivan, MO	2011/06/07	**M** 3.89, SLU	3.89	0	0	0

Table 7.2.3-1 (page 6 of 7)
Moment Magnitudes for Earthquake in Ground-Motion Database

EQID	Earthquake	Date	Moment Magnitude Information	Assigned Moment Magnitude (M)	Rift Code[1]	NE Code[2]	OA Code[3]
82	Eagle Lake, ME	2006/07/14	**M** 3.51, SLU	Not used **M** < 3.75	0	1	0
83	Val-des-Bois, QC aftershock	2010/06/24	**M** 2.9 Cramer et al. (2013)	Not used **M** < 3.75	1	1	0
84	Val-des-Bois, QC aftershock?	2010/07/22	**M** 2.7 Cramer et al. (2013)	Not used **M** < 3.75	1	1	0
85	Hawkesbury, ON	2011/03/16	**M** 3.48, SLU	Not used **M** < 3.75	1	1	0
86	Charlevoix, QC	2001/05/22	**M** 3.6, Atkinson (2004a, 2004b)	Not used **M** < 3.75	1	1	0
87	Baie Saint Paul, QC	2002/08/17	**M** 3.24, Atkinson (2004a, 2004b)	Not used **M** < 3.75	1	1	0
88	Mineral, VA	2011/08/23	**M** 5.68, Chapman (2013); **M** 5.68, SLU, **M** 5.74 & **M** 5.80, USGSMT; **M** 5.81, GCMT	5.74	0	0	0
89	Mineral, VA aftershock	2011/08/25	**M** 3.97, SLU	3.97	0	0	0
90	Sparks, OK	2011/11/05	**M** 4.73, SLU	4.73	0	0	1
91	Sparks, OK	2011/11/06	**M** 5.62, SLU	5.62	0	0	1
92	Cormal, TX	2011/10/20	**M** 4.62, SLU	4.62 Not used (propagation paths through Gulf region)	0	0	0
93	Miramichi, NB aftershock	1982/03/31	**M** 4.1, Atkinson (1993)	4.1	0	1	0
94	Miramichi, NB aftershock	1982/05/06	E(**M**) 3.45, NUREG-2115	Not used **M** < 3.75	0	1	0

Table 7.2.3-1 (page 7 of 7)
Moment Magnitudes for Earthquake in Ground-Motion Database

EQID	Earthquake	Date	Moment Magnitude Information	Assigned Moment Magnitude (M)	Rift Code[1]	NE Code[2]	OA Code[3]
95	Saguenay, QC foreshock	1988/11/23	**M** 4.2, Boore and Atkinson (1992)	4.2	1	1	0
96	Cape Girardeau, MO	1990/09/26	**M** 4.28, Herrmann and Ammon (1997)	4.28	1	0	0
97	New Madrid, MO	1989/04/27	**M** 4.3, EPRI (1993)	4.3	1	0	0
98	New Madrid, MO	1991/05/04	**M** 4.13, Herrmann and Ammon (1997); **M** 4.33, Johnston (1996)	4.23	1	0	0
99	Franklin Falls, NH	1982/01/19	**M** 4.28, EPRI (1993)	4.28	0	1	0

LDSN – http://www.ldeo.columbia.edu/LCSN/Eq/
NEDB – http://www.earthquakescanada.nrcan.gc.ca/index-eng.php
NUREG-2115 (EPRI/DOE/NRC, 2012)

PEER NGA-West – http://peer.berkeley.edu/ngawest/nga_flatfiles.html
SLU – http://www.eas.slu.edu/eqc/eqc_mt/MECH.NA/
[1] 1 indicates Rift earthquake, 0 indicates non-rift
[2] 1 indicates Northeast earthquake, 0 indicates otherwise
[3] 1 indicates central Oklahoma or central Arkansas earthquake, 0 indicates otherwise

Table 7.2.6-1
Number of Earthquakes in Final Ground-Motion Database Used to Develop Ground-Motion Model Weights

Magnitude Range	Number of Earthquakes for PSA at Frequency of:					
	25 Hz	**10 Hz**	**5 Hz**	**2.5 Hz**	**1 Hz**	**0.5 Hz**
$3.75 \leq \mathbf{M} < 4.75$	32	39	42	42	42	36
$\mathbf{M} \geq 4.75$	9	9	9	9	8	8

Table 7.2.6-2
Number of Rock Site Recordings in Final Ground-Motion Database Used to Develop GMM Weights

Magnitude Range	Distance Range	Rock Site Category	Number of Recordings for PSA at Frequency of:					
			25 Hz	10 Hz	5 Hz	2.5 Hz	1 Hz	0.5 Hz
$3.75 \le \mathbf{M} < 4.75$	$0 < R_{JB} \le 70$ km	Soft	16	22	22	22	22	15
		Intermediate	15	17	19	16	14	11
		Very Firm	29	29	29	29	28	21
	$70 < R_{JB} \le 150$ km	Soft	4	24	28	28	27	24
		Intermediate	1	13	18	18	18	17
		Very Firm	8	14	16	16	16	10
	$150 < R_{JB} \le 500$ km	Soft	21	126	201	205	200	173
		Intermediate	16	132	183	190	189	176
		Very Firm	29	63	74	75	73	45
$\mathbf{M} \ge 4.75$	$0 < R_{JB} \le 70$ km	Soft	12	13	13	13	12	8
		Intermediate	7	7	7	8	7	5
		Very Firm	2	2	2	2	2	2
	$70 < R_{JB} \le 150$ km	Soft	2	4	5	5	5	5
		Intermediate	0	1	2	2	3	1
		Very Firm	6	8	8	8	8	8
	$150 < R_{JB} \le 500$ km	Soft	21	44	49	49	49	46
		Intermediate	14	48	51	51	51	49
		Very Firm	20	29	29	29	29	28
Total			**223**	**596**	**756**	**766**	**753**	**644**

Table 7.2.6-3
Number of Recording Stations in Final Ground-Motion Database Used to Develop GMM Weights

Rock Site Category	Basis for Categorization	Number of Recording Stations for PSA at Frequency of:					
		25 Hz	**10 Hz**	**5 Hz**	**2.5 Hz**	**1 Hz**	**0.5 Hz**
Soft	Measured V_{S30}	17	24	24	24	24	22
	Inferred V_{S30}	31	62	68	69	68	55
	Geology Only	1	12	13	13	13	10
Intermediate	Measured V_{S30}	6	12	12	12	12	12
	Inferred V_{S30}	18	25	26	26	25	23
	Geology Only	4	46	60	61	63	56
Very Firm	Measured V_{S30}	3	3	3	3	3	2
	Inferred V_{S30}	33	46	46	47	46	38
	Geology Only	0	0	0	0	0	0
Total		**113**	**230**	**252**	**255**	**254**	**218**

Table 7.2.6-4
Number of Recording Stations with Measured V_S in Final Ground-Motion Database Used to Develop GMM Weights

V_{S30} Range	Number of Recording Stations for PSA at Frequency of:					
	25 Hz	**10 Hz**	**5 Hz**	**2.5 Hz**	**1 Hz**	**0.5 Hz**
Soft ($500 \leq V_{S30} < 1000$ m/s)	15	21	21	21	21	19
Intermediate ($1000 \leq V_{S30} < 1890$ m/s)	6	12	12	12	12	12
Very Firm ($V_{S30} \geq 1890$ m/s)	1	1	1	1	1	1
Total	**22**	**34**	**34**	**34**	**34**	**32**

Table 7.3.1.1-1 (page 1 of 3)
Stations with Shear-Wave-Velocity Profiles

Station	Data Source	Depth of Instrument Emplacement (m; if known and non-zero)	V_{S30} (m/s)	kappa (s)	Comments
AG.WHAR	GV		1162	0.0065	
CN.ACTO	NGA-East		966	0.0067	
CN.ALGO	NGA-East		303	0.0400	Not used (V_{S30}<500 m/s)
CN.OTT	NGA-East	13.00	1692	0.0064	
CN.PEMO	NGA-East		547	0.0073	
CN.WLVO	NGA-East		1137	0.0065	
ET.SWET	UT	2.44	940	0.0068	
GS.OK001	GV		610	0.0143	Modified top layer as done by GEOVision
GS.OK002	GV		708	0.0115	
GS.OK005	GV		580	0.0120	Used average of 2 arrays
GS.OK008	GV		610	0.0118	Top layer made equal to 2nd as per GEOVision
GS.OK009	GV		323	0.0136	Used average of array 2 Love + Rayleigh; layers 1 and 2--> layer 3 (stiffer below building). Not used (V_{S30}<500 m/s)
GS.OK010	GV		618	0.0116	Average of Love & Rayleigh; replaced 1st layer with 2nd
IU.SSPA	UT		899	0.0119	
LD.MVL	USGS		669	0.0073	Preliminary from USGS
NM.BLO	USGS	3.50	2324	0.0061	Preliminary from USGS
NM.CBHT	NGA-East		227	0.0400	Not used (V_{S30}<500 m/s)
NM.CVVA	UT	0.61	627	0.0120	
NM.HAIL	NGA-East		756	0.0098	
NM.JCMO	USGS	1.00	902	0.0071	Preliminary from USGS
NM.SEAR	GV	1.00	1200	0.0065	
NM.SIUC	GV	5.50	753	0.0171	
NM.UALR	GV		1242	0.0067	

Table 7.3.1.1-1 (page 2 of 3)
Stations with Shear-Wave-Velocity Profiles

Station	Data Source	Depth of Instrument Emplacement (m; if known and non-zero)	V_{S30} (m/s)	kappa (s)	Comments
NM.USIN	NGA-East		668	0.0074	
NM.WVIL	NGA-East		624	0.0076	
NP.2549	USGS		492	0.0400	Preliminary from USGS. Not used (V_{S30}<500 m/s)
NP.2555	USGS		364	0.0400	Preliminary from USGS. Not used (V_{S30}<500 m/s)
NP.2648	USGS		608	0.0083	Preliminary from USGS
NQ.Q793	GV		383	0.0124	Changed 1st layer as per GEOVision. Not used (V_{S30}<500 m/s)
PE.PAGS	USGS		453	0.0400	Preliminary from USGS (very strong V_S inversion). Not used (V_{S30}<500 m/s)
PE.PSUB	USGS		394	0.0372	Preliminary from USGS. Not used (V_{S30}<500 m/s)
PE.PSWB	GV	4.00	646	0.0121	Not used (no records meet criteria)
PN.PPBLN	GV	2.50	1916	0.0062	Not used (no records meet criteria)
PN.PPCWF	GV	4.50	640	0.0082	Not used (no records meet criteria)
PN.PPMOO	GV	4.00	555	0.0103	Use Rayleigh
PN.PPPCH	GV		436	0.0203	Use array 2 Rayleigh (~average value of V_{S30}). Not used (V_{S30}<500 m/s)
PN.PPPHS	GV	2.50	362	0.0400	Not used (V_{S30}<500 m/s)
SE.RCRC	UT	0.61	548	0.0084	
SE.URVA	UT	0.61	558	0.0075	Depth from Martin Chapman

Table 7.3.1.1-1 (page 3 of 3)
Stations with Shear-Wave-Velocity Profiles

Station	Data Source	Depth of Instrument Emplacement (m; if known and non-zero)	V_{S30} (m/s)	kappa (s)	Comments
SE.VWCC	UT	5.88	522	0.0218	Sensor depth taken as 19.3 ft (M. Chapman: "The sensor on a concrete pad poured directly on Paleozoic shale")
US.ACSO	USGS	1.00	473	0.0400	USGS preliminary; model 1AM. Not used (V_{S30}<500 m/s)
US.BLA	UT	30.48	1572	0.0070	Sensor depth is taken as depth to 5,000 fps as per M. Chapman's e-mail
US.CBN	UT	4.57	275	0.0157	Not used (V_{S30}<500 m/s)
US.CNNC	USGS		285	0.0400	Preliminary from USGS. Not used (V_{S30}<500 m/s)
US.GOGA	UT	0.10	302	0.0400	Not used (V_{S30}<500 m/s)
US.LBNH	GV	1.00	1016	0.0069	
US.LONY	GV	1.00	1416	0.0064	
US.LRAL	UT	0.10	556	0.0111	
US.MCWV	USGS		1488	0.0064	Preliminary from USGS
US.MIAR	GV	1.00	1257	0.0065	
US.MYNC	UT	0.30	543	0.0107	Not used (no records meet criteria)
US.NCB	GV	1.00	1247	0.0064	
US.TZTN	USGS		722	0.0080	Preliminary from USGS. Not used (no records meet criteria)
US.WMOK	GV	0.50	1809	0.0061	

Table 7.3.1.1-2
Reference Shear-Wave-Velocity Profile

Thickness (m)	V_S (m/s)	Density (gr/cc)
1,300	2,830	2.52
11,000	3,520	2.71
28,000	3,750	2.78
–	4,620	3.34

Table 7.4.1-1
Updated EPRI (2004, 2006) GMM Clusters and Models

Cluster	Model Types and Cluster Weights (repeated large-magnitude earthquake sources/area earthquake sources)	Models
1	Single-Corner Brune Source (0.15/0.185)	Silva et al. (2002) – SSCCSS[1] Silva et al. (2002) – SSCVS[1] Toro et al. (1997) – TEL Frankel et al. (1996) – FEL
2	Complex/Empirical Source $\sim R^{-1}$ Geometric spreading (0.31/0.383)	Silva et al. (2002) – SDCS Atkinson (2008) with 2011 modifications – A08′
3	Complex/Empirical Source $\sim R^{-1.3}$ Geometric spreading (0.35/0.432)	Atkinson-Boore (2006) with 2011 modifications – AB06′ Pezeshk et al. (2011) – PZT
4	Finite-Source /Green's Function (0.19/0)	Somerville et al. (2001); slightly different models for rifted and non-rifted (not used for distributed seismicity sources with large contribution from **M** < 6) – SEL

[1] Treated as one model for calculation of weights.

Table 7.4.2-1 (page 1 of 2)
Results of Statistical Analysis of Regionalization

GMPE	Regionalization Model with Lowest AIC Score for M ≥ 4.75 Residuals for Frequency of:					
	25 Hz	**10 Hz**	**5 Hz**	**2.5 Hz**	**1 Hz**	**0.5 Hz**
A08'	Both	NE Only	Both	NE Only	OA Only	Both
AB06'	NE Only	No Reg	No Reg	No Reg	No Reg	OA Only
FEL	NE Only	No Reg	No Reg	No Reg	No Reg	OA Only
PZT	NE Only	No Reg	No Reg	No Reg	No Reg	No Reg
SDCS	NE Only	No Reg	NE Only	NE Only	No Reg	No Reg
SSCCSS	NE Only	No Reg	NE Only	NE Only	No Reg	NE Only
SSCVS	NE Only	No Reg	NE Only	NE Only	No Reg	NE Only
SEL	OA Only	No Reg	No Reg	NE Only	No Reg	NE Only
TEL	NE Only	No Reg	No Reg	No Reg	No Reg	No Reg
GMPE	**Regionalization Model with Lowest AIC Score for M ≥ 3.75 Residuals for Frequency of:**					
	25 Hz	**10 Hz**	**5 Hz**	**2.5 Hz**	**1 Hz**	**0.5 Hz**
A08'	Both	Both	No Reg	No Reg	No Reg	No Reg
AB06'	Both	OA Only	No Reg	No Reg	No Reg	No Reg
FEL	Both	OA Only	No Reg	No Reg	No Reg	OA Only
PZT	Both	OA Only	No Reg	No Reg	No Reg	No Reg
SDCS	Both	OA Only	No Reg	No Reg	No Reg	No Reg
SSCCSS	Both	OA Only	No Reg	No Reg	No Reg	No Reg
SSCVS	Both	OA Only	No Reg	No Reg	No Reg	No Reg
SEL	NE Only	OA Only	No Reg	No Reg	No Reg	No Reg
TEL	Both	OA Only	No Reg	No Reg	No Reg	OA Only

Table 7.4.2-1 (page 2 of 2)
Results of Statistical Analysis of Regionalization

GMPE	Regionalization Model with Lowest BIC Score for M ≥ 4.75 Residuals for Frequency of:					
	25 Hz	**10 Hz**	**5 Hz**	**2.5 Hz**	**1 Hz**	**0.5 Hz**
A08'	NE Only	No Reg	NE Only	No Reg	No Reg	Both
AB06'	No Reg	No Reg	No Reg	No Reg	No Reg	No Reg
FEL	No Reg	No Reg	No Reg	No Reg	No Reg	No Reg
PZT	No Reg	No Reg	No Reg	No Reg	No Reg	No Reg
SDCS	No Reg	No Reg	No Reg	No Reg	No Reg	No Reg
SSCCSS	NE Only	No Reg	No Reg	No Reg	No Reg	No Reg
SSCVS	No Reg	No Reg	No Reg	No Reg	No Reg	No Reg
SEL	No Reg	No Reg	No Reg	No Reg	No Reg	No Reg
TEL	No Reg	No Reg	No Reg	No Reg	No Reg	No Reg
GMPE	**Regionalization Model with Lowest BIC Score for M ≥ 3.75 Residuals for Frequency of:**					
	25 Hz	**10 Hz**	**5 Hz**	**2.5 Hz**	**1 Hz**	**0.5 Hz**
A08'	OA Only	No Reg	No Reg	No Reg	No Reg	No Reg
AB06'	NE Only	No Reg	No Reg	No Reg	No Reg	No Reg
FEL	NE Only	No Reg	No Reg	No Reg	No Reg	No Reg
PZT	NE Only	No Reg	No Reg	No Reg	No Reg	No Reg
SDCS	Both	No Reg	No Reg	No Reg	No Reg	No Reg
SSCCSS	Both	No Reg	No Reg	No Reg	No Reg	No Reg
SSCVS	Both	No Reg	No Reg	No Reg	No Reg	No Reg
SEL	NE Only	No Reg	No Reg	No Reg	No Reg	No Reg
TEL	NE Only	No Reg	No Reg	No Reg	No Reg	No Reg

Table 7.5.2-1
Soft Rock Scaling Factors Used for Empirical Site Adjustments

GMPE	Soft-Rock Scaling Factor C_{SR} for Frequency of:					
	25 Hz	**10 Hz**	**5 Hz**	**2.5 Hz**	**1 Hz**	**0.5 Hz**
SSCCSC	0.43 ± 0.17	0.11 ± 0.14	0.09 ± 0.13	0.25 ± 0.13	0.34 ± 0.13	0.59 ± 0.12
SSCVS	0.44 ± 0.17	0.10 ± 0.14	0.09 ± 0.13	0.25 ± 0.13	0.34 ± 0.12	0.59 ± 0.12
TEL	0.44 ± 0.16	0.12 ± 0.13	0.12 ± 0.13	0.27 ± 0.12	0.34 ± 0.11	0.57 ± 0.11
FEL	0.46 ± 0.16	0.16 ± 0.13	0.15 ± 0.12	0.30 ± 0.12	0.36 ± 0.11	0.58 ± 0.11
A08'	0.35 ± 0.15	0.16 ± 0.13	0.15 ± 0.12	0.29 ± 0.11	0.34 ± 0.12	0.60 ± 0.11
SDCS	0.44 ± 0.17	0.11 ± 0.14	0.10 ± 0.13	0.25 ± 0.13	0.34 ± 0.13	0.59 ± 0.12
AB06'	0.50 ± 0.17	0.19 ± 0.14	0.16 ± 0.13	0.30 ± 0.12	0.35 ± 0.12	0.56 ± 0.11
PZT	0.49 ± 0.17	0.20 ± 0.15	0.17 ± 0.13	0.31 ± 0.12	0.36 ± 0.12	0.56 ± 0.11
SEL	0.43 ± 0.18	0.18 ± 0.14	0.16 ± 0.12	0.31 ± 0.12	0.38 ± 0.13	0.63 ± 0.13

Table 7.5.3-1
Calculation of GMPE Weights for Cluster 1, 25 Hz Spectral Acceleration, Using the Analytical Adjustment for Site Conditions

Mmin	Mmax	Rmin	Rmax	Equiv. Sample Size	Importance Factor	Exponent	SSCCSS	SSCVS	TEL	FEL
3.75	4.75	0	70	6.7	0.250	0.1355	1.000	0.451	0.101	0.066
3.75	4.75	70	150	2.2	0.083	0.0833	0.953	0.922	0.778	0.680
3.75	4.75	150	500	7.3	0.042	0.0207	1.000	0.907	0.723	0.645
4.75	-	0	70	3.6	1.000	1.0000	0.533	0.227	0.231	0.009
4.75	-	70	150	1.4	0.333	0.3333	0.630	0.658	0.676	0.538
4.75	-	150	500	3.1	0.167	0.1667	0.819	0.786	0.876	0.451
						Raw Product	0.131	0.022	0.008	0.000
						Normalized	0.814	0.137	0.048	0.000

Table 7.5.3-2
Calculation of GMPE Weights for Cluster 1, 25 Hz Spectral Acceleration, Using the Empirical Adjustment for Site Conditions

Mmin	Mmax	Rmin	Rmax	Equiv. Sample Size	Importance Factor	Exponent	SSCCSS	SSCVS	TEL	FEL
3.75	4.75	0	70	24.7	0.250	0.1144	0.999	0.591	0.083	0.084
3.75	4.75	70	150	9.2	0.083	0.0833	0.737	0.860	0.976	0.795
3.75	4.75	150	500	30.6	0.042	0.0154	1.000	0.846	0.544	0.457
4.75	-	0	70	11.3	1.000	1.0000	0.561	0.266	0.171	0.002
4.75	-	70	150	4.1	0.333	0.3333	0.394	0.503	0.491	0.885
4.75	-	150	500	12.6	0.167	0.1497	0.732	0.562	0.977	0.337
						Raw Product	0.060	0.016	0.004	0.000
						Normalized	**0.751**	**0.203**	**0.045**	**0.000**

Table 7.5.3-3
Calculation of GMPE Weights for Cluster 1, 10 Hz Spectral Acceleration, Using the Analytical Adjustment for Site Conditions

Mmin	Mmax	Rmin	Rmax	Equiv. Sample Size	Importance Factor	Exponent	SSCCSS	SSCVS	TEL	FEL
3.75	4.75	0	70	9.0	0.250	0.1103	0.999	0.598	0.140	0.266
3.75	4.75	70	150	5.9	0.083	0.0561	0.961	0.961	0.724	0.735
3.75	4.75	150	500	21.1	0.042	0.0078	1.000	0.926	0.650	0.801
4.75	-	0	70	4.0	1.000	1.0000	0.358	0.254	0.252	0.136
4.75	-	70	150	2.5	0.333	0.3333	0.668	0.680	0.627	0.520
4.75	-	150	500	6.7	0.167	0.0984	0.887	0.892	0.903	0.725
						Raw Product	0.102	0.041	0.009	0.008
						Normalized	**0.636**	**0.256**	**0.059**	**0.050**

Table 7.5.3-4
Calculation of GMPE Weights for Cluster 1, 10 Hz Spectral Acceleration, Using the Empirical Adjustment for Site Conditions

Mmin	Mmax	Rmin	Rmax	Equiv. Sample Size	Importance Factor	Exponent	SSCCSS	SSCVS	TEL	FEL
3.75	4.75	0	70	28.6	0.250	0.1039	0.989	0.789	0.128	0.362
3.75	4.75	70	150	30.3	0.083	0.0327	0.878	0.999	0.728	0.777
3.75	4.75	150	500	69.4	0.042	0.0071	1.000	0.953	0.636	0.950
4.75	-	0	70	11.9	1.000	1.0000	0.093	0.195	0.419	0.292
4.75	-	70	150	6.9	0.333	0.3333	0.341	0.478	0.606	0.857
4.75	-	150	500	15.3	0.167	0.1292	0.182	0.201	0.671	0.994
						Raw Product	0.003	0.007	0.010	0.067
						Normalized	**0.029**	**0.082**	**0.118**	**0.771**

Table 7.5.3-5
Calculation of GMPE Weights for Cluster 1, 5 Hz Spectral Acceleration, Using the Analytical Adjustment for Site Conditions

Mmin	Mmax	Rmin	Rmax	Equiv. Sample Size	Importance Factor	Exponent	SSCCSS	SSCVS	TEL	FEL
3.75	4.75	0	70	9.7	0.250	0.1033	0.999	0.624	0.030	0.134
3.75	4.75	70	150	6.8	0.083	0.0494	0.966	0.967	0.540	0.630
3.75	4.75	150	500	24.3	0.042	0.0069	1.000	0.969	0.555	0.704
4.75	-	0	70	4.0	1.000	1.0000	0.574	0.294	0.068	0.063
4.75	-	70	150	2.5	0.333	0.3333	0.665	0.693	0.585	0.557
4.75	-	150	500	7.2	0.167	0.0933	0.880	0.939	0.866	0.704
						Raw Product	0.162	0.056	0.000	0.001
						Normalized	**0.738**	**0.254**	**0.001**	**0.007**

Table 7.5.3-6
Calculation of GMPE Weights for Cluster 1, 5 Hz Spectral Acceleration, Using the Empirical Adjustment for Site Conditions

Mmin	Mmax	Rmin	Rmax	Equiv. Sample Size	Importance Factor	Exponent	SSCCSS	SSCVS	TEL	FEL
3.75	4.75	0	70	31.1	0.250	0.0988	1.000	0.586	0.002	0.041
3.75	4.75	70	150	34.3	0.083	0.0299	0.894	0.999	0.380	0.533
3.75	4.75	150	500	86.7	0.042	0.0059	0.947	1.000	0.420	0.673
4.75	-	0	70	12.3	1.000	1.0000	0.335	0.299	0.257	0.110
4.75	-	70	150	8.6	0.333	0.3333	0.079	0.133	0.403	0.977
4.75	-	150	500	17.1	0.167	0.1201	0.133	0.202	0.826	0.973
						Raw Product	0.001	0.002	0.000	0.002
						Normalized	**0.276**	**0.435**	**0.005**	**0.284**

Table 7.5.3-7
Calculation of GMPE Weights for Cluster 1, 2.5 Hz Spectral Acceleration, Using the Analytical Adjustment for Site Conditions

Mmin	Mmax	Rmin	Rmax	Equiv. Sample Size	Importance Factor	Exponent	SSCCSS	SSCVS	TEL	FEL
3.75	4.75	0	70	9.8	0.250	0.1113	0.985	0.793	0.114	0.110
3.75	4.75	70	150	7.2	0.250	0.1513	0.901	0.900	0.218	0.142
3.75	4.75	150	500	27.0	0.083	0.0134	0.971	0.998	0.434	0.416
4.75	-	0	70	4.4	1.000	1.0000	0.560	0.325	0.062	0.053
4.75	-	70	150	2.6	1.000	1.0000	0.251	0.305	0.282	0.162
4.75	-	150	500	7.6	1.000	0.5719	0.455	0.724	0.364	0.065
						Raw Product	0.028	0.026	0.000	0.000
						Normalized	**0.517**	**0.481**	**0.001**	**0.000**

Table 7.5.3-8
Calculation of GMPE Weights for Cluster 1, 2.5 Hz Spectral Acceleration, Using the Empirical Adjustment for Site Conditions

Mmin	Mmax	Rmin	Rmax	Equiv. Sample Size	Importance Factor	Exponent	SSCCSS	SSCVS	TEL	FEL
3.75	4.75	0	70	31.4	0.250	0.1045	0.998	0.649	0.006	0.006
3.75	4.75	70	150	35.1	0.250	0.0935	0.940	0.934	0.014	0.004
3.75	4.75	150	500	91.1	0.083	0.0120	0.760	1.000	0.253	0.212
4.75	-	0	70	13.1	1.000	1.0000	0.717	0.251	0.025	0.007
4.75	-	70	150	8.9	1.000	1.0000	0.056	0.134	0.543	0.267
4.75	-	150	500	18.0	1.000	0.7287	0.000	0.000	0.868	0.283
						Raw Product	0.000	0.000	0.000	0.000
						Normalized	**0.062**	**0.868**	**0.069**	**0.001**

Table 7.5.3-9
Calculation of GMPE Weights for Cluster 1, 1 Hz Spectral Acceleration, Using the Analytical Adjustment for Site Conditions

Mmin	Mmax	Rmin	Rmax	Equiv. Sample Size	Importance Factor	Exponent	SSCCSS	SSCVS	TEL	FEL
3.75	4.75	0	70	10.7	0.250	0.1070	0.925	0.932	0.176	0.333
3.75	4.75	70	150	7.6	0.250	0.1503	0.908	0.894	0.136	0.115
3.75	4.75	150	500	28.3	0.083	0.0135	0.928	1.000	0.520	0.538
4.75	-	0	70	4.6	1.000	1.0000	0.507	0.373	0.047	0.073
4.75	-	70	150	2.8	1.000	1.0000	0.520	0.454	0.019	0.008
4.75	-	150	500	7.7	1.000	0.5973	0.544	0.750	0.098	0.013
						Raw Product	0.056	0.053	0.000	0.000
						Normalized	**0.514**	**0.486**	**0.000**	**0.000**

Table 7.5.3-10
Calculation of GMPE Weights for Cluster 1, 1 Hz Spectral Acceleration, Using the Empirical Adjustment for Site Conditions

Mmin	Mmax	Rmin	Rmax	Equiv. Sample Size	Importance Factor	Exponent	SSCCSS	SSCVS	TEL	FEL
3.75	4.75	0	70	29.4	0.250	0.1000	0.920	0.944	0.012	0.065
3.75	4.75	70	150	33.8	0.250	0.0872	0.944	0.939	0.010	0.007
3.75	4.75	150	500	83.7	0.083	0.0117	0.775	1.000	0.294	0.295
4.75	-	0	70	11.8	1.000	1.0000	0.690	0.300	0.004	0.006
4.75	-	70	150	9.0	1.000	1.0000	0.448	0.517	0.029	0.006
4.75	-	150	500	16.4	1.000	0.7188	0.053	0.270	0.865	0.018
						Raw Product	0.006	0.019	0.000	0.000
						Normalized	**0.230**	**0.770**	**0.000**	**0.000**

Table 7.5.3-11
Calculation of GMPE Weights for Cluster 1, 0.5 Hz Spectral Acceleration, Using the Analytical Adjustment for Site Conditions

Mmin	Mmax	Rmin	Rmax	Equiv. Sample Size	Importance Factor	Exponent	SSCCSS	SSCVS	TEL	FEL
3.75	4.75	0	70	9.0	0.250	0.1233	0.875	0.872	0.618	0.866
3.75	4.75	70	150	7.4	0.250	0.1499	0.897	0.886	0.487	0.655
3.75	4.75	150	500	23.4	0.083	0.0158	0.942	0.996	0.835	0.974
4.75	-	0	70	4.4	1.000	1.0000	0.314	0.257	0.086	0.343
4.75	-	70	150	2.8	1.000	1.0000	0.451	0.413	0.069	0.067
4.75	-	150	500	7.0	1.000	0.6329	0.663	0.626	0.009	0.003
						Raw Product	0.035	0.026	0.000	0.000
						Normalized	**0.575**	**0.424**	**0.000**	**0.001**

Table 7.5.3-12
Calculation of GMPE Weights for Cluster 1, 0.5 Hz Spectral Acceleration, Using the Empirical Adjustment for Site Conditions

Mmin	Mmax	Rmin	Rmax	Equiv. Sample Size	Importance Factor	Exponent	SSCCSS	SSCVS	TEL	FEL
3.75	4.75	0	70	20.6	0.250	0.1043	0.864	0.886	0.257	0.918
3.75	4.75	70	150	27.2	0.250	0.0791	0.951	0.942	0.205	0.456
3.75	4.75	150	500	68.6	0.083	0.0105	0.883	1.000	0.657	0.894
4.75	-	0	70	8.6	1.000	1.0000	0.457	0.174	0.013	0.356
4.75	-	70	150	6.9	1.000	1.0000	0.598	0.401	0.001	0.000
4.75	-	150	500	13.6	1.000	0.6320	0.485	0.784	0.011	0.002
						Raw Product	0.048	0.023	0.000	0.000
						Normalized	**0.677**	**0.323**	**0.000**	**0.000**

Table 7.5.3-13
Combination of GMPE Weights for Cluster 1

	Analytical Site Adjustments				Empirical Site Adjustments			
	SSCCSS	**SSCVS**	**TEL**	**FEL**	**SSCCSS**	**SSCVS**	**TEL**	**FEL**
25 Hz	0.81	0.14	0.05	0.00	0.75	0.20	0.05	0.00
10 Hz	0.64	0.26	0.06	0.05	0.03	0.08	0.12	0.77
5 Hz	0.74	0.25	0.00	0.01	0.28	0.44	0.01	0.28
Combined HF	**0.84**	**0.16**	**0.01**	**0.00**	**0.44**	**0.47**	**0.04**	**0.05**
Comb. HF Analytical + Empirical	**0.64**	**0.31**	**0.022**	**0.026**				
2.5 Hz	0.52	0.48	0.00	0.00	0.06	0.87	0.07	0.00
1 Hz	0.51	0.49	0.00	0.00	0.23	0.77	0.00	0.00
0.5 Hz	0.57	0.42	0.00	0.00	0.68	0.32	0.00	0.00
Combined LF	**0.55**	**0.45**	**0.00**	**0.00**	**0.20**	**0.80**	**0.00**	**0.00**
Comb. LF Analytical + Empirical	**0.37**	**0.63**	**4.5E-06**	**8.8E-07**				

Table 7.5.3-14
Calculation of GMPE Weights for Cluster 2, 25 Hz Spectral Acceleration, Using the Analytical Adjustment for Site Conditions

Mmin	Mmax	Rmin	Rmax	Equiv. Sample Size	Importance Factor	Exponent	A08'	SDCS
3.75	4.75	0	70	6.7	0.250	0.1355	1.000	0.445
3.75	4.75	70	150	2.2	0.083	0.0833	0.936	0.951
3.75	4.75	150	500	7.3	0.042	0.0207	1.000	0.903
4.75	-	0	70	3.6	1.000	1.0000	0.028	0.972
4.75	-	70	150	1.4	0.333	0.3333	0.778	0.809
4.75	-	150	500	3.1	0.167	0.1667	0.833	0.935
						Raw Product	0.017	0.281
						Normalized	**0.057**	**0.943**

Table 7.5.3-15
Calculation of GMPE Weights for Cluster 2, 25 Hz Spectral Acceleration, Using the Empirical Adjustment for Site Conditions

Mmin	Mmax	Rmin	Rmax	Equiv. Sample Size	Importance Factor	Exponent	A08'	SDCS
3.75	4.75	0	70	24.7	0.250	0.1144	1.000	0.355
3.75	4.75	70	150	9.2	0.083	0.0833	0.618	1.000
3.75	4.75	150	500	30.6	0.042	0.0154	0.908	1.000
4.75	-	0	70	11.3	1.000	1.0000	0.167	0.833
4.75	-	70	150	4.1	0.333	0.3333	0.944	0.542
4.75	-	150	500	12.6	0.167	0.1497	1.000	0.147
						Raw Product	0.088	0.024
						Normalized	**0.788**	**0.212**

Table 7.5.3-16
Calculation of GMPE Weights for Cluster 2, 10 Hz Spectral Acceleration, Using the Analytical Adjustment for Site Conditions

Mmin	Mmax	Rmin	Rmax	Equiv. Sample Size	Importance Factor	Exponent	A08'	SDCS
3.75	4.75	0	70	9.0	0.250	0.1103	0.975	0.838
3.75	4.75	70	150	5.9	0.083	0.0561	0.911	0.988
3.75	4.75	150	500	21.1	0.042	0.0078	1.000	0.907
4.75	-	0	70	4.0	1.000	1.0000	0.200	0.800
4.75	-	70	150	2.5	0.333	0.3333	0.727	0.851
4.75	-	150	500	6.7	0.167	0.0984	0.592	1.000
						Raw Product	0.076	0.511
						Normalized	**0.130**	**0.870**

Table 7.5.3-17
Calculation of GMPE Weights for Cluster 2, 10 Hz Spectral Acceleration, Using the Empirical Adjustment for Site Conditions

Mmin	Mmax	Rmin	Rmax	Equiv. Sample Size	Importance Factor	Exponent	A08'	SDCS
3.75	4.75	0	70	28.6	0.250	0.1039	0.914	0.945
3.75	4.75	70	150	30.3	0.083	0.0327	0.814	1.000
3.75	4.75	150	500	69.4	0.042	0.0071	0.835	1.000
4.75	-	0	70	11.9	1.000	1.0000	0.893	0.107
4.75	-	70	150	6.9	0.333	0.3333	0.990	0.313
4.75	-	150	500	15.3	0.167	0.1292	1.000	0.220
						Raw Product	0.549	0.007
						Normalized	**0.987**	**0.013**

Table 7.5.3-18
Calculation of GMPE Weights for Cluster 2, 5 Hz Spectral Acceleration, Using the Analytical Adjustment for Site Conditions

Mmin	Mmax	Rmin	Rmax	Equiv. Sample Size	Importance Factor	Exponent	A08'	SDCS
3.75	4.75	0	70	9.7	0.250	0.1033	1.000	0.458
3.75	4.75	70	150	6.8	0.083	0.0494	0.932	0.986
3.75	4.75	150	500	24.3	0.042	0.0069	0.969	1.000
4.75	-	0	70	4.0	1.000	1.0000	0.333	0.667
4.75	-	70	150	2.5	0.333	0.3333	0.808	0.779
4.75	-	150	500	7.2	0.167	0.0933	0.788	0.993
						Raw Product	0.192	0.233
						Normalized	**0.452**	**0.548**

Table 7.5.3-19
Calculation of GMPE Weights for Cluster 2, 5 Hz Spectral Acceleration, Using the Empirical Adjustment for Site Conditions

Mmin	Mmax	Rmin	Rmax	Equiv. Sample Size	Importance Factor	Exponent	A08'	SDCS
3.75	4.75	0	70	31.1	0.250	0.0988	1.000	0.351
3.75	4.75	70	150	34.3	0.083	0.0299	0.791	1.000
3.75	4.75	150	500	86.7	0.042	0.0059	0.642	1.000
4.75	-	0	70	12.3	1.000	1.0000	0.788	0.212
4.75	-	70	150	8.6	0.333	0.3333	1.000	0.045
4.75	-	150	500	17.1	0.167	0.1201	1.000	0.213
						Raw Product	0.400	0.001
						Normalized	**0.998**	**0.002**

Table 7.5.3-20
Calculation of GMPE Weights for Cluster 2, 2.5 Hz Spectral Acceleration, Using the Analytical Adjustment for Site Conditions

Mmin	Mmax	Rmin	Rmax	Equiv. Sample Size	Importance Factor	Exponent	A08'	SDCS
3.75	4.75	0	70	9.8	0.250	0.1113	0.997	0.668
3.75	4.75	70	150	7.2	0.250	0.1513	0.802	0.961
3.75	4.75	150	500	27.0	0.083	0.0134	0.895	1.000
4.75	-	0	70	4.4	1.000	1.0000	0.516	0.484
4.75	-	70	150	2.6	1.000	1.0000	0.578	0.422
4.75	-	150	500	7.6	1.000	0.5719	0.963	0.208
						Raw Product	0.205	0.027
						Normalized	**0.882**	**0.118**

Table 7.5.3-21
Calculation of GMPE Weights for Cluster 2, 2.5 Hz Spectral Acceleration, Using the Empirical Adjustment for Site Conditions

Mmin	Mmax	Rmin	Rmax	Equiv. Sample Size	Importance Factor	Exponent	A08'	SDCS
3.75	4.75	0	70	31.4	0.250	0.1045	1.000	0.491
3.75	4.75	70	150	35.1	0.250	0.0935	0.739	0.996
3.75	4.75	150	500	91.1	0.083	0.0120	0.570	1.000
4.75	-	0	70	13.1	1.000	1.0000	0.757	0.243
4.75	-	70	150	8.9	1.000	1.0000	0.998	0.002
4.75	-	150	500	18.0	1.000	0.7287	1.000	0.000
						Raw Product	0.318	0.000
						Normalized	**1.000**	**0.000**

Table 7.5.3-22
Calculation of GMPE Weights for Cluster 2, 1 Hz Spectral Acceleration, Using the Analytical Adjustment for Site Conditions

Mmin	Mmax	Rmin	Rmax	Equiv. Sample Size	Importance Factor	Exponent	A08'	SDCS
3.75	4.75	0	70	10.7	0.250	0.1070	0.865	0.969
3.75	4.75	70	150	7.6	0.250	0.1503	0.553	0.997
3.75	4.75	150	500	28.3	0.083	0.0135	0.703	1.000
4.75	-	0	70	4.6	1.000	1.0000	0.490	0.510
4.75	-	70	150	2.8	1.000	1.0000	0.492	0.508
4.75	-	150	500	7.7	1.000	0.5973	0.999	0.015
						Raw Product	0.081	0.004
						Normalized	**0.955**	**0.045**

Table 7.5.3-23
Calculation of GMPE Weights for Cluster 2, 1 Hz Spectral Acceleration, Using the Empirical Adjustment for Site Conditions

Mmin	Mmax	Rmin	Rmax	Equiv. Sample Size	Importance Factor	Exponent	A08'	SDCS
3.75	4.75	0	70	29.4	0.250	0.1000	0.873	0.971
3.75	4.75	70	150	33.8	0.250	0.0872	0.339	1.000
3.75	4.75	150	500	83.7	0.083	0.0117	0.396	1.000
4.75	-	0	70	11.8	1.000	1.0000	0.717	0.283
4.75	-	70	150	9.0	1.000	1.0000	1.000	0.000
4.75	-	150	500	16.4	1.000	0.7188	1.000	0.000
						Raw Product	0.084	0.000
						Normalized	**1.000**	**0.000**

Table 7.5.3-24
Calculation of GMPE Weights for Cluster 2, 0.5 Hz Spectral Acceleration, Using the Analytical Adjustment for Site Conditions

Mmin	Mmax	Rmin	Rmax	Equiv. Sample Size	Importance Factor	Exponent	A08'	SDCS
3.75	4.75	0	70	9.0	0.250	0.1233	0.785	0.981
3.75	4.75	70	150	7.4	0.250	0.1499	0.408	1.000
3.75	4.75	150	500	23.4	0.083	0.0158	0.593	1.000
4.75	-	0	70	4.4	1.000	1.0000	0.512	0.488
4.75	-	70	150	2.8	1.000	1.0000	0.500	0.500
4.75	-	150	500	7.0	1.000	0.6329	0.890	0.324
						Raw Product	0.043	0.078
						Normalized	**0.358**	**0.642**

Table 7.5.3-25
Calculation of GMPE Weights for Cluster 2, 0.5 Hz Spectral Acceleration, Using the Empirical Adjustment for Site Conditions

Mmin	Mmax	Rmin	Rmax	Equiv. Sample Size	Importance Factor	Exponent	A08'	SDCS
3.75	4.75	0	70	20.6	0.250	0.1051	0.893	0.957
3.75	4.75	70	150	27.8	0.250	0.0781	0.361	1.000
3.75	4.75	150	500	69.6	0.083	0.0104	0.392	1.000
4.75	-	0	70	8.7	1.000	1.0000	0.313	0.687
4.75	-	70	150	6.9	1.000	1.0000	0.590	0.410
4.75	-	150	500	13.7	1.000	0.6348	1.000	0.001
						Raw Product	0.023	0.000
						Normalized	**0.987**	**0.013**

Table 7.5.3-26
Combination of GMPE Weights for Cluster 2

	Analytical Site Adjustments		Empirical Site Adjustments	
	A08′	**SDCS**	**A08′**	**SDCS**
25 Hz	0.06	0.94	0.79	0.21
10 Hz	0.13	0.87	0.99	0.01
5 Hz	0.45	0.55	1.00	0.00
Combined HF	**0.10**	**0.90**	**1.00**	**0.00**
Comb. HF Analytical + Empirical	**0.55**	**0.45**		
2.5 Hz	0.88	0.12	1.00	0.00
1 Hz	0.95	0.05	1.00	0.00
0.5 Hz	0.36	0.64	0.99	0.01
Combined LF	**0.88**	**0.12**	**1.00**	**0.00**
Comb. LF Analytical + Empirical	**0.94**	**0.06**		

Table 7.5.3-27
Calculation of GMPE Weights for Cluster 3, 25 Hz Spectral Acceleration, Using the Analytical Adjustment for Site Conditions

Mmin	Mmax	Rmin	Rmax	Equiv. Sample Size	Importance Factor	Exponent	AB06'	PZT
3.75	4.75	0	70	6.7	0.250	0.1355	1.000	0.068
3.75	4.75	70	150	2.2	0.083	0.0833	0.989	0.843
3.75	4.75	150	500	7.3	0.042	0.0207	1.000	0.811
4.75	-	0	70	3.6	1.000	1.0000	0.793	0.207
4.75	-	70	150	1.4	0.333	0.3333	0.800	0.787
4.75	-	150	500	3.1	0.167	0.1667	0.928	0.844
						Raw Product	0.583	0.006
						Normalized	**0.989**	**0.011**

Table 7.5.3-28
Calculation of GMPE Weights for Cluster 3, 25 Hz Spectral Acceleration, Using the Empirical Adjustment for Site Conditions

Mmin	Mmax	Rmin	Rmax	Equiv. Sample Size	Importance Factor	Exponent	AB06'	PZT
3.75	4.75	0	70	24.7	0.250	0.1144	1.000	0.132
3.75	4.75	70	150	9.2	0.083	0.0833	0.862	0.985
3.75	4.75	150	500	30.6	0.042	0.0154	1.000	0.653
4.75	-	0	70	11.3	1.000	1.0000	0.109	0.891
4.75	-	70	150	4.1	0.333	0.3333	0.624	0.911
4.75	-	150	500	12.6	0.167	0.1497	0.993	0.631
						Raw Product	0.058	0.043
						Normalized	**0.573**	**0.427**

Table 7.5.3-29
Calculation of GMPE Weights for Cluster 3, 10 Hz Spectral Acceleration, Using the Analytical Adjustment for Site Conditions

Mmin	Mmax	Rmin	Rmax	Equiv. Sample Size	Importance Factor	Exponent	AB06'	PZT
3.75	4.75	0	70	9.0	0.250	0.1103	1.000	0.326
3.75	4.75	70	150	5.9	0.083	0.0561	0.998	0.835
3.75	4.75	150	500	21.1	0.042	0.0078	1.000	0.805
4.75	-	0	70	4.0	1.000	1.0000	0.505	0.495
4.75	-	70	150	2.5	0.333	0.3333	0.820	0.765
4.75	-	150	500	6.7	0.167	0.0984	0.960	0.898
						Raw Product	0.397	0.075
						Normalized	**0.842**	**0.158**

Table 7.5.3-30
Calculation of GMPE Weights for Cluster 3, 10 Hz Spectral Acceleration, Using the Empirical Adjustment for Site Conditions

Mmin	Mmax	Rmin	Rmax	Equiv. Sample Size	Importance Factor	Exponent	AB06'	PZT
3.75	4.75	0	70	28.6	0.250	0.1039	1.000	0.515
3.75	4.75	70	150	30.3	0.083	0.0327	1.000	0.822
3.75	4.75	150	500	69.4	0.042	0.0071	1.000	0.725
4.75	-	0	70	11.9	1.000	1.0000	0.345	0.655
4.75	-	70	150	6.9	0.333	0.3333	0.821	0.764
4.75	-	150	500	15.3	0.167	0.1292	0.894	0.932
						Raw Product	0.253	0.143
						Normalized	**0.638**	**0.362**

Table 7.5.3-31
Calculation of GMPE Weights for Cluster 3, 5 Hz Spectral Acceleration, Using the Analytical Adjustment for Site Conditions

Mmin	Mmax	Rmin	Rmax	Equiv. Sample Size	Importance Factor	Exponent	AB06'	PZT
3.75	4.75	0	70	9.7	0.250	0.1033	1.000	0.220
3.75	4.75	70	150	6.8	0.083	0.0494	0.999	0.835
3.75	4.75	150	500	24.3	0.042	0.0069	1.000	0.798
4.75	-	0	70	4.0	1.000	1.0000	0.601	0.399
4.75	-	70	150	2.5	0.333	0.3333	0.808	0.779
4.75	-	150	500	7.2	0.167	0.0933	0.982	0.852
						Raw Product	0.476	0.039
						Normalized	**0.925**	**0.075**

Table 7.5.3-32
Calculation of GMPE Weights for Cluster 3, 5 Hz Spectral Acceleration, Using the Empirical Adjustment for Site Conditions

Mmin	Mmax	Rmin	Rmax	Equiv. Sample Size	Importance Factor	Exponent	AB06'	PZT
3.75	4.75	0	70	31.1	0.250	0.0988	1.000	0.144
3.75	4.75	70	150	34.3	0.083	0.0299	0.999	0.902
3.75	4.75	150	500	86.7	0.042	0.0059	1.000	0.701
4.75	-	0	70	12.3	1.000	1.0000	0.321	0.679
4.75	-	70	150	8.6	0.333	0.3333	0.592	0.926
4.75	-	150	500	17.1	0.167	0.1201	0.861	0.960
						Raw Product	0.163	0.055
						Normalized	**0.748**	**0.252**

Table 7.5.3-33
Calculation of GMPE Weights for Cluster 3, 2.5 Hz Spectral Acceleration, Using the Analytical Adjustment for Site Conditions

Mmin	Mmax	Rmin	Rmax	Equiv. Sample Size	Importance Factor	Exponent	AB06'	PZT
3.75	4.75	0	70	9.8	0.250	0.1113	1.000	0.310
3.75	4.75	70	150	7.2	0.250	0.1513	0.966	0.787
3.75	4.75	150	500	27.0	0.083	0.0134	1.000	0.750
4.75	-	0	70	4.4	1.000	1.0000	0.495	0.505
4.75	-	70	150	2.6	1.000	1.0000	0.489	0.511
4.75	-	150	500	7.6	1.000	0.5719	0.792	0.535
						Raw Product	0.185	0.025
						Normalized	**0.880**	**0.120**

Table 7.5.3-34
Calculation of GMPE Weights for Cluster 3, 2.5 Hz Spectral Acceleration, Using the Empirical Adjustment for Site Conditions

Mmin	Mmax	Rmin	Rmax	Equiv. Sample Size	Importance Factor	Exponent	AB06'	PZT
3.75	4.75	0	70	31.4	0.250	0.1045	1.000	0.151
3.75	4.75	70	150	35.1	0.250	0.0935	1.000	0.589
3.75	4.75	150	500	91.1	0.083	0.0120	1.000	0.637
4.75	-	0	70	13.1	1.000	1.0000	0.507	0.493
4.75	-	70	150	8.9	1.000	1.0000	0.605	0.395
4.75	-	150	500	18.0	1.000	0.7287	0.511	0.691
						Raw Product	0.157	0.008
						Normalized	**0.954**	**0.046**

Table 7.5.3-35
Calculation of GMPE Weights for Cluster 3, 1 Hz Spectral Acceleration, Using the Analytical Adjustment for Site Conditions

Mmin	Mmax	Rmin	Rmax	Equiv. Sample Size	Importance Factor	Exponent	AB06'	PZT
3.75	4.75	0	70	10.7	0.250	0.1070	0.938	0.918
3.75	4.75	70	150	7.6	0.250	0.1503	0.848	0.941
3.75	4.75	150	500	28.3	0.083	0.0135	1.000	0.952
4.75	-	0	70	4.6	1.000	1.0000	0.533	0.467
4.75	-	70	150	2.8	1.000	1.0000	0.532	0.468
4.75	-	150	500	7.7	1.000	0.5973	0.675	0.647
						Raw Product	0.152	0.116
						Normalized	**0.567**	**0.433**

Table 7.5.3-36
Calculation of GMPE Weights for Cluster 3, 1 Hz Spectral Acceleration, Using the Empirical Adjustment for Site Conditions

Mmin	Mmax	Rmin	Rmax	Equiv. Sample Size	Importance Factor	Exponent	AB06'	PZT
3.75	4.75	0	70	29.4	0.250	0.1000	0.723	0.996
3.75	4.75	70	150	33.8	0.250	0.0872	0.729	0.998
3.75	4.75	150	500	83.7	0.083	0.0117	1.000	0.947
4.75	-	0	70	11.8	1.000	1.0000	0.528	0.472
4.75	-	70	150	9.0	1.000	1.0000	0.700	0.300
4.75	-	150	500	16.4	1.000	0.7188	0.506	0.703
						Raw Product	0.099	0.094
						Normalized	**0.513**	**0.487**

Table 7.5.3-37
Calculation of GMPE Weights for Cluster 3, 0.5 Hz Spectral Acceleration, Using the Analytical Adjustment for Site Conditions

Mmin	Mmax	Rmin	Rmax	Equiv. Sample Size	Importance Factor	Exponent	AB06'	PZT
3.75	4.75	0	70	9.0	0.250	0.1233	0.868	0.954
3.75	4.75	70	150	7.4	0.250	0.1499	0.807	0.960
3.75	4.75	150	500	23.4	0.083	0.0158	0.978	0.996
4.75	-	0	70	4.4	1.000	1.0000	0.608	0.392
4.75	-	70	150	2.8	1.000	1.0000	0.565	0.435
4.75	-	150	500	7.0	1.000	0.6329	0.616	0.673
						Raw Product	0.145	0.105
						Normalized	**0.580**	**0.420**

Table 7.5.3-38
Calculation of GMPE Weights for Cluster 3, 0.5 Hz Spectral Acceleration, Using the Empirical Adjustment for Site Conditions

Mmin	Mmax	Rmin	Rmax	Equiv. Sample Size	Importance Factor	Exponent	AB06'	PZT
3.75	4.75	0	70	20.6	0.250	0.1051	0.724	0.995
3.75	4.75	70	150	27.8	0.250	0.0781	0.795	0.996
3.75	4.75	150	500	69.6	0.083	0.0104	0.972	0.999
4.75	-	0	70	8.7	1.000	1.0000	0.584	0.416
4.75	-	70	150	6.9	1.000	1.0000	0.706	0.294
4.75	-	150	500	13.7	1.000	0.6348	0.633	0.655
						Raw Product	0.146	0.079
						Normalized	**0.649**	**0.351**

Table 7.5.3-39
Combination of GMPE Weights for Cluster 3

	Analytical Site Adjustments		Empirical Site Adjustments	
	AB06'	**PZT**	**AB06'**	**PZT**
25 Hz	0.99	0.01	0.57	0.43
10 Hz	0.84	0.16	0.64	0.36
5 Hz	0.92	0.08	0.75	0.25
Combined HF	**0.98**	**0.02**	**0.70**	**0.30**
Comb. HF Analytical + Empirical	**0.84**	**0.16**		
2.5 Hz	0.88	0.12	0.95	0.05
1 Hz	0.57	0.43	0.51	0.49
0.5 Hz	0.58	0.42	0.65	0.35
Combined LF	**0.76**	**0.24**	**0.84**	**0.16**
Comb. LF Analytical + Empirical	**0.80**	**0.20**		

Table 7.5.3-40
Raw and Moderated Within-Cluster Weights

Raw Weights

Cluster	1				2		3	
GMPE	**SSCCSS**	**SSCVS**	**TEL**	**FEL**	**A08'**	**SDCS**	**AB06'**	**PZT**
HF Weight	0.64	0.31	2.2E-02	2.6E-02	0.55	0.45	0.84	0.16
LF Weight	0.37	0.63	4.5E-06	8.8E-07	0.94	0.06	0.80	0.20

Moderated Weights

Cluster	1				2		3	
GMPE	**SSCCSS**	**SSCVS**	**TEL**	**FEL**	**A08'**	**SDCS**	**AB06'**	**PZT**
HF Weight	0.344	0.322	0.181	0.152	0.548	0.452	0.667	0.333
LF Weight	0.343	0.324	0.175	0.159	0.667	0.333	0.667	0.333

Table 7.7.1-1
Parameters of Data Constraint Within-Cluster Standard Deviation

Ground-Motion Parameter	P1	P2	P3	P4
PGA	0.22	0.18	0.12	2.63e-04
25 Hz PSA	0.22	0.18	0.12	2.63e-04
10 Hz PSA	0.22	0.18	0.12	2.63e-04
5 Hz PSA	0.21	0.16	0.11	2.11e-04
2.5 Hz PSA	0.21	0.16	0.11	2.10e-04
1 Hz PSA	0.22	0.17	0.11	2.15e-04
0.5 Hz PSA	0.24	0.18	0.12	2.28e-04

Table 7.7.1-2
Magnitude Scaling Variability Across All GMPEs

Joyner-Boore Distance (km)	$\sigma_{\ln(MSF)}(\mathbf{M}=8)$			$\frac{\text{Cluster}-\text{to}-\text{cluster}\ \sigma^2_{\ln(MSF)}(\mathbf{M}=8)}{\text{Total}\ \sigma^2_{\ln(MSF)}(\mathbf{M}=8)}$
	Total Across All Nine GMPEs	**Across Cluster 1-4 Medians**	**Computed Residual Intra-cluster**	
1	0.59	0.58	0.11	0.97
5	0.48	0.45	0.17	0.88
10	0.43	0.41	0.13	0.91
20	0.38	0.39	0.00	1.05
30	0.36	0.37	0.00	1.06
50	0.34	0.35	0.00	1.06
70	0.36	0.34	0.12	0.89
100	0.41	0.38	0.15	0.90
140	0.48	0.44	0.19	0.84
200	0.53	0.46	0.26	0.79
300	0.60	0.50	0.33	0.69
500	0.70	0.57	0.41	0.64

Table 7.7.1-3
Magnitude Scaling Variability Across Cluster 1-3 GMPEs

Joyner-Boore Distance (km)	$\sigma_{\ln(MSF)}(\mathbf{M}=8)$			$\frac{\text{Cluster}-\text{to}-\text{cluster}\ \sigma^2_{\ln(MSF)}(\mathbf{M}=8)}{\text{Total}\ \sigma^2_{\ln(MSF)}(\mathbf{M}=8)}$
	Total Across Cluster 1-3 GMPEs	Across Cluster 1-3 Medians	Computed Residual Intra-cluster	
1	0.56	0.47	0.30	0.70
5	0.41	0.29	0.29	0.50
10	0.36	0.21	0.29	0.34
20	0.31	0.22	0.22	0.50
30	0.29	0.22	0.19	0.58
50	0.29	0.23	0.18	0.63
70	0.32	0.24	0.21	0.56
100	0.39	0.32	0.22	0.67
140	0.47	0.40	0.25	0.72
200	0.53	0.45	0.28	0.72
300	0.61	0.50	0.35	0.67
500	0.72	0.58	0.43	0.65

Table 7.9-1
Calculation of Data-Consistency Cluster Weights for 25 Hz Spectral Acceleration, Using the Analytical Adjustment for Site Conditions

Mmin	Mmax	Rmin	Rmax	Equiv. Sample Size	Importance Factor	Exponent	Cluster 1	Cluster 2	Cluster 3	Cluster 4
3.75	4.75	0	70	6.7	0.250	0.1355	0.064	0.142	0.346	1.000
3.75	4.75	70	150	2.2	0.083	0.0833	0.892	0.937	0.835	0.863
3.75	4.75	150	500	7.3	0.042	0.0207	0.816	1.000	0.782	0.667
4.75	-	0	70	3.6	1.000	1.0000	0.025	0.003	0.398	0.574
4.75	-	70	150	1.4	0.333	0.3333	0.644	0.635	0.611	0.630
4.75	-	150	500	3.1	0.167	0.1667	0.837	0.765	0.818	0.734
						Raw Product	0.001	0.000	0.045	0.153
						Normalized	**0.003**	**0.001**	**0.226**	**0.770**

Table 7.9-2
Calculation of Data-Consistency Cluster Weights for 25 Hz Spectral Acceleration, Using the Empirical Adjustment for Site Conditions

Mmin	Mmax	Rmin	Rmax	Equiv. Sample Size	Importance Factor	Exponent	Cluster 1	Cluster 2	Cluster 3	Cluster 4
3.75	4.75	0	70	24.7	0.250	0.1144	0.238	0.804	0.982	0.252
3.75	4.75	70	150	9.2	0.083	0.0833	0.968	0.722	0.821	0.878
3.75	4.75	150	500	30.6	0.042	0.0154	0.677	1.000	0.681	0.485
4.75	-	0	70	11.3	1.000	1.0000	0.293	0.210	0.068	0.429
4.75	-	70	150	4.1	0.333	0.3333	0.559	0.878	0.386	0.451
4.75	-	150	500	12.6	0.167	0.1497	0.286	0.976	0.753	0.335
						Raw Product	0.007	0.105	0.011	0.007
						Normalized	**0.056**	**0.806**	**0.084**	**0.054**

Table 7.9-3
Calculation of Data-Consistency Cluster Weights for 10 Hz Spectral Acceleration, Using the Analytical Adjustment for Site Conditions

Mmin	Mmax	Rmin	Rmax	Equiv. Sample Size	Importance Factor	Exponent	Cluster 1	Cluster 2	Cluster 3	Cluster 4
3.75	4.75	0	70	9.0	0.250	0.1103	0.246	0.374	0.871	0.963
3.75	4.75	70	150	5.9	0.083	0.0561	0.954	0.956	0.811	0.875
3.75	4.75	150	500	21.1	0.042	0.0078	0.848	1.000	0.698	0.749
4.75	-	0	70	4.0	1.000	1.0000	0.191	0.085	0.320	0.405
4.75	-	70	150	2.5	0.333	0.3333	0.664	0.637	0.563	0.647
4.75	-	150	500	6.7	0.167	0.0984	0.946	0.745	0.772	0.890
						Raw Product	0.024	0.014	0.069	0.147
						Normalized	**0.094**	**0.057**	**0.270**	**0.580**

Table 7.9-4
Calculation of Data-Consistency Cluster Weights for 10 Hz Spectral Acceleration, Using the Empirical Adjustment for Site Conditions

Mmin	Mmax	Rmin	Rmax	Equiv. Sample Size	Importance Factor	Exponent	Cluster 1	Cluster 2	Cluster 3	Cluster 4
3.75	4.75	0	70	28.6	0.250	0.1039	0.426	0.613	0.999	0.266
3.75	4.75	70	150	30.3	0.083	0.0327	0.996	0.886	0.860	0.917
3.75	4.75	150	500	69.4	0.042	0.0071	0.877	1.000	0.697	0.768
4.75	-	0	70	11.9	1.000	1.0000	0.182	0.807	0.007	0.004
4.75	-	70	150	6.9	0.333	0.3333	0.443	0.950	0.215	0.355
4.75	-	150	500	15.3	0.167	0.1292	0.424	0.924	0.756	0.870
						Raw Product	0.013	0.385	0.001	0.000
						Normalized	**0.032**	**0.966**	**0.002**	**0.001**

Table 7.9-5
Calculation of Data-Consistency Cluster Weights for 5 Hz Spectral Acceleration, Using the Analytical Adjustment for Site Conditions

Mmin	Mmax	Rmin	Rmax	Equiv. Sample Size	Importance Factor	Exponent	Cluster 1	Cluster 2	Cluster 3	Cluster 4
3.75	4.75	0	70	9.7	0.250	0.1033	0.122	0.945	0.914	0.156
3.75	4.75	70	150	6.8	0.083	0.0494	0.963	0.921	0.948	0.772
3.75	4.75	150	500	24.3	0.042	0.0069	0.927	1.000	0.783	0.812
4.75	-	0	70	4.0	1.000	1.0000	0.084	0.097	0.525	0.295
4.75	-	70	150	2.5	0.333	0.3333	0.630	0.641	0.627	0.621
4.75	-	150	500	7.2	0.167	0.0933	0.932	0.848	0.799	0.885
						Raw Product	0.005	0.046	0.179	0.016
						Normalized	**0.022**	**0.186**	**0.727**	**0.064**

Table 7.9-6
Calculation of Data-Consistency Cluster Weights for 5 Hz Spectral Acceleration, Using the Empirical Adjustment for Site Conditions

Mmin	Mmax	Rmin	Rmax	Equiv. Sample Size	Importance Factor	Exponent	Cluster 1	Cluster 2	Cluster 3	Cluster 4
3.75	4.75	0	70	31.1	0.250	0.0988	0.042	0.998	0.662	0.038
3.75	4.75	70	150	34.3	0.083	0.0299	0.968	0.563	0.988	0.723
3.75	4.75	150	500	86.7	0.042	0.0059	1.000	0.699	0.737	0.832
4.75	-	0	70	12.3	1.000	1.0000	0.160	0.336	0.033	0.470
4.75	-	70	150	8.6	0.333	0.3333	0.315	0.855	0.216	0.694
4.75	-	150	500	17.1	0.167	0.1201	0.504	0.710	0.762	0.979
						Raw Product	0.001	0.080	0.003	0.007
						Normalized	**0.011**	**0.879**	**0.029**	**0.080**

Table 7.9-7
Calculation of Data-Consistency Cluster Weights for 2.5 Hz Spectral Acceleration, Using the Analytical Adjustment for Site Conditions

Mmin	Mmax	Rmin	Rmax	Equiv. Sample Size	Importance Factor	Exponent	Cluster 1	Cluster 2	Cluster 3	Cluster 4
3.75	4.75	0	70	9.8	0.250	0.1113	0.096	0.992	0.744	0.159
3.75	4.75	70	150	7.2	0.250	0.1513	0.808	0.474	0.947	0.640
3.75	4.75	150	500	27.0	0.083	0.0134	1.000	0.772	0.890	0.943
4.75	-	0	70	4.4	1.000	1.0000	0.054	0.278	0.513	0.155
4.75	-	70	150	2.6	1.000	1.0000	0.347	0.189	0.166	0.298
4.75	-	150	500	7.6	1.000	0.5719	0.513	0.467	0.356	0.464
						Raw Product	0.001	0.009	0.019	0.002
						Normalized	**0.024**	**0.290**	**0.619**	**0.067**

Table 7.9-8
Calculation of Data-Consistency Cluster Weights for 2.5 Hz Spectral Acceleration, Using the Empirical Adjustment for Site Conditions

Mmin	Mmax	Rmin	Rmax	Equiv. Sample Size	Importance Factor	Exponent	Cluster 1	Cluster 2	Cluster 3	Cluster 4
3.75	4.75	0	70	31.4	0.250	0.1045	0.011	0.997	0.680	0.032
3.75	4.75	70	150	35.1	0.250	0.0935	0.330	0.146	1.000	0.198
3.75	4.75	150	500	91.1	0.083	0.0120	1.000	0.180	0.829	0.707
4.75	-	0	70	13.1	1.000	1.0000	0.035	0.660	0.135	0.171
4.75	-	70	150	8.9	1.000	1.0000	0.305	0.125	0.011	0.560
4.75	-	150	500	18.0	1.000	0.7287	0.056	0.039	0.978	0.000
						Raw Product	0.000	0.000	0.001	0.000
						Normalized	**0.002**	**0.095**	**0.903**	**0.000**

Table 7.9-9
Calculation of Data-Consistency Cluster Weights for 1 Hz Spectral Acceleration, Using the Analytical Adjustment for Site Conditions

Mmin	Mmax	Rmin	Rmax	Equiv. Sample Size	Importance Factor	Exponent	Cluster 1	Cluster 2	Cluster 3	Cluster 4
3.75	4.75	0	70	10.7	0.250	0.1070	0.549	0.950	0.901	0.547
3.75	4.75	70	150	7.6	0.250	0.1503	0.772	0.393	0.917	0.815
3.75	4.75	150	500	28.3	0.083	0.0135	0.974	0.470	0.998	0.870
4.75	-	0	70	4.6	1.000	1.0000	0.084	0.338	0.199	0.379
4.75	-	70	150	2.8	1.000	1.0000	0.112	0.357	0.242	0.289
4.75	-	150	500	7.7	1.000	0.5973	0.584	0.274	0.620	0.123
						Raw Product	0.002	0.006	0.025	0.005
						Normalized	**0.060**	**0.153**	**0.649**	**0.138**

Table 7.9-10
Calculation of Data-Consistency Cluster Weights for 1 Hz Spectral Acceleration, Using the Empirical Adjustment for Site Conditions

Mmin	Mmax	Rmin	Rmax	Equiv. Sample Size	Importance Factor	Exponent	Cluster 1	Cluster 2	Cluster 3	Cluster 4
3.75	4.75	0	70	29.4	0.250	0.1000	0.200	0.980	0.842	0.248
3.75	4.75	70	150	33.8	0.250	0.0872	0.565	0.150	1.000	0.598
3.75	4.75	150	500	83.7	0.083	0.0117	0.889	0.109	1.000	0.505
4.75	-	0	70	11.8	1.000	1.0000	0.015	0.514	0.071	0.400
4.75	-	70	150	9.0	1.000	1.0000	0.652	0.135	0.135	0.077
4.75	-	150	500	16.4	1.000	0.7188	0.478	0.013	0.725	0.000
						Raw Product	0.000	0.000	0.006	0.000
						Normalized	**0.074**	**0.002**	**0.923**	**0.000**

Table 7.9-11
Calculation of Data-Consistency Cluster Weights for 0.5 Hz Spectral Acceleration, Using the Analytical adjustment for Site Conditions

Mmin	Mmax	Rmin	Rmax	Equiv. Sample Size	Importance Factor	Exponent	Cluster 1	Cluster 2	Cluster 3	Cluster 4
3.75	4.75	0	70	9.0	0.250	0.1233	0.954	0.817	0.499	0.771
3.75	4.75	70	150	7.4	0.250	0.1499	0.800	0.377	0.856	0.877
3.75	4.75	150	500	23.4	0.083	0.0158	0.989	0.510	0.989	0.930
4.75	-	0	70	4.4	1.000	1.0000	0.117	0.390	0.090	0.402
4.75	-	70	150	2.8	1.000	1.0000	0.178	0.347	0.146	0.329
4.75	-	150	500	7.0	1.000	0.6329	0.268	0.517	0.475	0.377
						Raw Product	0.004	0.011	0.003	0.031
						Normalized	**0.086**	**0.223**	**0.054**	**0.637**

Table 7.9-12
Calculation of Data-Consistency Cluster Weights for 0.5 Hz Spectral Acceleration, Using the Empirical Adjustment for Site Conditions

Mmin	Mmax	Rmin	Rmax	Equiv. Sample Size	Importance Factor	Exponent	Cluster 1	Cluster 2	Cluster 3	Cluster 4
3.75	4.75	0	70	20.6	0.250	0.1051	0.722	0.995	0.572	0.441
3.75	4.75	70	150	27.8	0.250	0.0781	0.757	0.326	0.998	0.563
3.75	4.75	150	500	69.6	0.083	0.0104	0.968	0.292	1.000	0.714
4.75	-	0	70	8.7	1.000	1.0000	0.001	0.525	0.176	0.299
4.75	-	70	150	6.9	1.000	1.0000	0.015	0.665	0.065	0.255
4.75	-	150	500	13.7	1.000	0.6348	0.177	0.245	0.885	0.000
						Raw Product	0.000	0.008	0.006	0.000
						Normalized	**0.000**	**0.584**	**0.416**	**0.000**

Table 7.9-13
Combination of Data-Consistency Cluster Weights Across Frequencies and Across Approaches for Site Adjustment

	Analytical Site Adjustments				Empirical Site Adjustments			
	Cluster 1	Cluster 2	Cluster 3	Cluster 4	Cluster 1	Cluster 2	Cluster 3	Cluster 4
25 Hz	0.00	0.00	0.23	0.77	0.06	0.81	0.08	0.05
10 Hz	0.09	0.06	0.27	0.58	0.03	0.97	0.00	0.00
5 Hz	0.02	0.19	0.73	0.06	0.01	0.88	0.03	0.08
Combined HF	**0.01**	**0.01**	**0.54**	**0.44**	**0.01**	**0.98**	**0.00**	**0.00**
Comb. HF Analytical + Empirical	**0.01**	**0.50**	**0.27**	**0.22**				
2.5 Hz	0.02	0.29	0.62	0.07	0.00	0.09	0.90	0.00
1 Hz	0.06	0.15	0.65	0.14	0.07	0.00	0.92	0.00
0.5 Hz	0.09	0.22	0.05	0.64	0.00	0.58	0.42	0.00
Combined LF	**0.04**	**0.30**	**0.42**	**0.24**	**0.00**	**0.03**	**0.97**	**0.00**
Comb. LF Analytical + Empirical	**0.02**	**0.16**	**0.70**	**0.12**				

Table 7.9-14
Calculation of Cluster Weights on the Basis of Combined Data-Consistency Weights and Confidence Weights

	Cluster 1	Cluster 2	Cluster 3	Cluster 4
Weight Based on Consistency with Data (avg. HF and LF) – 25%	0.02	0.33	0.48	0.17
Weight Based on Confidence in GMPEs – 75%	0.20	0.30	0.30	0.20
Combined Weight	0.15	0.31	0.35	0.19

Table 7.10.2-1
Aleatory Variability for Active Tectonic Regions Based on the NGA Projects

Spectral Frequency (Hz)	Components of Aleatory Variability for ln(Peak Ground-Motion Amplitude) Based On:											
	Preliminary NGA Used by EPRI (2006)*		Average for 2008 NGA				Incorporation of Preliminary NGA-West 2 Results					
			M ≤ 5		M ≥ 7		M 5		M 6		M ≥ 7	
	τ	φ	τ	φ	τ	φ	τ	φ	T	φ	T	φ
PGA	0.34	0.51	0.32	0.54	0.26	0.48	0.35	0.55	0.33	0.51	0.31	0.50
10	0.40	0.56	0.38	0.58	0.31	0.51	0.39	0.60	0.37	0.56	0.35	0.54
5	0.40	0.56	0.35	0.58	0.29	0.52	0.36	0.60	0.34	0.57	0.32	0.55
2.5	0.40	0.56	0.32	0.59	0.28	0.54	0.35	0.61	0.33	0.59	0.31	0.57
1.0	0.40	0.60	0.32	0.59	0.31	0.56	0.39	0.62	0.38	0.62	0.36	0.61
0.5	0.40	0.62	0.36	0.58	0.36	0.56	0.45	0.61	0.44	0.61	0.42	0.61

* Values reported by EPRI (2006) for 2 Hz used for 2.5 Hz.

Table 7.10.2-2
Update Aleatory Variability CEUS Ground Motions

Spectral Frequency (Hz)	Aleatory Variability Components for ln(Peak Ground-Motion Amplitude) for Magnitude:					
	M 5		M 6		M ≥ 7	
	τ	φ	τ	φ	τ	φ
PGA (100 Hz)	0.38	0.55	0.36	0.51	0.34	0.50
40	0.42	0.60	0.40	0.56	0.38	0.54
25	0.42	0.60	0.40	0.56	0.38	0.54
10	0.42	0.60	0.40	0.56	0.38	0.54
5	0.39	0.60	0.37	0.57	0.35	0.55
2.5	0.38	0.61	0.36	0.59	0.34	0.57
1.0	0.42	0.62	0.41	0.62	0.39	0.61
0.5	0.48	0.61	0.47	0.61	0.45	0.61
0.25	0.50	0.61	0.48	0.62	0.47	0.61

Table 7.11.1-1
Earthquakes Used for of Analysis of Gulf Coast Region Q

State	Date	Magnitude	Latitude	Longitude	Depth
Arkansas	10/15/2010	3.83	35.28	-92.32	5.0
Arkansas	11/20/2010	3.87	35.32	-92.32	5.0
Arkansas	2/17/2011	3.80	35.28	-92.36	6.0
Arkansas	2/18/2011	3.88	35.26	-92.37	8.0
Arkansas	2/18/2011	4.07	35.27	-92.38	8.0
Arkansas	2/28/2011	4.65	35.26	-92.34	4.0
Arkansas	4/7/2011	3.73	35.25	-92.37	3.0
Arkansas	4/8/2011	3.86	35.26	-92.36	4.0
Oklahoma	2/27/2010	4.15	35.54	-96.75	4.0
Oklahoma	10/13/2010	4.30	35.20	-97.31	14.0
Oklahoma	11/24/2010	3.93	35.63	-97.25	3.0
Oklahoma	12/12/2010	3.20	35.39	-97.00	4.0
Oklahoma	11/6/2011	5.59	35.54	-96.75	8.0
Texas	9/11/2011	4.40	32.87	-100.8	5.0
Texas	10/20/2011	4.59	28.81	-98.15	3.0
Texas	5/17/2012	4.83	31.90	-94.33	4.0

Table 7.11.1-2
Estimated Values of Q for Gulf Coast Region

Frequency (Hz)	Geometric Spreading Model 1		Geometric Spreading Model 2	
	Q	Standard Error	Q	Standard Error
0.25	182	37	179	37
.035	180	17	179	16
0.50	254	22	252	23
0.70	265	17	265	16
1.00	352	21	350	22
1.40	451	25	449	25
2.00	537	25	535	25
2.80	620	25	617	25
4.00	806	32	805	32
5.60	1013	40	1013	40
8.00	1377	62	1374	61

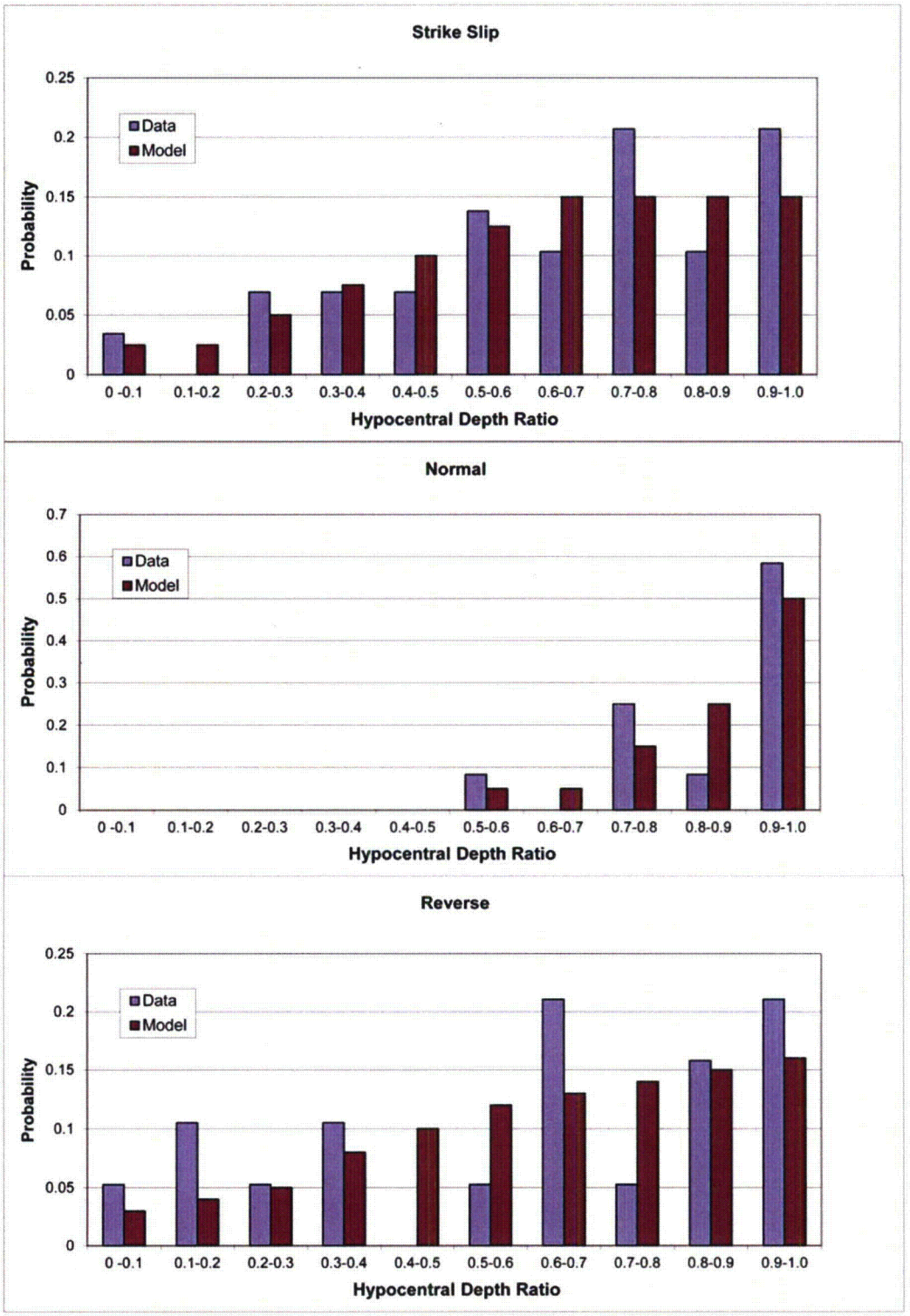

Figure 7.2.4-1
Empirical distributions for vertical location of hypocenter in rupture plane developed by Chiou and Youngs (2008b)

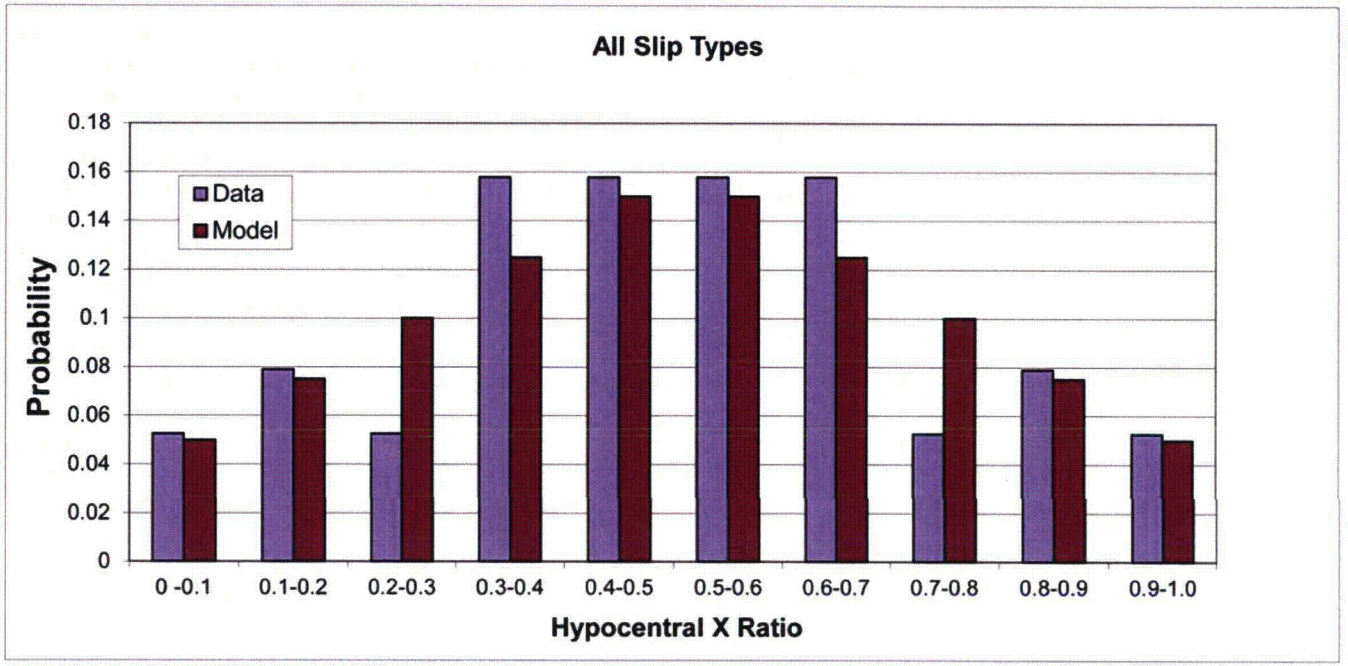

Figure 7.2.4-2
Distributions for horizontal location of hypocenter in rupture plane developed by Chiou and Youngs (2008b).

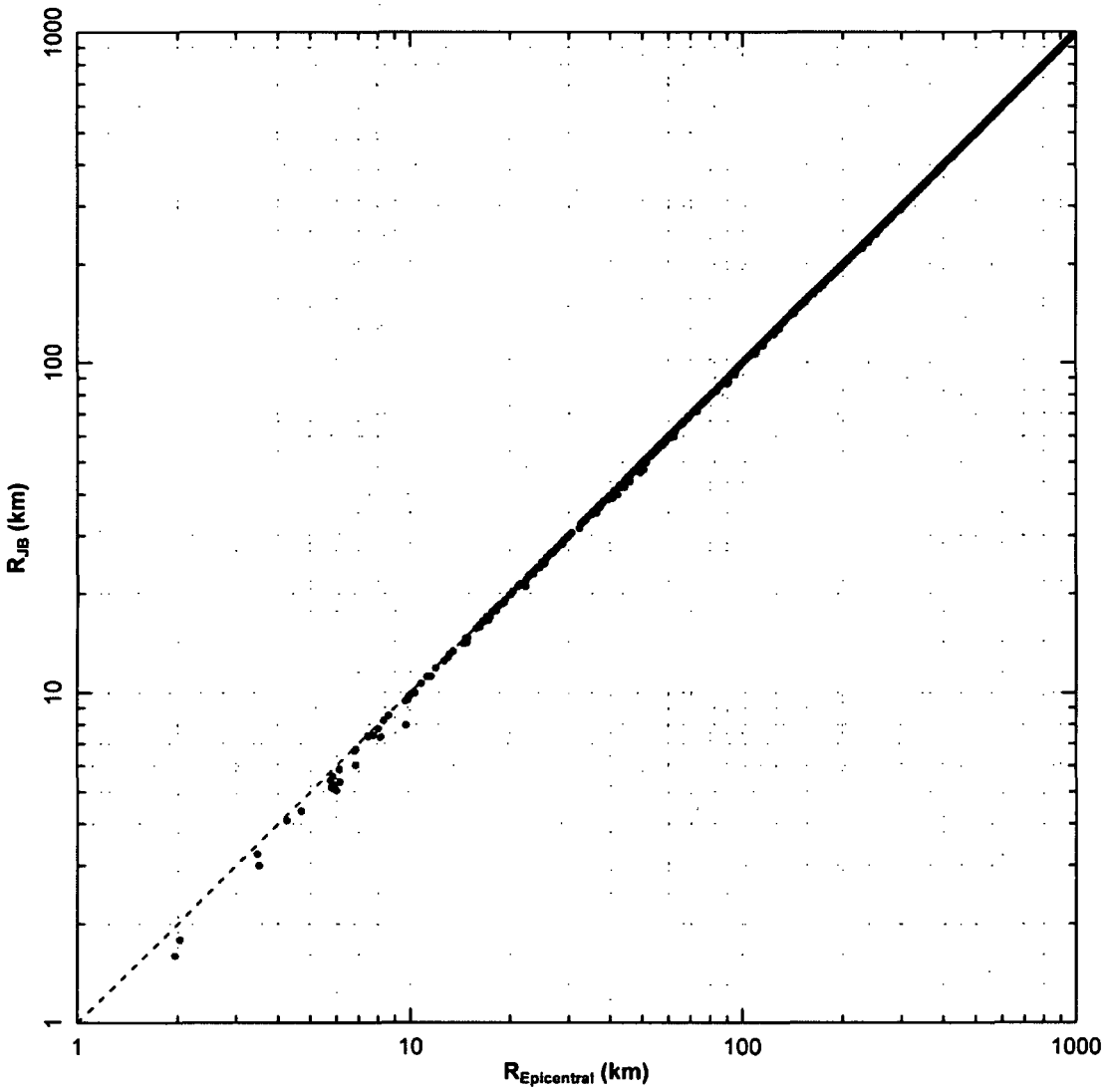

Figure 7.2.4-3
Comparison of epicentral and simulated Joyner-Boore distances for the ground motion database.

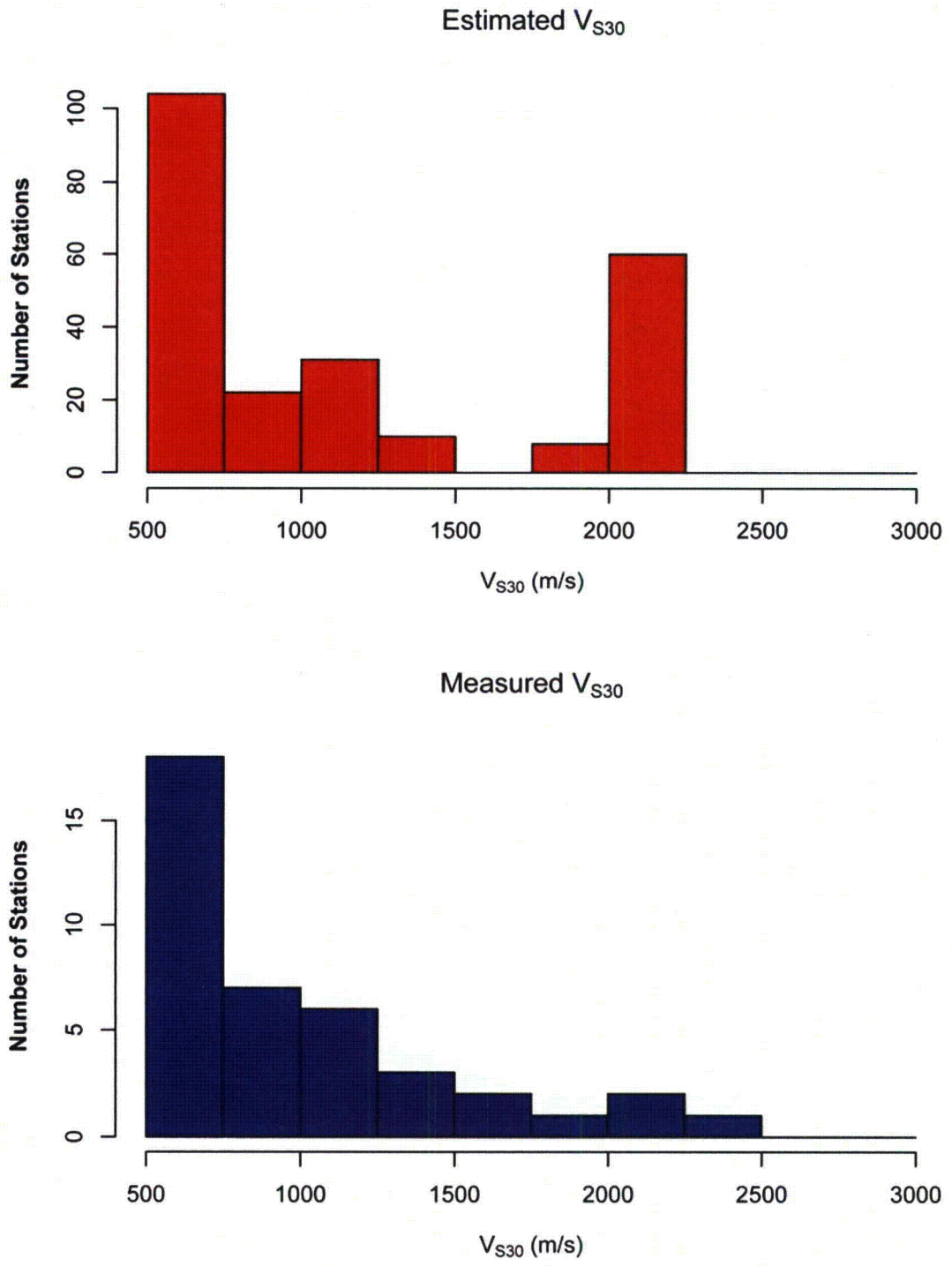

Figure 7.2.5-1
Distribution of V_{S30} values for recording stations in final ground-motion database

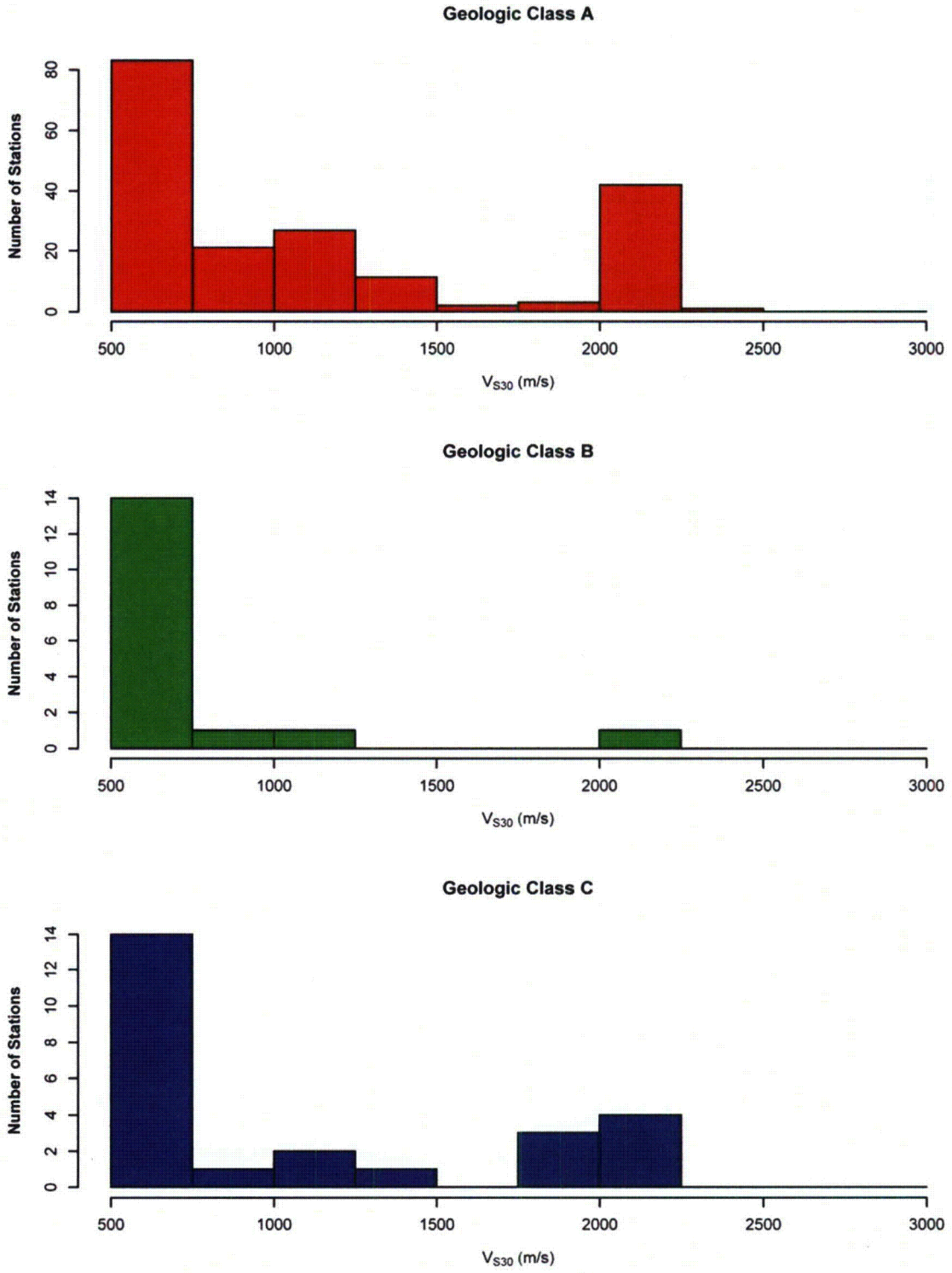

Figure 7.2.5-2
Distribution of V_{S30} values for recording stations with geological classifications

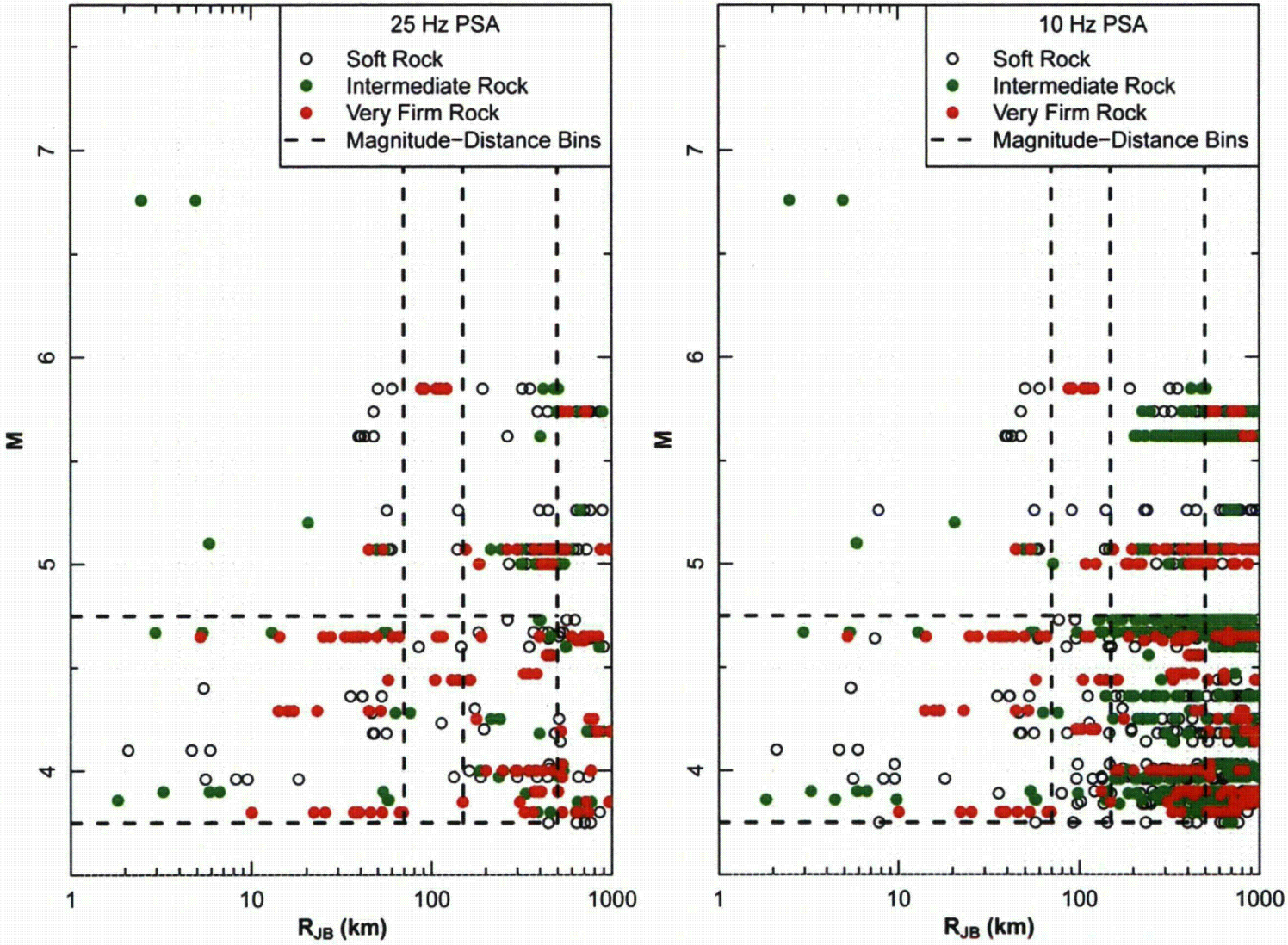

Figure 7.2.6-1 (1 of 3)
Magnitude-distance distribution of rock site ground-motion data

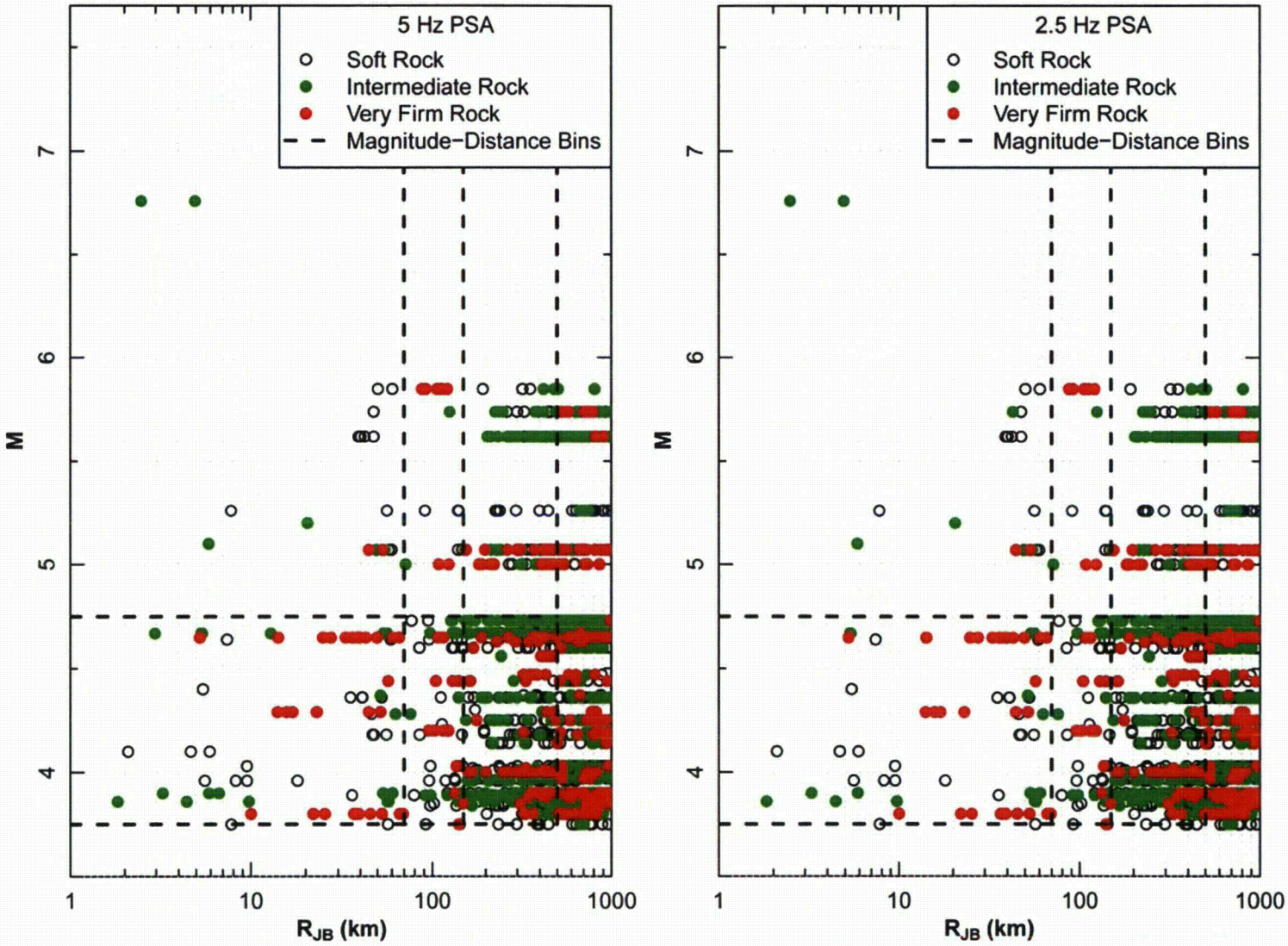

Figure 7.2.6-1 (2 of 3)
Magnitude-distance distribution of rock site ground-motion data

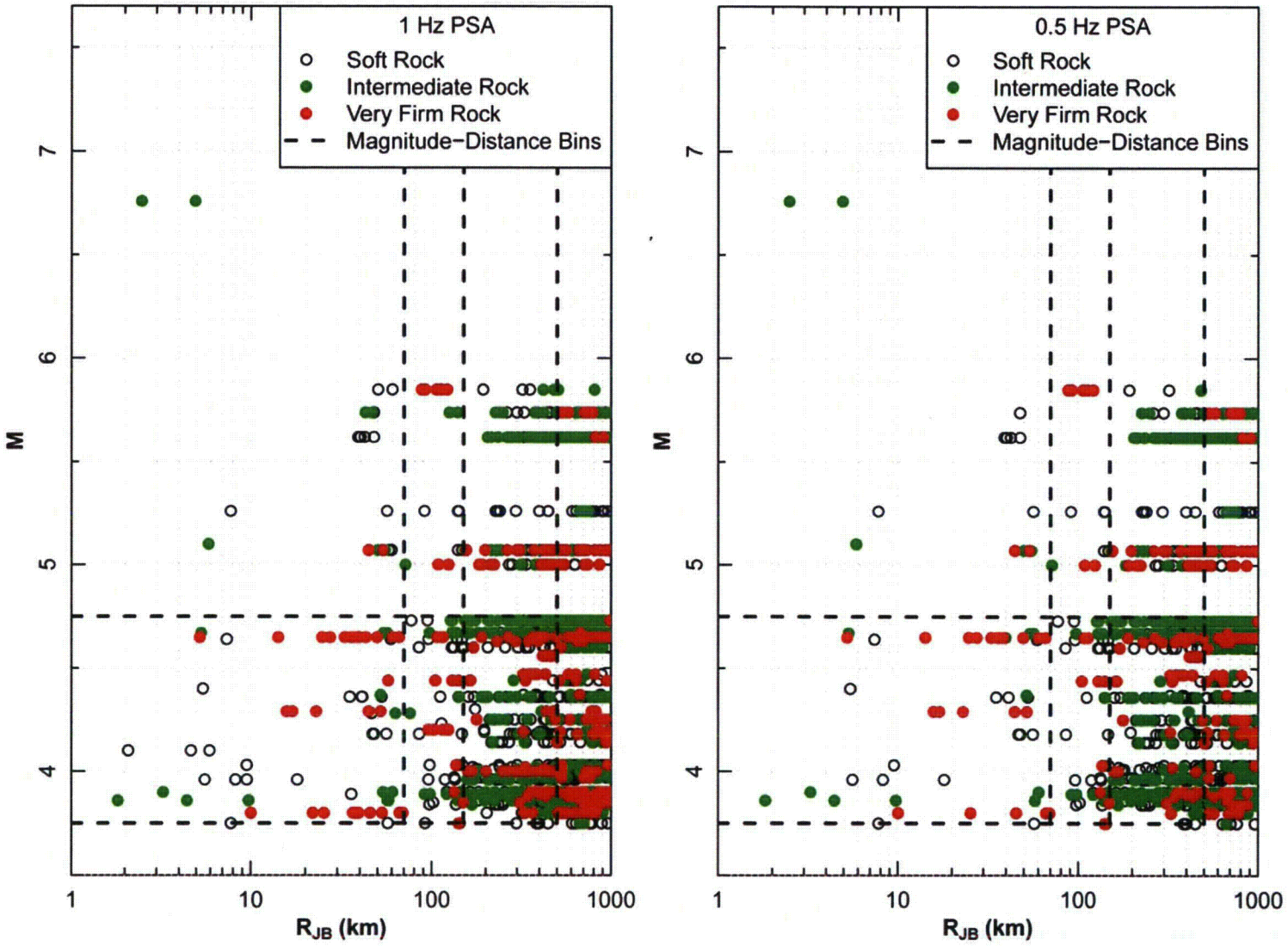

Figure 7.2.6-1 (3 of 3)
Magnitude-distance distribution of rock site ground-motion data

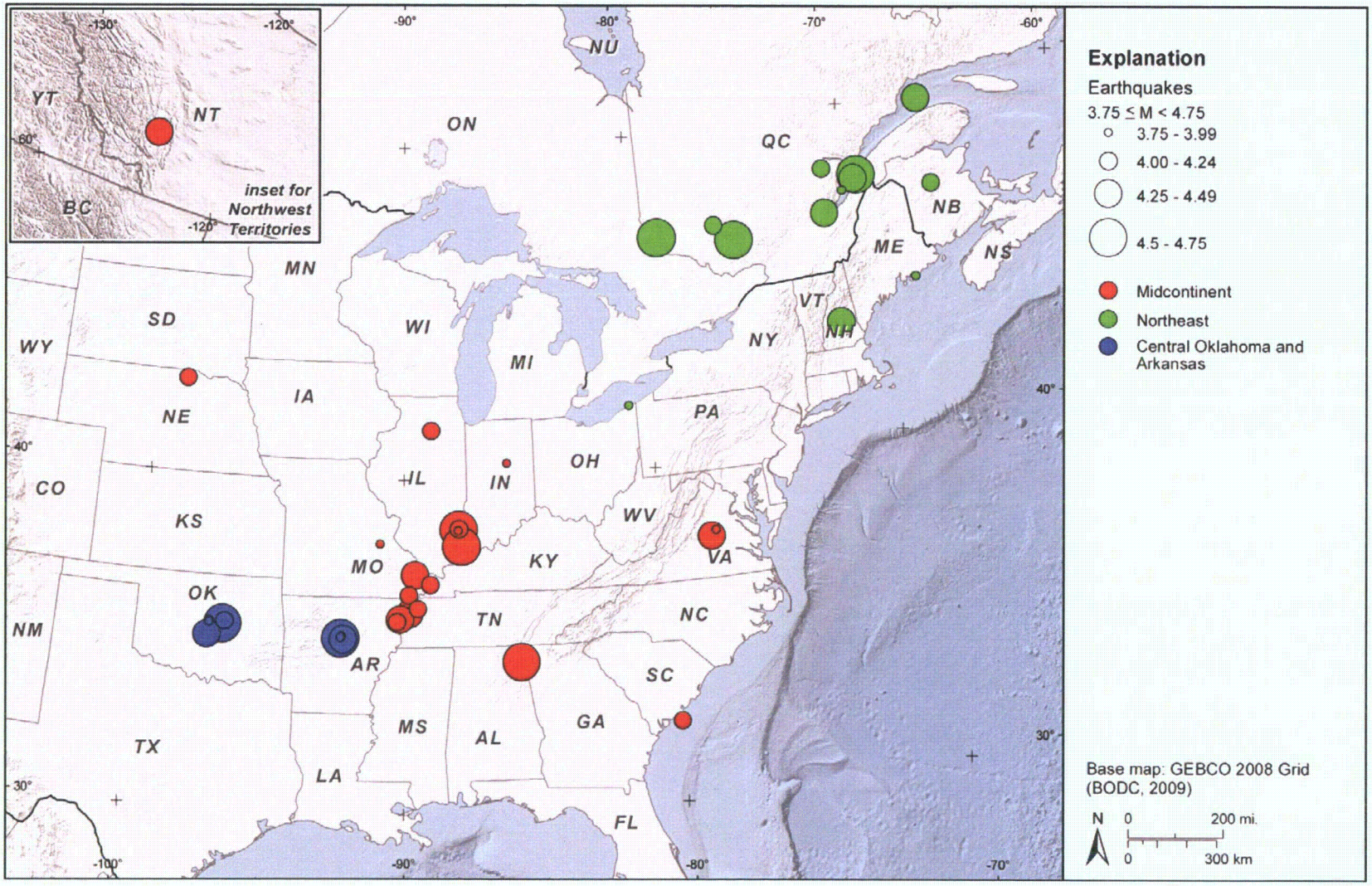

Figure 7.2.6-2
Map of earthquakes of magnitude 3.75 ≤ M < 4.75 in project ground-motion database. Note: the number of earthquakes may appear to be different from the number in Table 7.2.6-1 because some epicentral locations may coincide.

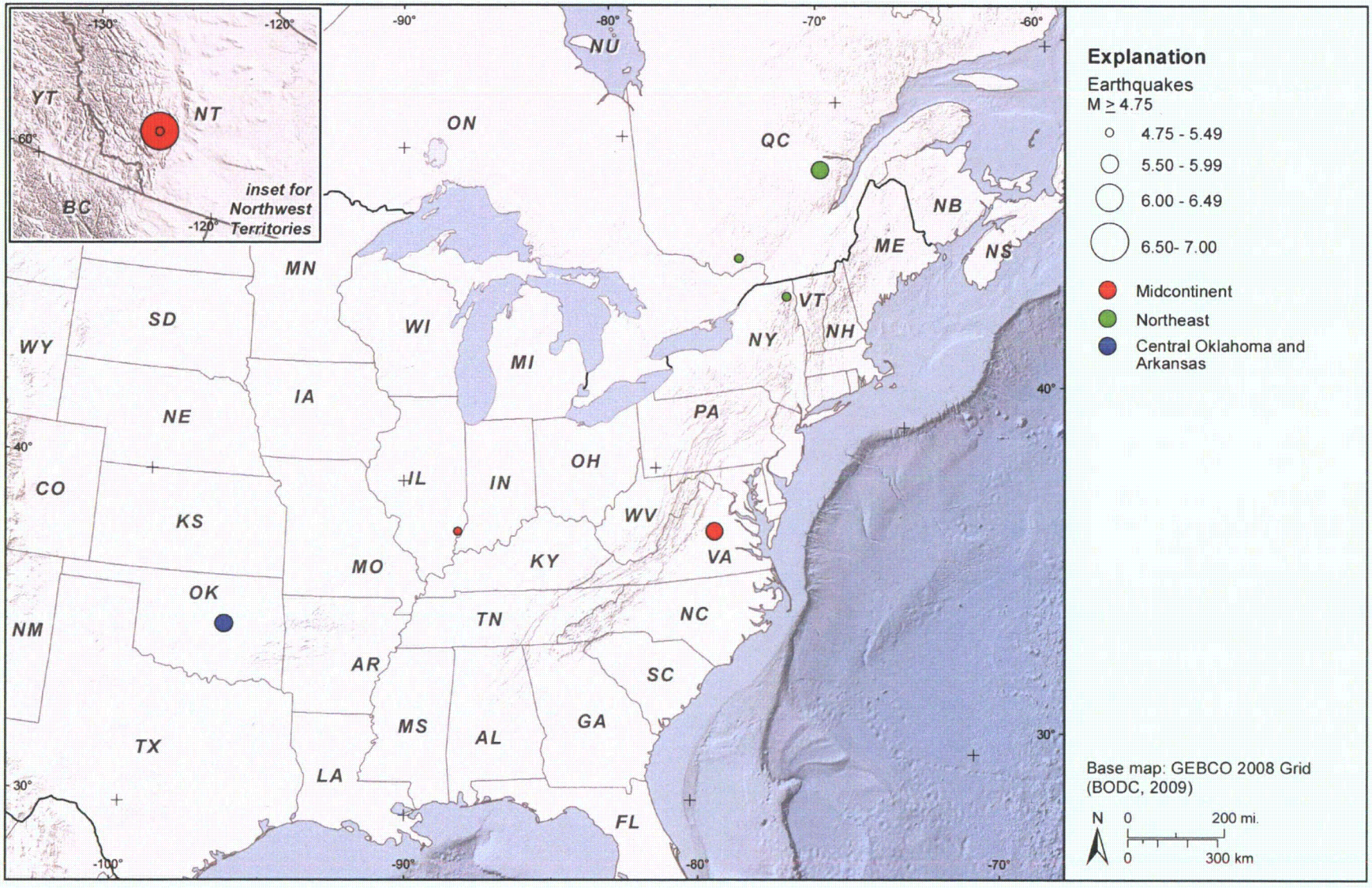

Figure 7.2.6-3
Map of earthquakes of magnitude M ≥ 4.75 in project ground-motion database

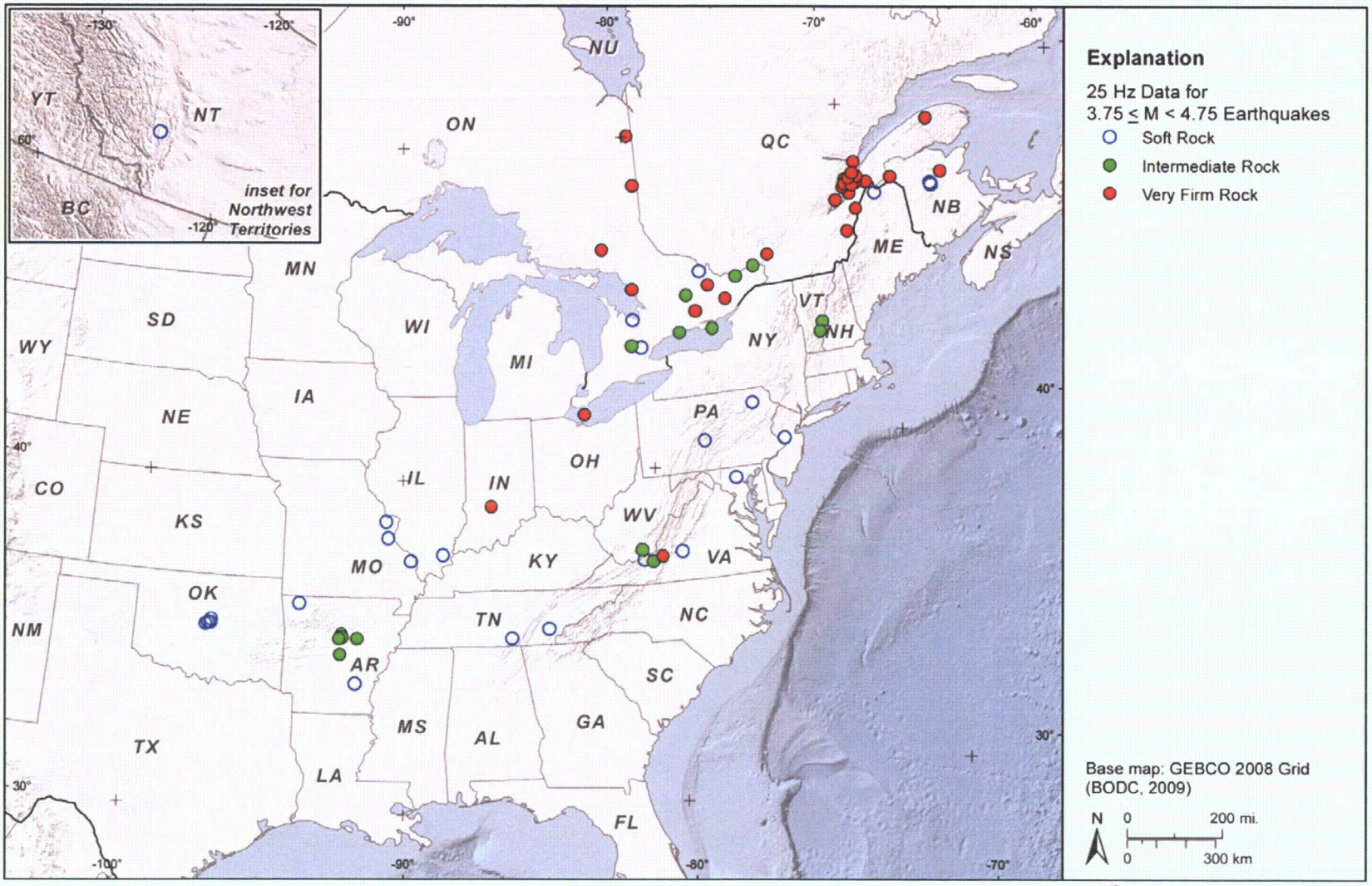

Figure 7.2.6-4a
Map of recording stations for earthquakes of magnitude 3.75 ≤ M < 4.75 and R_{JB} ≤ 500 km contributing 25 Hz PSA data to project ground-motion database

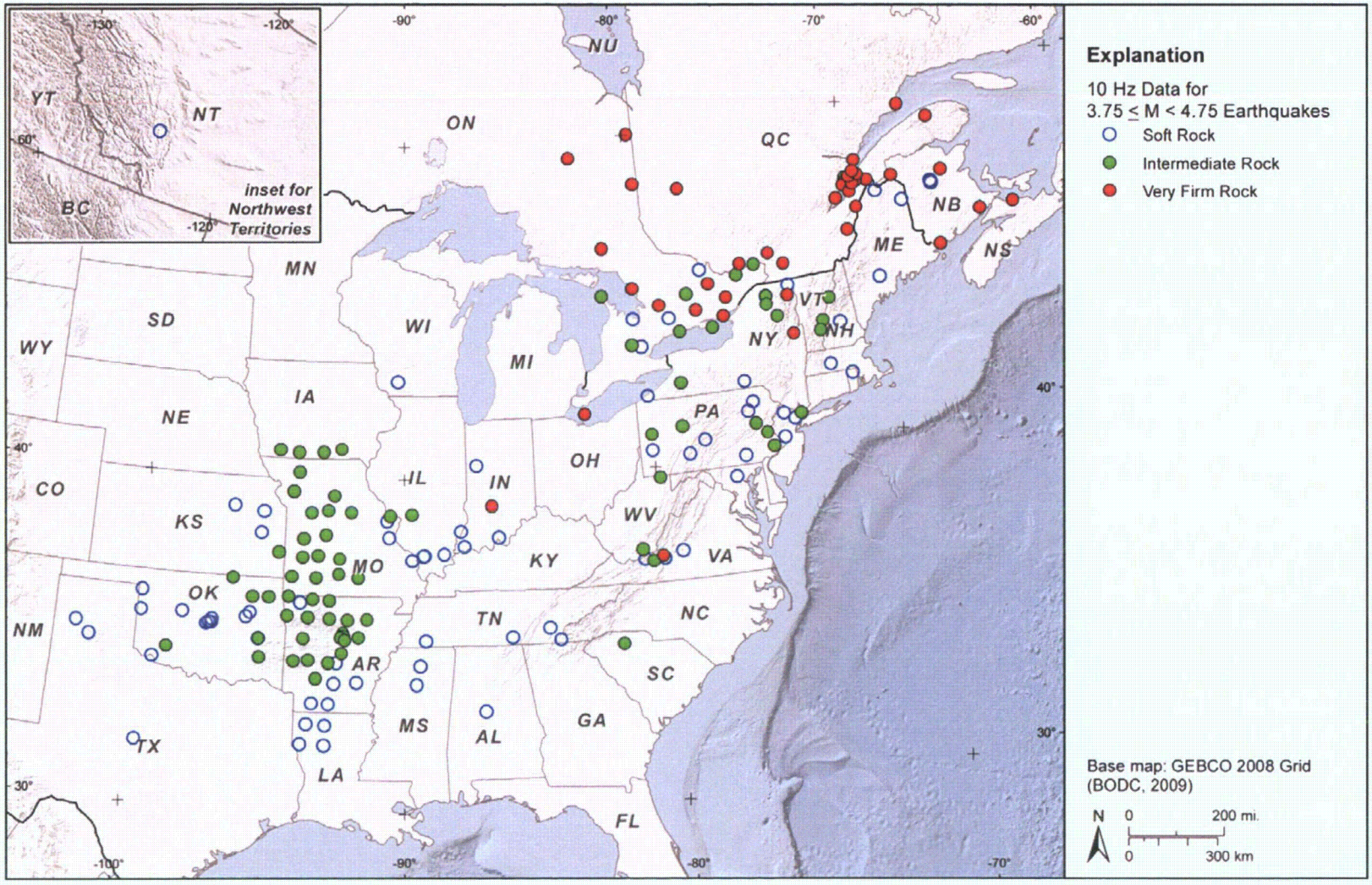

Figure 7.2.6-4b
Map of recording stations for earthquakes of magnitude 3.75 ≤ M < 4.75 and R_{JB} ≤ 500 km contributing 10 Hz PSA data to project ground-motion database

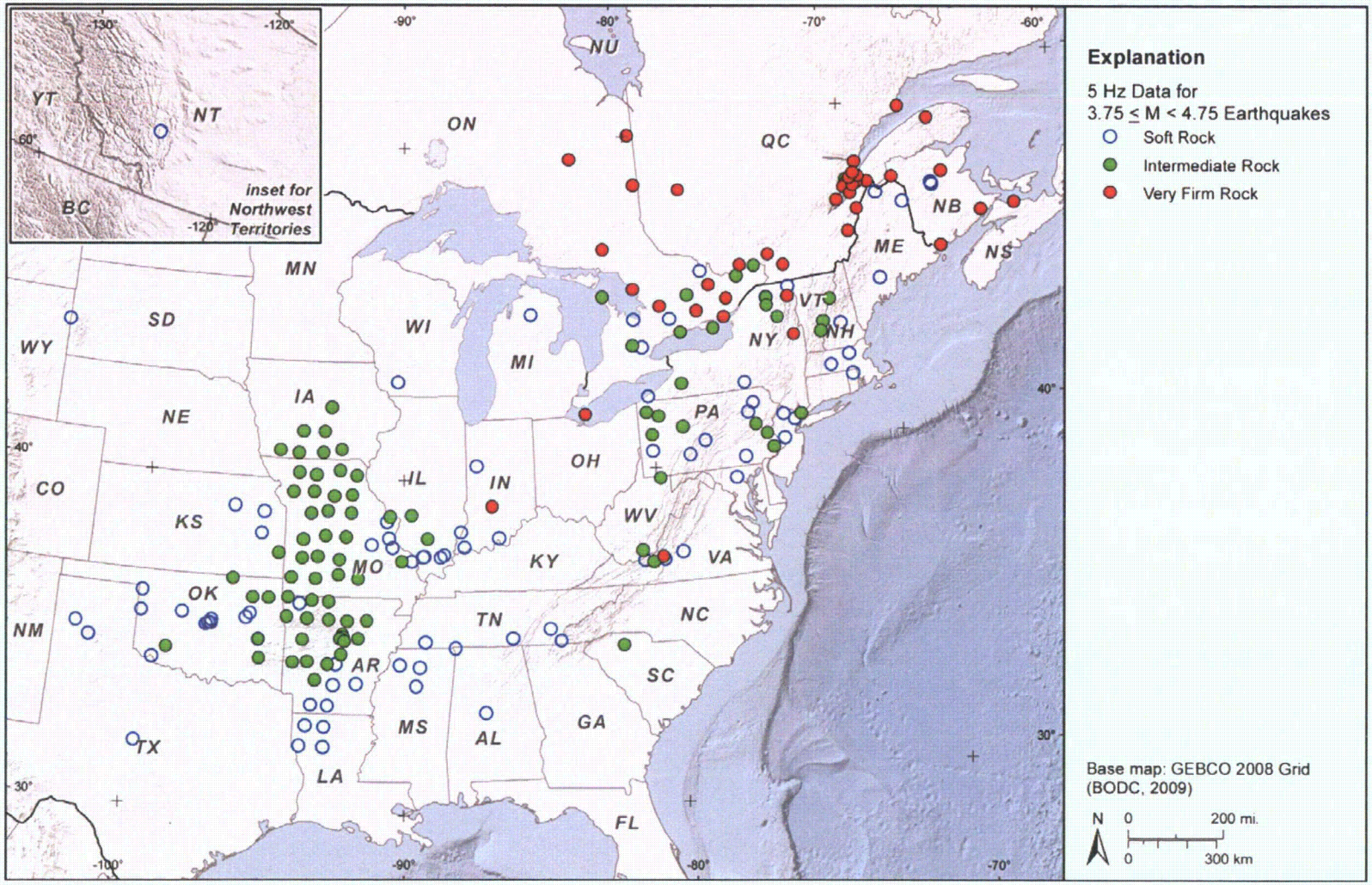

Figure 7.2.6-4c
Map of recording stations for earthquakes of magnitude 3.75 ≤ M < 4.75 and R_{JB} ≤ 500 km contributing 5 Hz PSA data to project ground-motion database

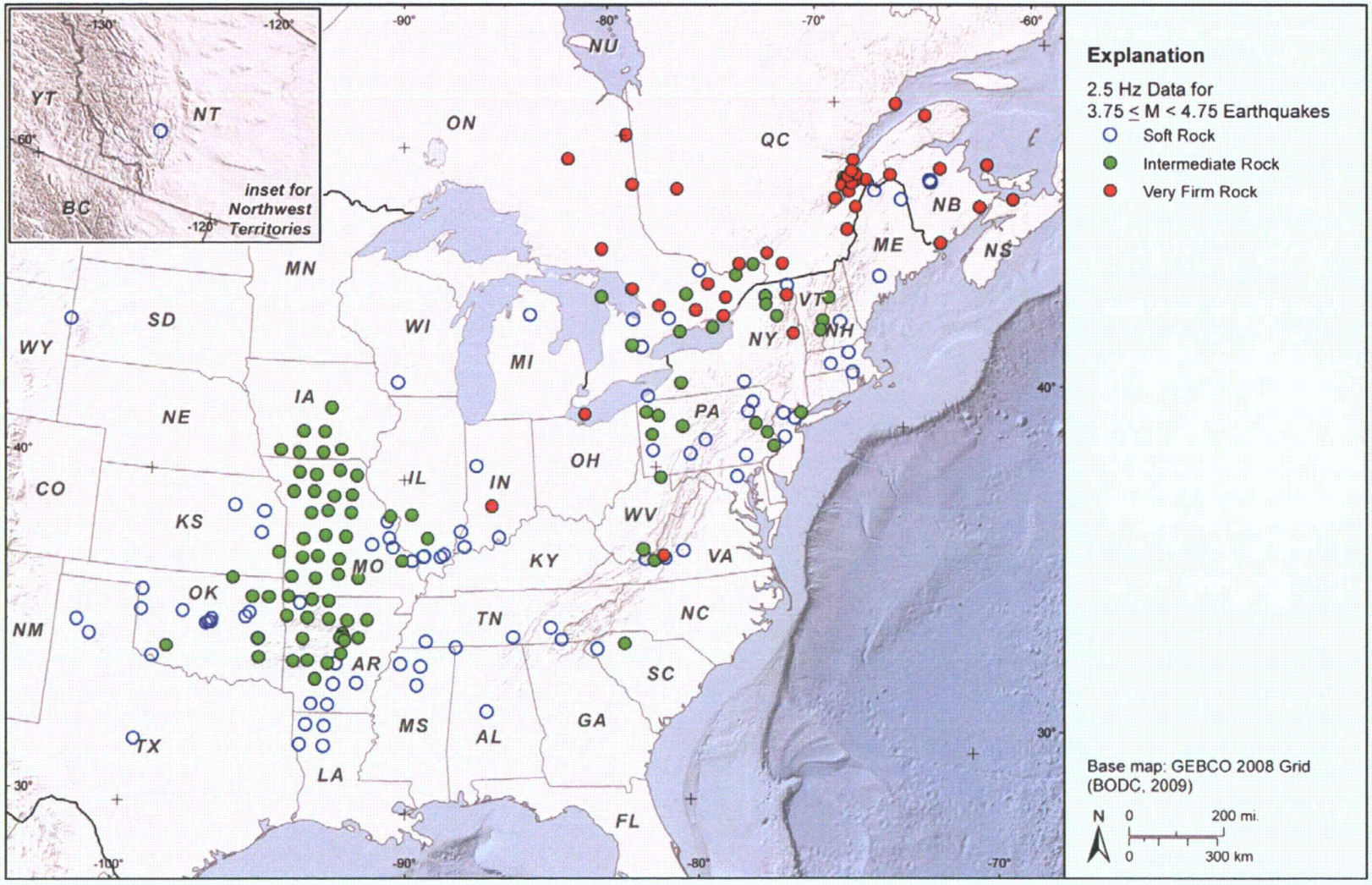

Figure 7.2.6-4d
Map of recording stations for earthquakes of magnitude 3.75 ≤ M < 4.75 and R_{JB} ≤ 500 km contributing 2.5 Hz PSA data to project ground-motion database

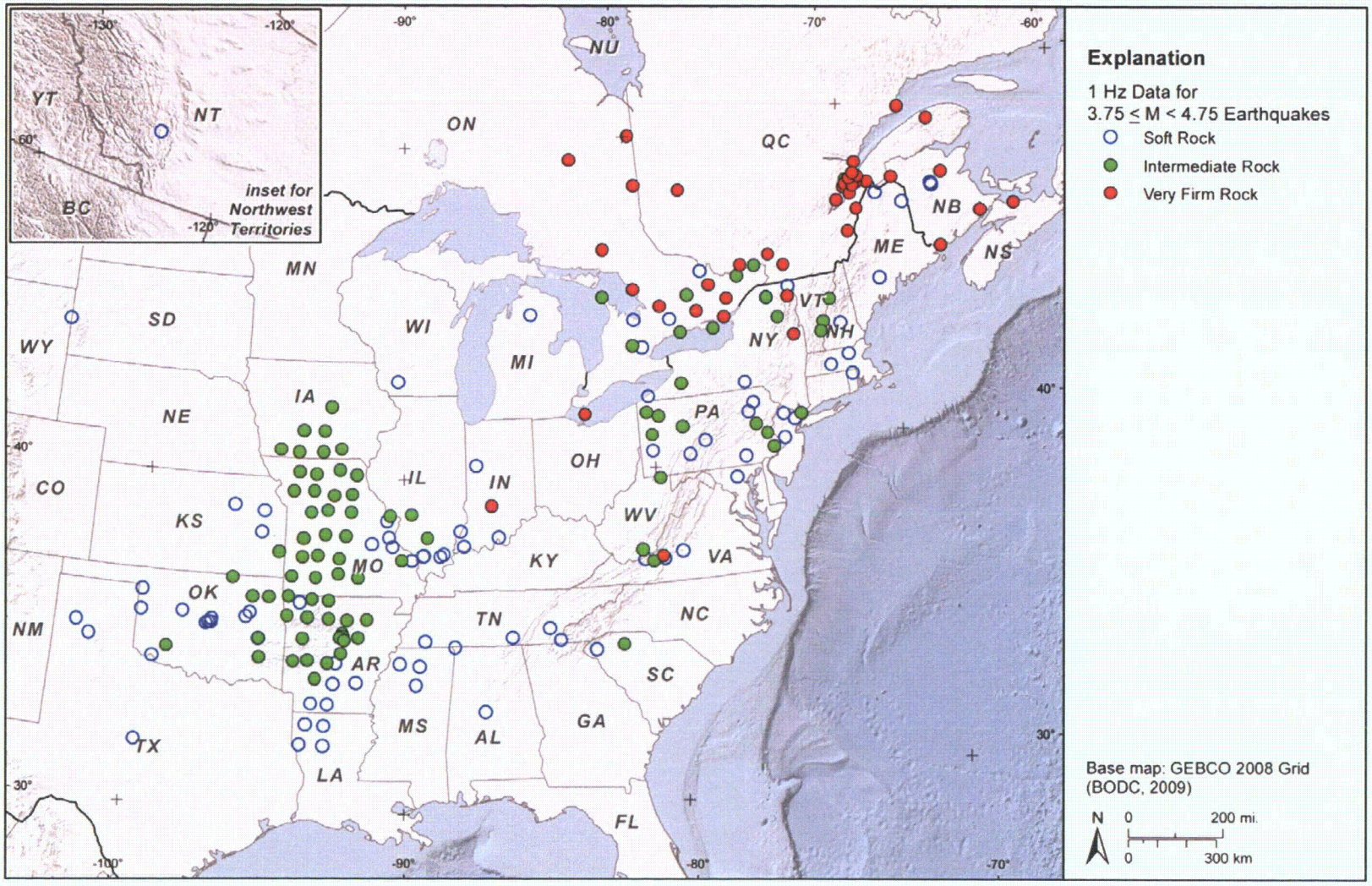

Figure 7.2.6-4e
Map of recording stations for earthquakes of magnitude 3.75 ≤ M < 4.75 and R_{JB} ≤ 500 km contributing 1 Hz PSA data to project ground-motion database

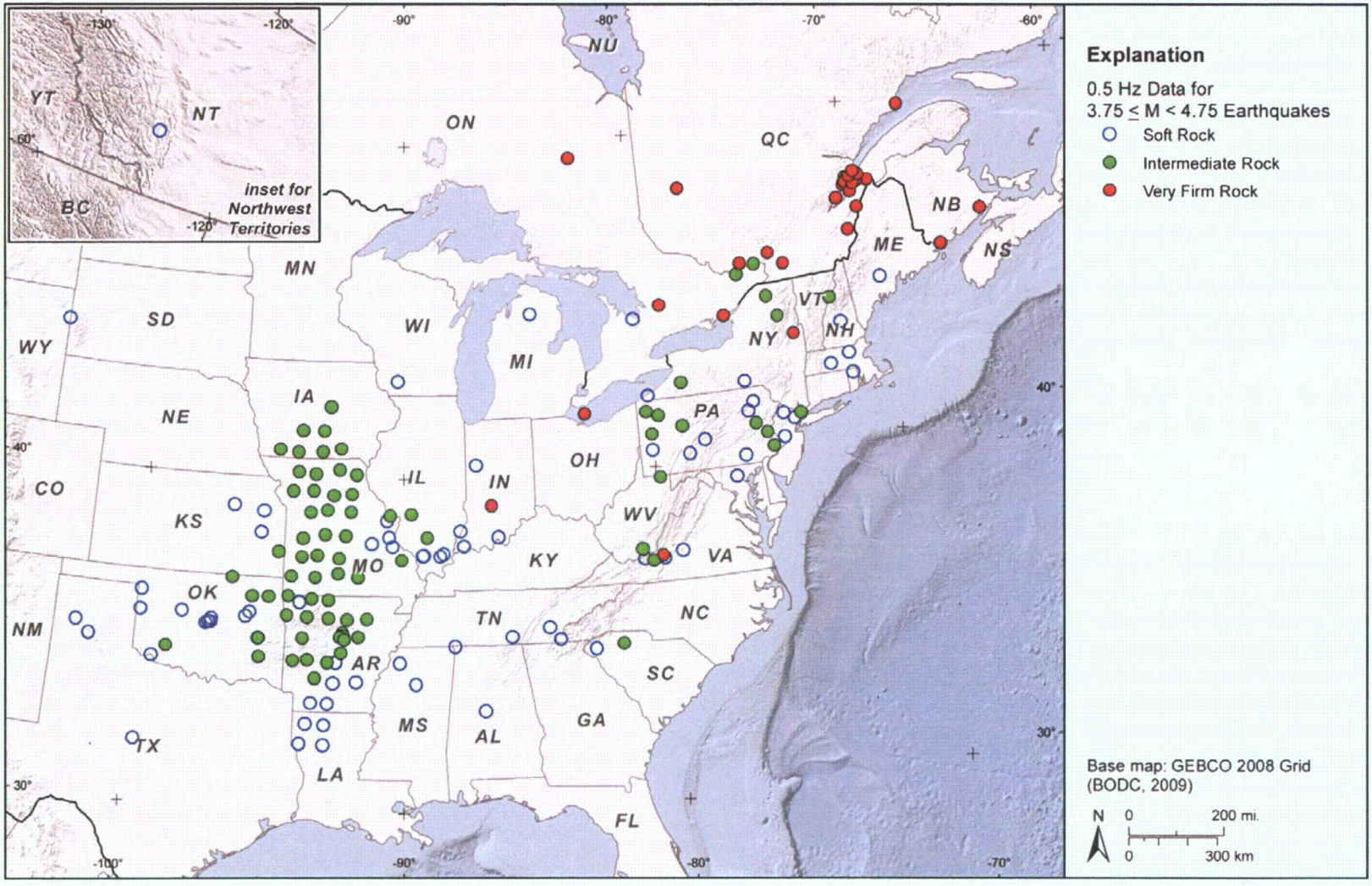

Figure 7.2.6-4f
Map of recording stations for earthquakes of magnitude 3.75 ≤ M < 4.75 and R_{JB} ≤ 500 km contributing 0.5 Hz PSA data to project ground-motion database

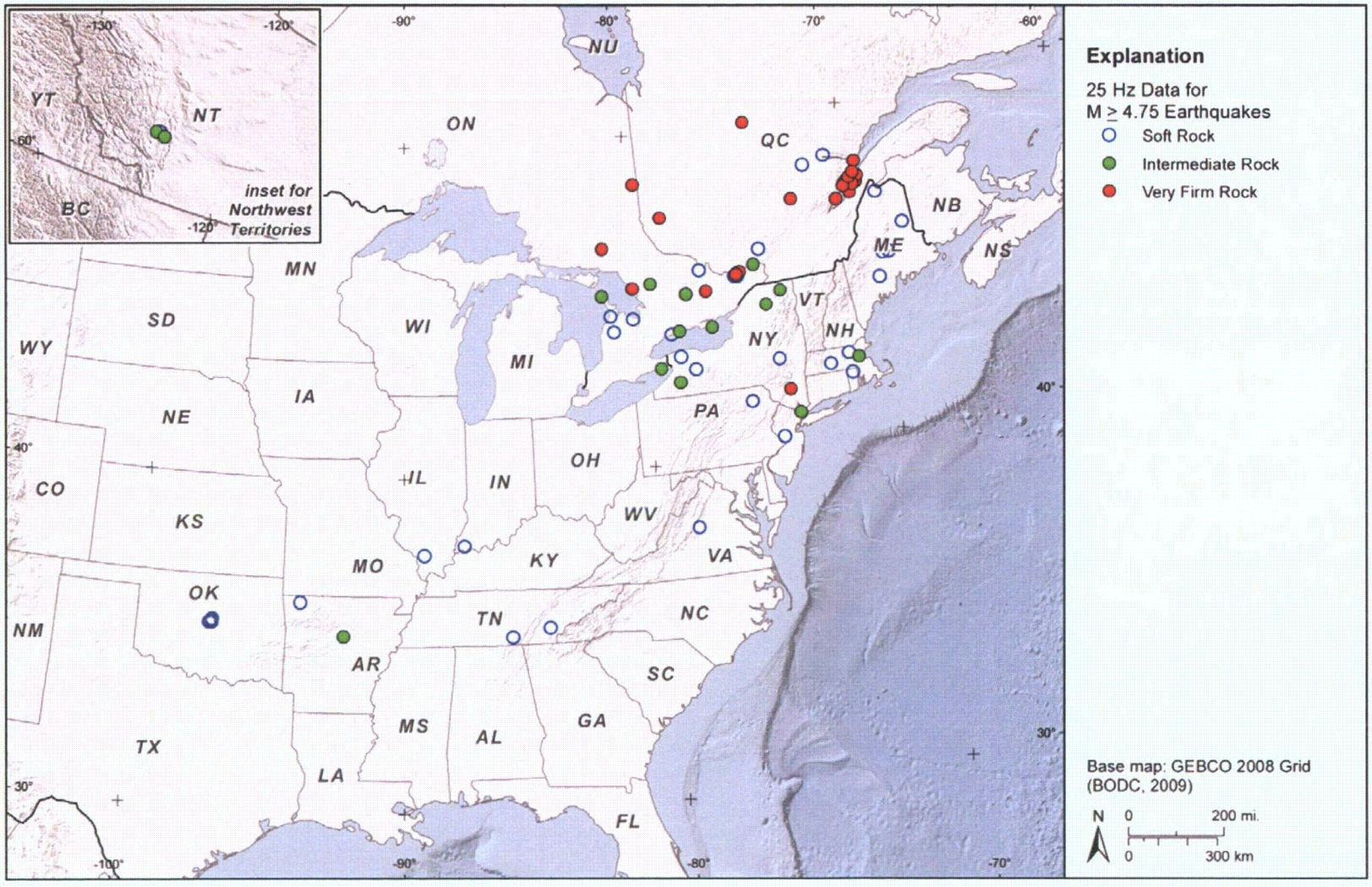

Figure 7.2.6-5a
Map of recording stations for earthquakes of magnitude M ≥ 4.75 and R_{JB} ≤ 500 km contributing 25 Hz PSA data to project ground-motion database

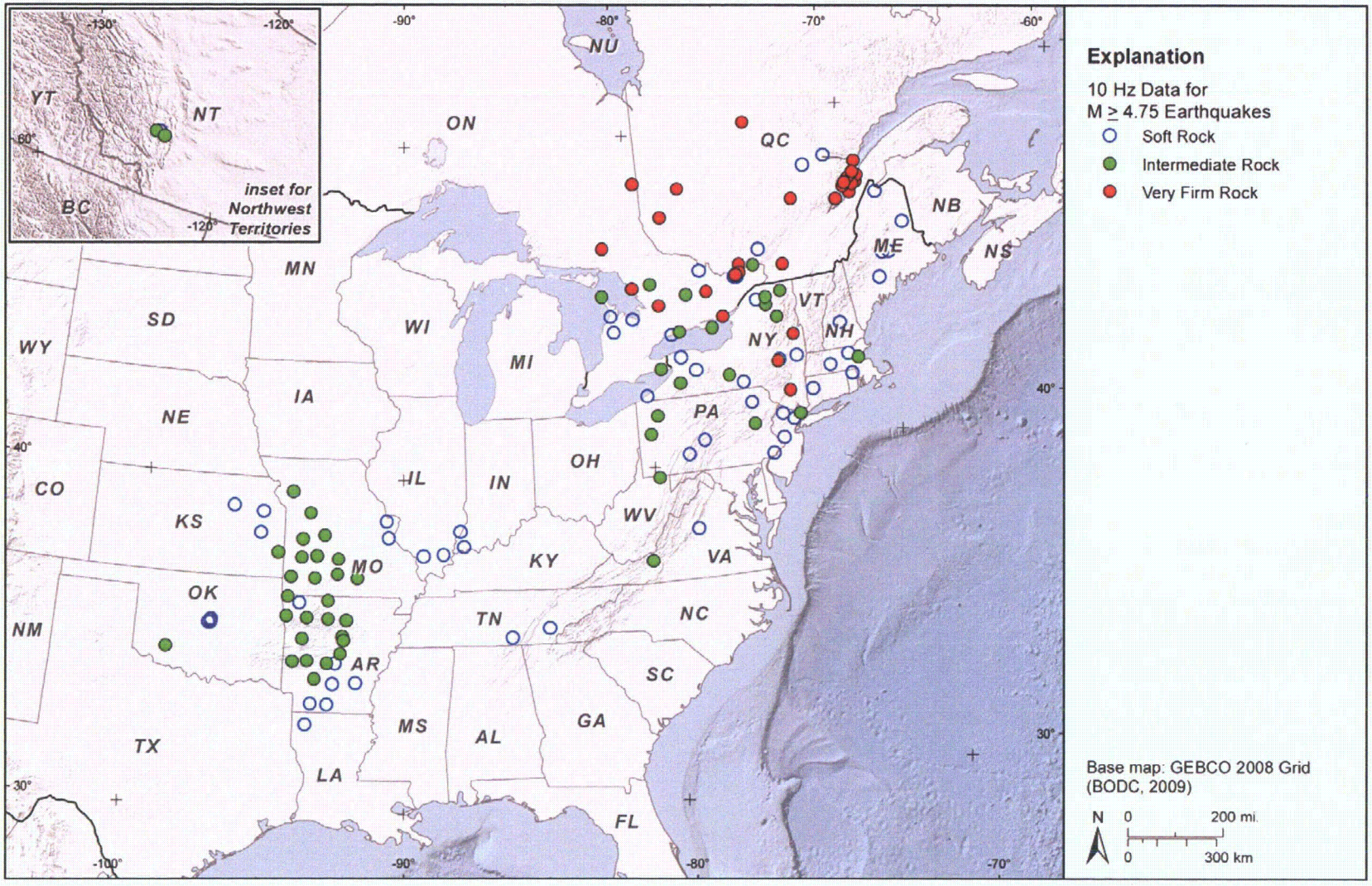

Figure 7.2.6-5b
Map of recording stations for earthquakes of magnitude M ≥ 4.75 and R_{JB} ≤ 500 km contributing 10 Hz PSA data to project ground-motion database

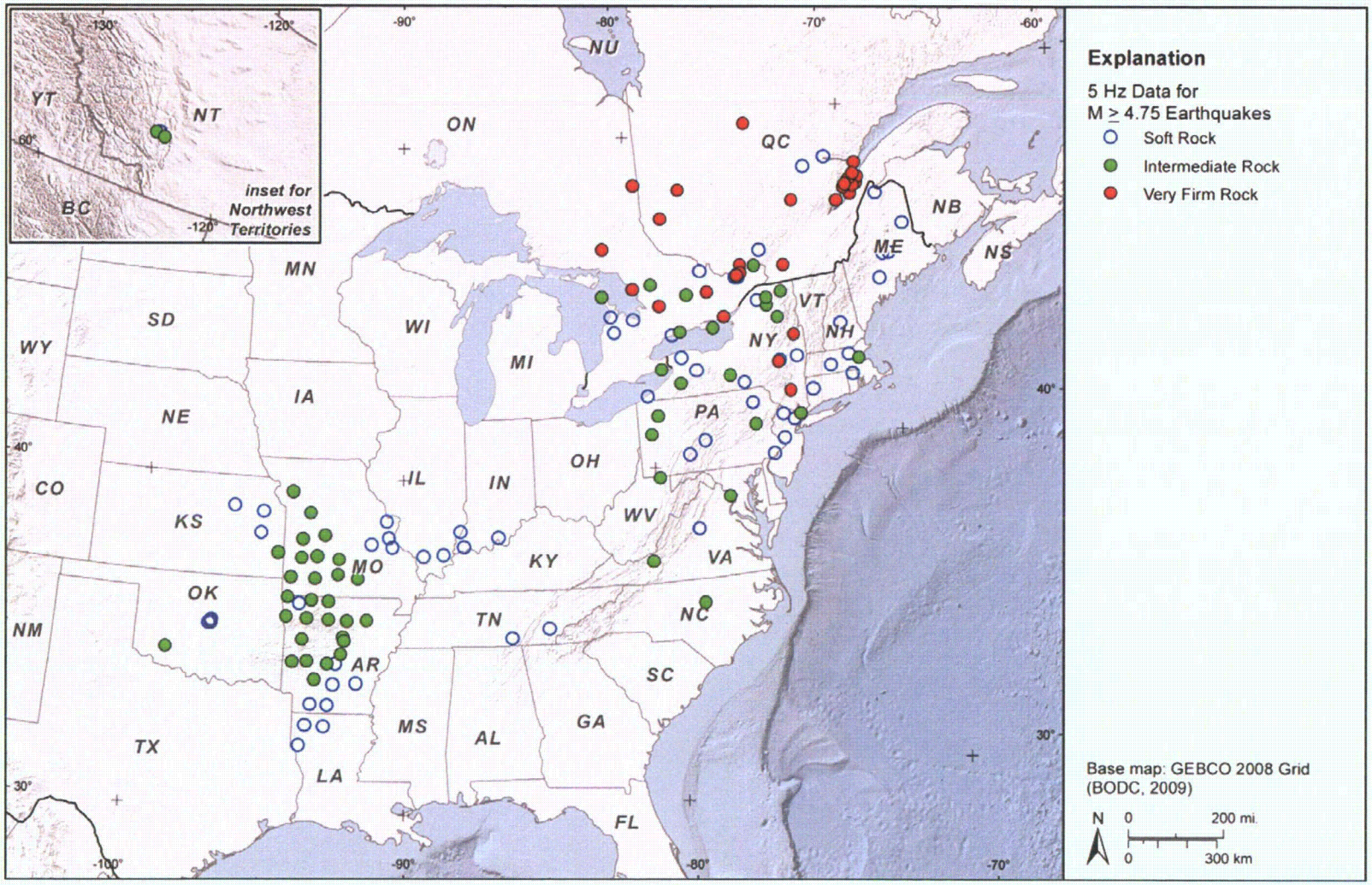

Figure 7.2.6-5c
Map of recording stations for earthquakes of magnitude M ≥ 4.75 and R_{JB} ≤ 500 km contributing 5 Hz PSA data to project ground-motion database

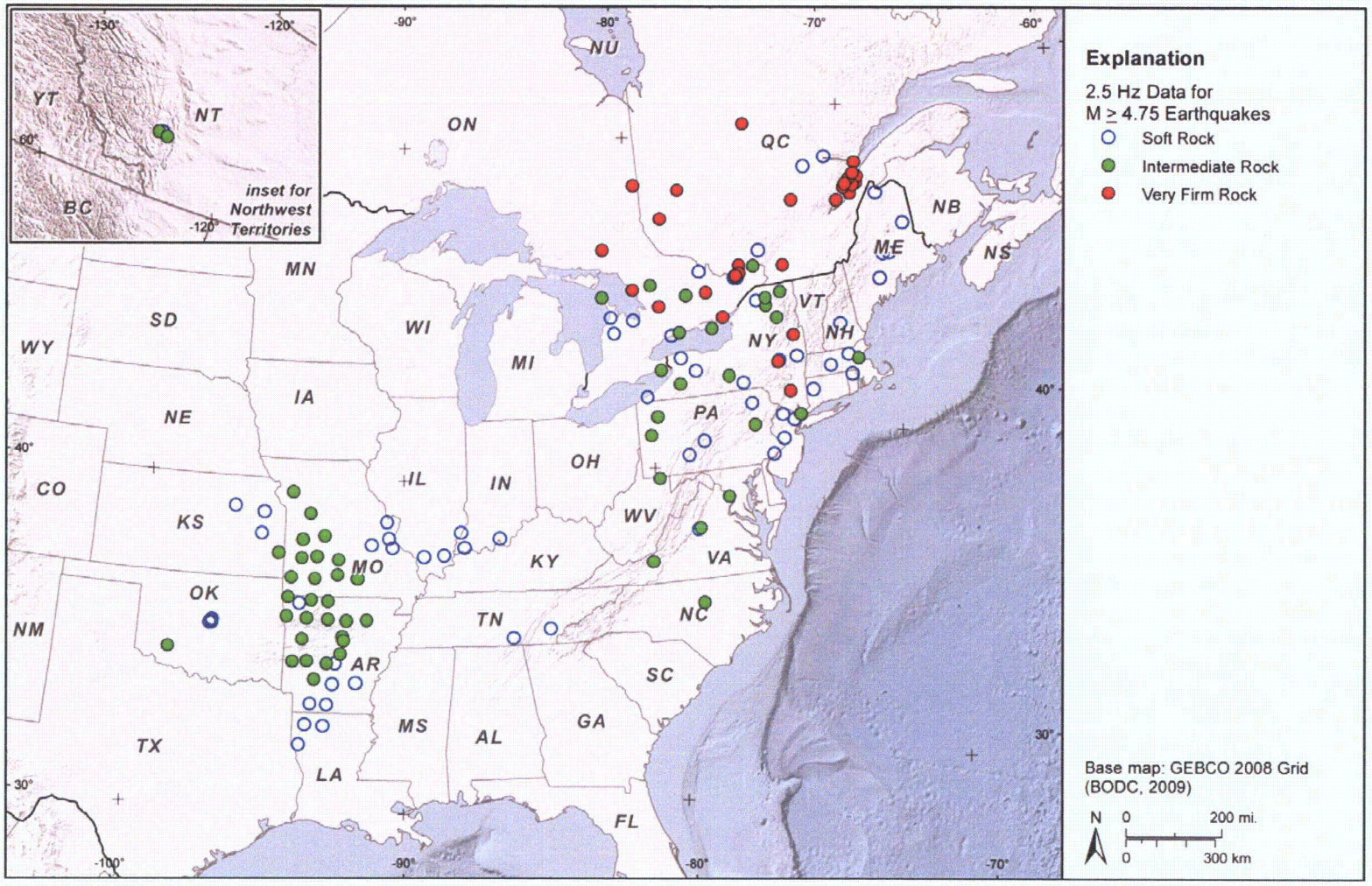

Figure 7.2.6-5d
Map of recording stations for earthquakes of magnitude M ≥ 4.75 and R_{JB} ≤ 500 km contributing 2.5 Hz PSA data to project ground-motion database

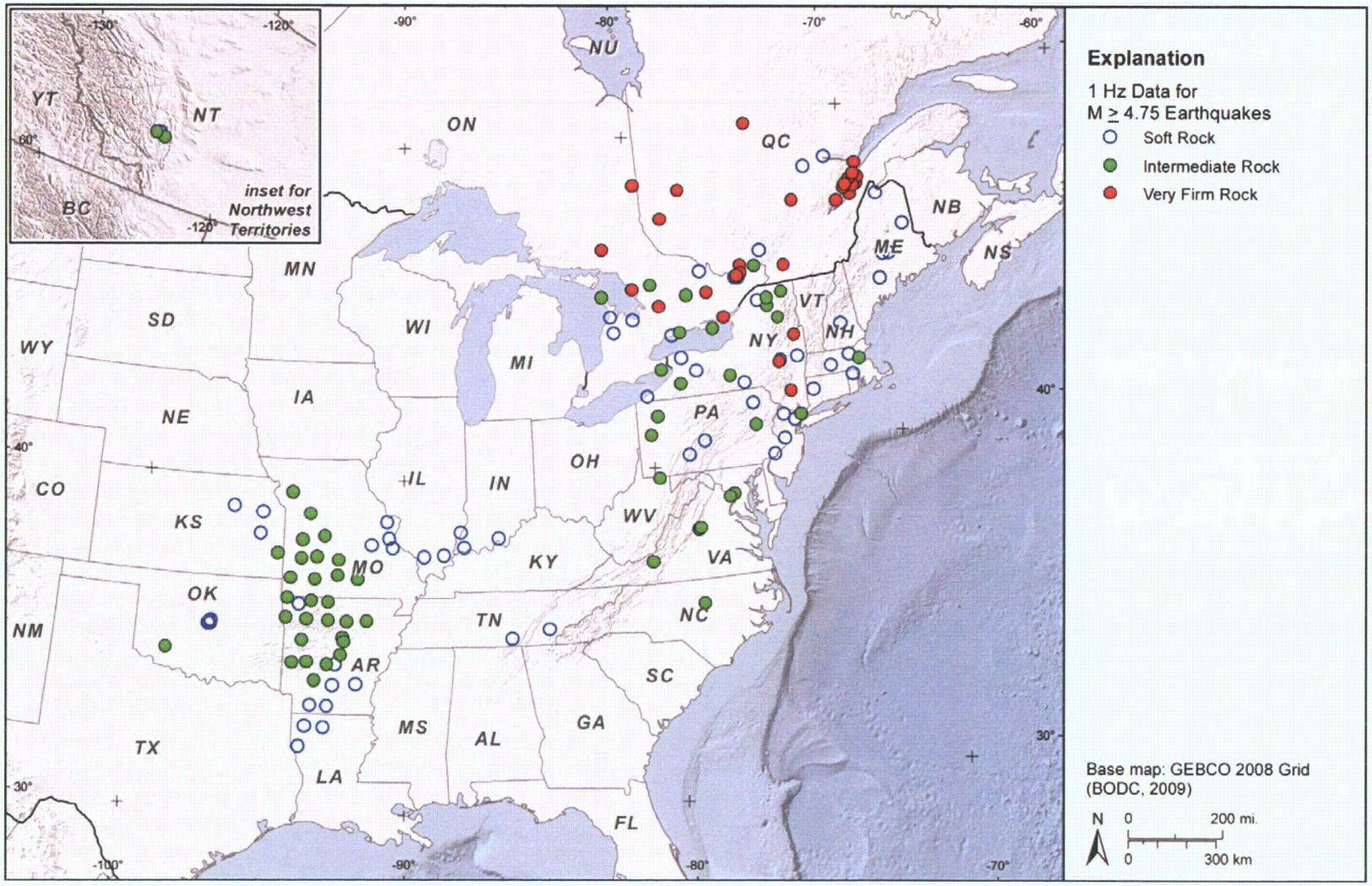

Figure 7.2.6-5e
Map of recording stations for earthquakes of magnitude M ≥ 4.75 and R_{JB} ≤ 500 km contributing 1 Hz PSA data to project ground-motion database

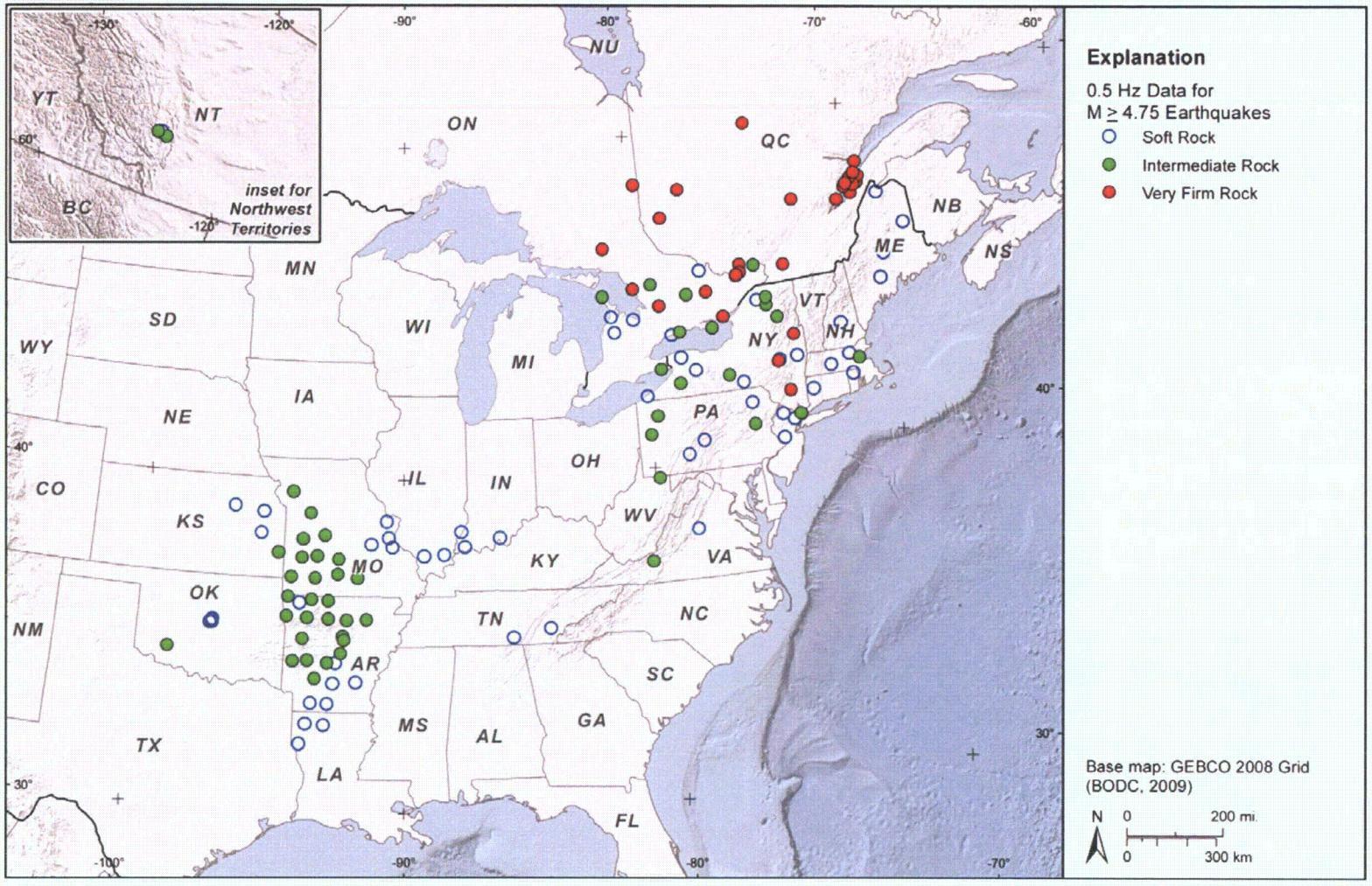

Figure 7.2.6-5f
Map of recording stations for earthquakes of magnitude M ≥ 4.75 and R_{JB} ≤ 500 km contributing 0.5 Hz PSA data to project ground-motion database